

University of Southampton Research Repository

Copyright © and Moral Rights for this thesis and, where applicable, any accompanying data are retained by the author and/or other copyright owners. A copy can be downloaded for personal non-commercial research or study, without prior permission or charge. This thesis and the accompanying data cannot be reproduced or quoted extensively from without first obtaining permission in writing from the copyright holder/s. The content of the thesis and accompanying research data (where applicable) must not be changed in any way or sold commercially in any format or medium without the formal permission of the copyright holder/s.

When referring to this thesis and any accompanying data, full bibliographic details must be given, e.g.

Thesis: Marcus Toy (2024) "The effect of environment on the properties of type Ia supernovae", University of Southampton, School of Physics and Astronomy, PhD Thesis, pagination.

Data: Marcus Toy (2024) The effect of environment on the properties of type Ia supernovae. URI [dataset]

University of Southampton

Faculty of Engineering and Physical Sciences School of Physics and Astronomy

The effect of environment on the properties of type Ia supernovae

DOI: 10.1002/0470841559.ch1

by

[Marcus Stephen Alexander Toy]

[MPhys with Astronomy]

ORCiD: 0000-0001-6882-0230

A thesis for the degree of Doctor of Philosophy

April 2025

University of Southampton

Abstract

Faculty of Engineering and Physical Sciences School of Physics and Astronomy

Doctor of Philosophy

The effect of environment on the properties of type Ia supernovae

by [Marcus Stephen Alexander Toy]

Since the discovery that the expansion of the Universe is accelerating, the field of modern observational cosmology with type Ia supernovae has strived to ratify and confirm this result. While one way to do so is to reduce uncertainties on measured cosmological parameters via the increase in sample size, recent years have seen an increased focus on understanding the underlying astrophysical phenomena that alter the measurable properties of type Ia supernovae. Many alterations currently are simply corrected for, without a complete understanding of the underlying cause. In this Thesis, we use the Dark Energy Survey's 5 year, photometrically confirmed type Ia supernovae (SNe Ia) sample, and investigate the effects of large and small scale environment on many properties of type Ia supernovae. We aim to investigate how these properties affect the supernovae themselves, and probe the underlying causes of some of these changes.

We identify that 66 of these supernovae have occurred within red-sequence selected galaxy clusters from the redMaPPer SVA1 catalogue. We compare light-curve and host galaxy properties of the cluster SNe to 1024 SNe Ia located in field galaxies, the largest comparison of two such samples at high redshift (z > 0.1) to date. We find that cluster SN light curves decline faster than those in the field at 97.7 per cent confidence. However, when limiting these samples to host galaxies of similar colour and mass, there is no significant difference in the SN light curve properties.

Additionally, we measure the intrinsic rate of SNe Ia in cluster and field environments. We find the average ratio of the SN Ia rate per galaxy between high mass ($10 \le \log{(M_*/M_\odot)} \le 11.25$) cluster and field galaxies to be 0.594 ± 0.068 . This difference is mass-dependent, with the ratio declining with increasing mass, which suggests that the stellar populations in cluster hosts are older than those in field hosts. We show that the mass-normalised rate (or SNe per unit mass) in massive-passive galaxies is consistent between cluster and field environments. Additionally, both of these rates are consistent with rates previously measured in clusters at similar redshifts. We conclude that in massive-passive galaxies, which are the dominant hosts of cluster SNe, the cluster delay time distribution, determining the expected rate of supernovae as a function of the time passed since a sample of white dwarfs is formed, is comparable to the field.

Motivated by our detection of a declining light curve width as a function of normalised galactic separation, we also investigate the effects of this separation on SNe Ia light curves and standardisation.

We use 1533 SNe Ia and show, for the first time, that the difference in SN Ia post-standardisation brightnesses between high and low-mass hosts reduces from 0.078 ± 0.011 mag in the full sample to 0.036 ± 0.018 mag for SNe Ia located in the outer regions of their host galaxies, while increasing to 0.100 ± 0.014 mag for SNe in the inner regions. In these inner regions, the difference in post-standardisation brightness between high and low mass hosts between can be reduced (but not removed) using a model where the R_V of dust along the line-of-sight to the SN changes as a function of galaxy properties. Various other probes also show a difference in post-standardisation brightness, such as intrinsically red or blue galaxies, or between star forming and passive galaxies. We show that selecting outer region SNe Ia only reduces this effect in all investigated probes. We conclude that the standardised distances of SNe Ia located in the outer regions of galaxies are less affected by their global host galaxy properties than those in the inner regions.

Contents

Li	st of 1	Figures		vi
Li	st of T	Fables		xi
De	eclara	tion of	Authorship	xiii
Ac	know	ledgem	ents	XV
De	efiniti	ons and	Abbreviations	xix
1	Intr	oductio	n	1
	1.1	Type I	a supernovae, from antiquity to the modern day	1
		1.1.1	The first rungs are set	4
		1.1.2	The climb further	5
		1.1.3	Testing the Universe	6
		1.1.4	Other measurements of H_0	8
			1.1.4.1 Progenitors of type Ia supernova	8
		1.1.5	Possible causes of light curve differences	9
	1.2	Enviro	onments of type Ia supernovae	9
		1.2.1	Effect of environment on the light curve properties of type Ia supernovae	10
		1.2.2	Effects of environment on distance measurements	13
2	Data	a and M	lethods	17
	2.1	The Su	apernova Sample	17
		2.1.1	The Dark Energy Survey	17
		2.1.2	The DES Supernova Program	18
		2.1.3	Transient Detection	21
		2.1.4	Spectroscopic Data	22
		2.1.5	SN Classification	23
		2.1.6	SN Light Curve Fitting	24
		2.1.7	Supernova Standardisation	26
		2.1.8	Galaxy Clusters	26
	2.2	Metho	ds	28
		2.2.1	Host Galaxy Matching	28
		2.2.2	Calculating host galaxy properties	29
		2.2.3	Bias Corrections	31
		2.2.4	Identification of Passive Galaxies	32
	2.3	Summ	arv	33

vi *CONTENTS*

3	Prop	perties (of Type Ia SNe within Clusters	35
	3.1	Superr	nova within Clusters	35
		3.1.1	Finding Supernovae Within Clusters	36
		3.1.2	SN Ia properties in field and cluster galaxies	39
			3.1.2.1 SN Ia light-curve width	41
			3.1.2.2 SN Ia colour	41
			3.1.2.3 SN Ia host galaxy stellar masses	44
			3.1.2.4 SN Ia host specific star formation rates	44
			3.1.2.5 The Effect of Progenitor Age	48
		3.1.3	Other causes of host distribution differences	51
			3.1.3.1 Host Confusion	52
	3.2	Summ	ary	53
4			pe Ia SNe within Clusters	57
	4.1	_	nova Rates in Clusters and the Field	57
		4.1.1	Calculating the SN Ia rate per unit stellar mass	58
		4.1.2	Discussion of rates	64
			4.1.2.1 The effect of age on the SN Ia rate	65
			4.1.2.2 The SN Ia rate in passive galaxies	67
	4.2	Summ	ary	68
5	A co	smolog	ical conundrum - Galactic location and its impact on the properties an	d
		_	ation of supernova	71
	5.1	The in	nportance of galactocentric separation for supernova properties	71
	5.2		Curve Properties as a function of Host Galaxy Radius	73
		5.2.1	Light Curve Properties	73
		5.2.2	What could drive these light curve differences?	74
	5.3	Superr	nova Standardisation	76
		5.3.1	The Host Mass Step	
		5.3.2	Host Mass Step as a function of d_{DLR}	78
		5.3.3	Line of sight effects	80
		5.3.4		84
		5.3.5	Could it be dust?	87
		5.5.5	5.3.5.1 Other influences on the mass step	92
	5.4	Summ	ary	96
6		clusions		99
	6.1		usions	99
		6.1.1	Differences in light curve properties and rates between cluster and field based type Ia supernovae	100
		6.1.2	Differences in light curve properties and post-standardisation brightness of type Ia supernovae between inner and outer regions of their host galaxies.	es 100
	6.2	Lookir	ng to the future	101
Δı	nend	lix A A	Appendix A	103
[1]	_		.1 Investigating the effects of Cluster Richness on SNe within clusters .	103
г				
K	eferen	ces		107

List of Figures

1.1	An image of the Crab Nebula in optical wavelengths (Emission from OI, [SII], [OIII]) taken by the Hubble Space Telescope. Credit:NASA, ESA and Allison	
	Loll/Jeff Hester (Arizona State University)	3
1.2	Distances to a given SNe as a function of redshift. Over-plotted are 3 different cosmological models, a low-mass Universe with no cosmological constant (dotted), a high mass Universe with no cosmological constant (dashed) and a low-mass Universe with a cosmological constant (solid). The data are in excellent agreement with a Universe that contains a non-zero cosmological constant.	
	Credits: Riess et al. (1998), Figure 4	7
1.3	Artists impression of the double degenerate (left) and single degenerate (right) progenitor systems of type Ia SNe. Credit: Wikipedia Commons, Discover	
	Magazine, Astrobites	10
1.4	Hubble Space Telescope image of the galaxy cluster eMACS J1823.1+7822. Credit: ESA/Hubble & NASA, H. Ebeling	12
1.5	Manifestation of the 'mass step', where SNe Ia in massive galaxies are ~ 0.06 -0.09 mag brighter than those in less massive galaxies. Credit Sullivan et al.	1.4
	(2010), Figure 4	14
2.1	A figure showing the relative transmission for each of the DES photometric passbands <i>grizY</i>	19
2.2	A comparison of the co-adds in the r band between the SVA1 and deep images. There is a clear increase in the number of sources detected in the deep images.	
	Figure from Wiseman et al. (2020)	22
2.3	A 'Flux Surface' for a type Ia SN at $z = 0.01$, with $x_0 = 0$, $c_{SN} = 0$	25
2.4	Upper Panel: Corrected distances to the DES 5 year photometric sample, along with an assumed Flat Λ CDM cosmology with parameters of $H_0 = 70$ km/s/mpc and $\Omega_M = 0.3, 0.1$ and 1.0. Lower Panel: The difference between the corrected distances and the assumed cosmology, along with the weighted average in equally	
	spaced redshift bins of 0.1	27
2.5	A stamp of DES13C1juw. Shown are the location of the SN (red cross) along with a $d_{\rm DLR}$ of 1.0 (green ellipse) and 4.0 (white ellipse). Note that as $d_{\rm DLR}$ is	
	directional it is ellipsoidal, and takes the shape of the host galaxy	30
2.6	The UVJ diagram for the zFOURGE sample from Tomczak et al. (2014)	32
3.1	SN Ia host galaxy stellar mass versus redshift for our two SN Ia samples (cluster SNe as red triangles, and field SNe as grey circles). Average uncertainties on the host masses are $<\sim 0.04$ dex. We note a lack of SNe Ia in field and cluster galaxies at $z>0.7$ and $\log{(M/M_{\odot})}<10$. As such we make a redshift selection	20
	of $z < 0.7$, shown by the dashed line	39

viii LIST OF FIGURES

3.2	U-R rest-frame colour versus stellar mass for SN Ia host galaxies. Cluster host	
	galaxies are redder and more massive on average than those in the field. The	
	horizontal and vertical lines indicate our selection of red, massive galaxies, with	
	masses $\log (M/M_{\odot}) > 10$ and $U - R > 1$	40
2 2		10
3.3	SN Ia x_1 distributions for events located in clusters versus those in the field.	
	Upper: x_1 values in bins of width 0.5. Lower: CDFs of the x_1 data. A K-S	
	test measures a 0.023 probability that the distributions are drawn from the same	
	parent distribution	42
3.4	SN Ia x_1 distributions for events located in clusters versus those in the field. In	
	these plots, both samples have been selected to be only red and massive host	
	galaxies (i.e., $U - R > 1$ and $\log(M_*/M_{\odot}) \ge 10$) as described in Section 3.1.1.	
	A K-S test measures a 0.068 probability that the distributions are drawn from the	40
	same parent distribution	43
3.5	SN Ia colour distributions for events found in clusters and those found in the	
	field. Upper: Histograms binned in steps of 0.05. Lower: CDFs of the colour	
	distributions. A two sided K-S test gives a p-value of 0.801, indicating no	
	statistical evidence that the CDFs are from different parent distributions	45
3.6	Host galaxy stellar mass distributions for SNe Ia occurring within clusters and	
2.0	in the field. Upper: Cluster and field data binned in steps 0.25. There is a lack of	
	cluster hosts with stellar masses between $9 \le \log(M_*/M_{\odot}) \le 10$, skewing the	
	distribution to the more massive end. Lower: CDFs of the host stellar masses.	
	A two-sided K-S test performed on the CDFs returned a p-value of 0.0006,	
	indicating strong evidence that the two distributions are drawn from different	
	base distributions	46
3.7	SN Ia x_1 versus host galaxy stellar mass for SNe Ia in clusters and the field, shown	
	both as individual points (yellow stars/grey crosses) and as weighted means (red	
	diamonds/blue pentagons). We recover the expected trend of higher mass hosts	
	containing SNe Ia with smaller values of x_1	47
3.8	Upper: SN Ia host specific star formation rate distributions for those location in	
2.0	clusters verses those in the field. There are a higher proportion of hosts with	
	more vigorous star formation in the field than in clusters. Lower: A CDF of the	
	above distributions. The cluster SN hosts have a clear shift to lower specific star	
	formation rates. A two sided K-S test returns a p-value of 0.0009, giving strong	40
	evidence for two separate populations	49
3.9	Distributions of the specific star formation rates of high mass hosts within clusters	
	and the field. The two distributions are nearly identical, with a two-sided K-S	
	test returning a p-value of 0.77	50
3.10	SN Ia x_1 versus host galaxy specific star formation rate in clusters (red triangles)	
	and the field (black circles). Weighted means are shown in purple (cluster) and	
	thistle (field). We confirm previous results that more vigorously star forming	
	galaxies (in both the cluster and field environments) host longer lived SNe	51
2 11	SN x_1 vs fractional host galaxy distance (d_{DLR}) for SNe Ia in clusters and the	<i>J</i> 1
3.11	• • • • • • • • • • • • • • • • • • • •	
	field, with the mean values for x_1 within d_{DLR} bins of width 0.25 plotted. Due	
	to few SNe Ia at these distances, we use one bin between $1.75 \le d_{\rm DLR} \le 2.5$.	52
3.12	A cartoon showing the behaviour of the host confusion parameter. Regions of	
	space where the SN is close to or within a specific host having a low degree of	
	confusion, while regions with SN spread more equally between several potential	
	hosts have a higher degree of confusion. From Gupta et al. (2016)	53

LIST OF FIGURES ix

Host confusion distributions for cluster and field based hosts. There is no significant difference between the two samples, with a two sided K-S test returning a p-value of 0.94	54
The efficiency of SN detection as a function of stretch (x_1) , colour (c_{SN}) , field and redshift. Figure adapted from Wiseman et al. (2021).	60
The number of SNe per year per Mpc ³ , as a function of redshift. Also shown are the data from Perrett et al. (2012). Our results are consistent within the 1σ	62
The number of SNe per $10^{10}~M_{\odot}$ per century, as a function of stellar mass of the host galaxy for cluster SNe and field SNe. The final cluster data points are the 1σ (dark red) and 3σ (light pink) upper limits for a non detection from Gehrels	63
A comparison of our field and cluster SNuMs, in host galaxies with $\log(M_*/M_{\odot}) \ge 10$, compared to other literature examples. The gold markers are rates measured in clusters from the literature. The black filled point is the field rate per stellar mass, and the black circle is the estimated field rate per formed mass, assuming a similar SFH to cluster environments, the error of which should be treated as a lower limit. Both cluster and field are presented in terms of formed mass. The	03
redshift range of this work spans $0.1 \le z \le 0.7$. Data are in Table 4.1 A similar comparison to 4.4, but instead both field and cluster have been limited to galaxies passing the UVJ cut described in Section 4.1.2.2. Errors on these passive rates should be treated as a lower limit	6465
SALT3 x_1 for our sample as a function of d_{DLR} along with the weighted averages. We see that, on average, the light curve width is centred on 0. However, in the centre-most bins the average x_1 is more negative.	74
SALT3 $c_{\rm SN}$ for our sample as a function of $d_{\rm DLR}$ along with the weighted averages. The average colour in the inner-most regions of galaxies are redder,	75
Hubble residuals for our sample as a function of d_{DLR} . There is no significant	77
The Hubble Residuals for the DES 5 year photometric sample, fit with 1 dimensional bias corrections only as a function of their host galaxy stellar mass. When split into bins above and below a stellar mass of $10^{10} M_{\odot}$, there is a difference of	
0.078 ± 0.011 magnitudes between the low and high mass weighted averages Top - As Fig. 5.4, but limited to SNe with $d_{\rm DLR} \leq 1$. The observed step between the SNe in low and high mass hosts increases to 0.100 ± 0.014 mag. Bottom - As Fig. 5.4, but limited to SNe with $d_{\rm DLR} > 1$. The observed step between the	78
SNe in low and high mass hosts decreases to 0.036 ± 0.018 mag Upper panel: The size of the host mass step, calculated for each realisation of our resampling, outlined in Section 5.3.2. The distribution appears broadly Gaussian, centred on a step size of 0.08 mag. Such a step size is consistent with the host mass step observed in our full sample. Lower panel: As the upper panel but instead the significance of the host mass step. It is centred between $3\sigma - 4\sigma$, showing that on average, a statistically significant step is found in our resampled SNe. Shown by the dashed red line in both are size and significance of the host mass step measured in the outer regions	81
	The efficiency of SN detection as a function of stretch (x_1) , colour (c_{SN}) , field and redshift. Figure adapted from Wiseman et al. (2021)

x LIST OF FIGURES

5.7	Upper: The host mass step observed in smaller d_{DLR} bins, with a span of 0.25 dex between $0 \le d_{DLR} \le 1$, increasing to 0.5 dex up to a $d_{DLR} \le 2$ and finally 1	
	dex at $d_{DLR} > 2$. We fit both a step function and a linear function to our data, and	
	find both have similar goodness-of-fit values, outlined in 5.3. Numbers show	
	the amount of SNe within each d_{DLR} bin. Lower: The reduced χ^2 for differing	
	step positions. Due to binning this only changes once the bin centres (shown in	
	the dotted black lines) have been passed. We see that the best fit step function is	0.0
5.8	located around 1.0, verifying the choice of location for our previous d_{DLR} split. Eccentricities of host galaxies within our inner region sample	83 84
5.9	As the upper panel of Figure 5.5 but limited to host galaxies with an eccentricity	
5.7	below 0.5, calculated with Equation 5.3	85
5.10	As Fig. 5.5 but for host galaxy rest-frame $U - R$ colour. The step sizes are	
	0.106 ± 0.013 mag (left) and 0.039 ± 0.018 mag (right)	86
5.11	The host mass step observed in smaller d_{DLR} bins of 0.25 dex over $0 \le d_{DLR} \le 1$,	
	$0.5 \text{dex over} 1 < d_{\text{DLR}} \le 2$, and $2 \text{dex at} d_{\text{DLR}} > 2$. The Hubble residuals split	
	into low and high stellar mass samples (top panel), split by the global host galaxy	
	rest-frame $U - R$ colour (middle panel), and split by an aperture $U - R$ colour	
	(lower panel)	87
5 12	Colour distributions for our sample, split by low (black) and high (red) mass	0.
3.12	hosts. Over-plotted are the best fit to the data. In this case both high and low	
	mass hosts are best fit by a Gaussian with an exponential tail	9(
5.13		,
5.15	the low mass SNe hosts in outer regions are the only distribution not best fit by	
	· · · · · · · · · · · · · · · · · · ·	91
5 1 <i>1</i>	a Gaussian with an exponential tail.	91
5.14	Hubble residuals for our inner (upper panel) and outer (lower panel) regions as a	
	function of SALT3 colour. We observe no significant difference in mean Hubble	01
	residual between low and high mass hosts at any SNe colour in the outer regions.	93
5.15	Hubble residuals for our inner (upper) and outer (lower) regions as a function	
	of SALT3 colour c_{SN} , plotted separately for events in low and high-mass host	
	galaxies, after having made a BBC 4D correction for the colour-dependent	
	selection and dust bias	94
5.16	Hubble residuals for our inner (upper panel) and outer (lower panel) regions as	
	a function of their host specific star formation rate, split at $\log_{ssfr} = -10$	95
Appe	endix A.1 Host galaxy stellar mass distributions for SNe Ia occurring within	
11	clusters and in the field. Shown is the CDF of our uncut sample, with clusters of	
	*	104
Anne	endix A.2 Host galaxy stellar mass distributions for SNe Ia occurring within	-
ppc	clusters and in the field. Show is the CDF of our restricted sample, with clusters	
	of richness \geq 15 Visually, there is little difference between this sample and A.1,	
	•	105

List of Tables

2.1	A summary of the 10 DES-SN fields, including the location of the field centre and the legacy surveys that observed them	20
2.2	The total exposure time, number of exposures and typical median limiting magnitude for each filter, per visit, used in the DES-SN program	20
3.1	The purity of a given cluster in a richness bin, estimated using Hao et al. (2010).	38
3.2	The number of SNe that are removed from our sample at each stage of selection.	40
4.1	Overall SN Ia rates (with host mass cuts applied) from this work with comparisons from the literature, as recalculated by Freundlich & Maoz (2021)	66
5.1	Weighted mean values of SN Ia light curve properties x_1 and c_{SN} and Hubble residuals in different d_{DLR} ranges	74
5.2	Statistics related to the steps in SN Ia luminosity as a function of stellar mass (the mass step) in our samples	79
5.3	The best fit parameters and reduced χ^2 for a linear trend and a step function to Figure 5.7	80
5.4	A table showing the reduced χ^2 values for both an exponential and regular Gaussian for both high and low mass hosts for each of our samples. Additionally, the best fit parameters are shown. They may also be found in the legends of Figures 5.12 and 5.13	89
App	pendix A.1 Significance's of our cluster vs field analysis for a richness cut of	102
	$\lambda/S > 5$ and for $\lambda/S > 15$	103

Declaration of Authorship

I declare that this thesis and the work presented in it is my own and has been generated by me as the result of my own original research.

I confirm that:

- 1. This work was done wholly or mainly while in candidature for a research degree at this University;
- 2. Where any part of this thesis has previously been submitted for a degree or any other qualification at this University or any other institution, this has been clearly stated;
- 3. Where I have consulted the published work of others, this is always clearly attributed;
- 4. Where I have quoted from the work of others, the source is always given. With the exception of such quotations, this thesis is entirely my own work;
- 5. I have acknowledged all main sources of help;
- 6. Where the thesis is based on work done by myself jointly with others, I have made clear exactly what was done by others and what I have contributed myself;
- 7. Parts of this work have been published as: Toy et al. (2023), Toy et al. (2024)

Signed:	Date:

Acknowledgements

There are so many people I wish to thank who've supported me during my time as an PhD student at Southampton University. Firstly, I'd like to thank my wonderful supervisory team. Mark, no matter how many times I'd joke around in my work you managed to keep the chaos focused, no small feat. Thank you for being so understanding with any problem I faced during the PhD, always offering additional meetings/proof readings/support. I hope you have learned from all the Gen Z slang I've thrown your way. Phil, you were round the corner for the majority of my PhD, and I honestly think that's been the deciding factor. Whether it was a pandas question or just checking if a given sentence made *any* sort of sense, you were always happy (I hope!) to help. I think with any other supervisors I wouldn't have made it this far, and I am eternally grateful.

Additionally, I had the joy of joining the absolute best group at Southampton, the Supernova Squad. Chris, when I had no clue what I was doing in first year and didn't understand you sat down with me for hours and helped me debug code, fix computing problems and just navigate the minefield of MacOS. Ed, CG, thank you for our SNeetings and joint adventures in hot pink graphs. Best of luck to you both with your PhD's, you'll both absolutely smash it.

I'd like to thank the entirety of the Southampton astronomy group - you all took in an anxious and jittery 22 year old and made me feel so welcome in this group. I'll cherish the Winchester trips, Hobbit expeditions and mental health breaks you took me on. I wish all of you the best. I'd like to particularly thank (in no particular order!): Charlotte, no matter how many times I'd whinge about work or medication or drag you along for a second pub trip you were always happy to listen or join for a breath of fresh air. Amy, thank you for all the coffees and connections, I'm sure we annoyed most of our office with our discussions on video games or other inane topics. Megan, somehow I've known you 8 years, and you've just about put up with me for most of them. Thank you for distracting me from work when I needed it, and the encouragements to just write this damn thesis. Matt, while I may have been the best physics dad, that wouldn't have been possible without the best physics son. Keep cracking at it, your father has high expectations! Arianna, thank you for always being there when I needed an ear to listen, your excellent suggestions on how to deal with any problem was always appreciated. Thank you for dragging me to my first metal concert! Martyna, good luck up North and thank for you all the reels you send me about hydrating and sleeping!

Finally I'd like to thank my wonderful family and friends. Mum, Dad, if you're reading this - I am doctor now. You've always been there whenever I need you and have helped me grow into the person I am today. Katie, you are my absolute rock, never far when I need someone to lean on or cry at. Thank you for staying beside this little ball of stress throughout the last 7 years. Here's to 7 more, hopefully less stressful, years. I'd also like to thank Lili, Tom, Rowland, Noe, and so many more but I'm out of space so, thank you all.

This work is dedicated to my grandparents. I miss you all so much.

Thank you for always supporting and guiding me. Each of you have left indelible marks on my soul, and I hope that wherever you are, you're looking down with pride at your grandson.

With all my love, Marcus.

'While you may not remember the kindnesses you did to me when I was little, I do, and I will remember them for both of us. And if one day I have children I will tell them of you, so that even when I am gone, your kindnesses will thread on down the hooks of your decedents and then your kindnesses will never die, and when both of us are gone, when we're only stories, it will still live on until there in all of time and space snuffed to dust and dust enough, there will be two facts lying leftover in dead eternity: that you were my grandparents, and I loved you.'

exurb1a, 'The Rememberer'

Definitions and Abbreviations

c The speed of light

 x_1 Decline rate of type Ia supernovae light curves

 $c_{\rm SN}$ Supernovae rest frame colour

SN/SNe Supernova/Supernovae
DES Dark Energy Survey

Ni⁵⁶ Nickel-56

MeV Mega electron-volts

pc parsec z Redshift

 $\mu_{\rm obs}$ Distance modulus

v Velocity

H₀ Hubble Constant

 R_V Slope of the dust extinction law (L)sSFR (Local) Specific star formation rate $\Omega_{\rm M}$ Fraction of matter within the Universe W Equation of state of the Universe

ZTF Zwicky Transient Facility

ASAS-SN Automated Survey for Supernovae

DECam Dark Energy Camera

CTIO Cerro Tololo Inter-American Observatory

S/N Signal-to-noise

SV Science Verification

DES-SN Dark Energy Survey Supernova Program

SNANA SuperNova ANAlysis framework

DESDM DES Data Management
CCD Charge coupled devices
VLT Very Large Telescope

LSST Legacy Survey of Space and Time

SNN SuperNNova

SCONE Supernova Classification with a Convolutional Neural Network

SED Spectral Energy Distribution

redMaPPer/RM red-sequence Matched-filter Probabilistic Percolation

K-S Kolmogorov–Smirnov

HC Host Confusion

DTD Delay Time Distribution SMF Stellar Mass Function

 $M_{\odot} \hspace{1cm} Solar \ mass$

SNuM Rate of supernovae per $10^{10}~{\rm M}_{\odot}$ per century

Chapter 1

Introduction

I also don't care if heaven exists or not. But even if it doesn't exist...I think it's something that should. It's more convenient that way. The final destination for those who kept on living despite all of life's hardships shouldn't be oblivion. Wouldn't it be nicer to think that they're indulging in luxury up in heaven?

Heiter, Frieren: Beyond Journey's End, Volume. 1

1.1 Type Ia supernovae, from antiquity to the modern day

The study of astronomy has long been pursued by humans. Star maps have been in use for millennia (von Spaeth, 2000), to track the sky and navigate the oceans. These mapped constellations do not change on human time scales. Thus, when the night sky changes, humans seek an answer. Typically, these changes were due to comets approaching the sun, illuminating part of the night sky for potentially weeks to months (e.g. Halleys Comet, Sicoli et al., 2024), or other solar based objects such as the planets. However, some events are visible in the sky for longer, and were more distant, though this distance was not known at the time.

The first 'guest star' was recorded in 185AD in the Houhanshu during the Han dynasty. Translated, the text reads - 'In the second year of the Zhongping reign period, the tenth month, on a Guihai day, a 'guest star' emerged within the Southern Gate. It seemed to be as large as half a yan, with scintillating, variegated colors, and it then grew smaller, until in the sixth month of the hou-year it disappeared' (Zhao et al., 2006). While the Han Chinese were unsure of what the new star meant, observations continued for thousands of years, with ~20 similar events recorded in Chinese records alone over the next couple millennia (Clark & Stephenson, 1982).

European observations of these 'guest stars' are often more sparse. However, some examples exist. SN 1006 was recorded by European, Asian and Native American sources, with the remnant from this explosion identified 900 years later (Gardner & Milne, 1965; Murdin & Murdin, 2011). SN 1054, which created the crab nebula (Lampland, 1921) was detailed in Eastern records, but not in European records. The lack of detailed European recordings, where such a bright event would have been visible for years, can be possibly attributed to the 'Great Schism', with recordings suppressed by the Roman Catholic Church (Collins et al., 1999).

These guest stars began to be known as 'novae', after Tycho Brahe's report on SN 1572 'De nova et nullius aevi memoria prius visa stella' ("Concerning the Star, new and never before seen in the life or memory of anyone") (Brahe, 1969, written in 1573, but re-published in 1969.).

Observations of these novae continued for many centuries, though there was no clear consensus as to their origin. This began to change in the mid 20th century, when Edwin Hubble attributed the changes in the shape of the crab nebula (see Fig. 1.1) to the result of a stellar explosion. These novae were then further defined between normal novae and super-novae by Walter Baade and Fritz Zwicky, who determined that the luminosity of a super-novae must come from a large fraction of the total mass of the progenitor (Baade & Zwicky, 1934; Zwicky, 1940).

Further advancements were made when Minkowski (1941) obtained spectra of a handful of supernova, and determined there were a group of highly homogeneous supernova, with spectra that contained no hydrogen (denoted as type I supernova) and a heterogeneous sample, with spectra all containing Balmer lines, but otherwise varied in their composition (type II supernova). Previously, many white dwarves had begun to be discovered. These faint stars were postulated to be the end product of stars around the mass of our sun. Curiously, these objects were dimmer than expected for stellar objects of their mass, and were soon discovered to only give off light due to the emission of thermal radiation. As such, they were understood to be composed of matter which supported itself against further collapse to due electron degeneracy pressure (Weidemann, 1968).

The nature of type I supernovae (SNe Ia) was proposed by Hoyle & Fowler (1960) to be the ignition of degenerate material, and further suggested by Whelan & Iben (1973) to be the ignition of a carbon-oxygen white dwarf. Degenerate matter is only supported against collapse by electron degeneracy pressure, thus as the mass of degenerate matter is increased, the radius of the object decreases, and correspondingly temperature and density increase. As such, should a carbon-oxygen white dwarf be in a binary system, and able to accrete matter from its companion, it would invariably become a smaller and hotter white dwarf.

Such degenerate pressure can only support a given amount of mass. Beyond ~ 1.44 times the mass of the sun the object will collapse (Chandrasekhar, 1931), however typically carbon fusion is ignited, and thus a type Ia SNe generated, before this limit reached. Fusion within the white dwarf is triggered by the increase in density and temperature, although the exact nature of the ignition is still a source of debate.

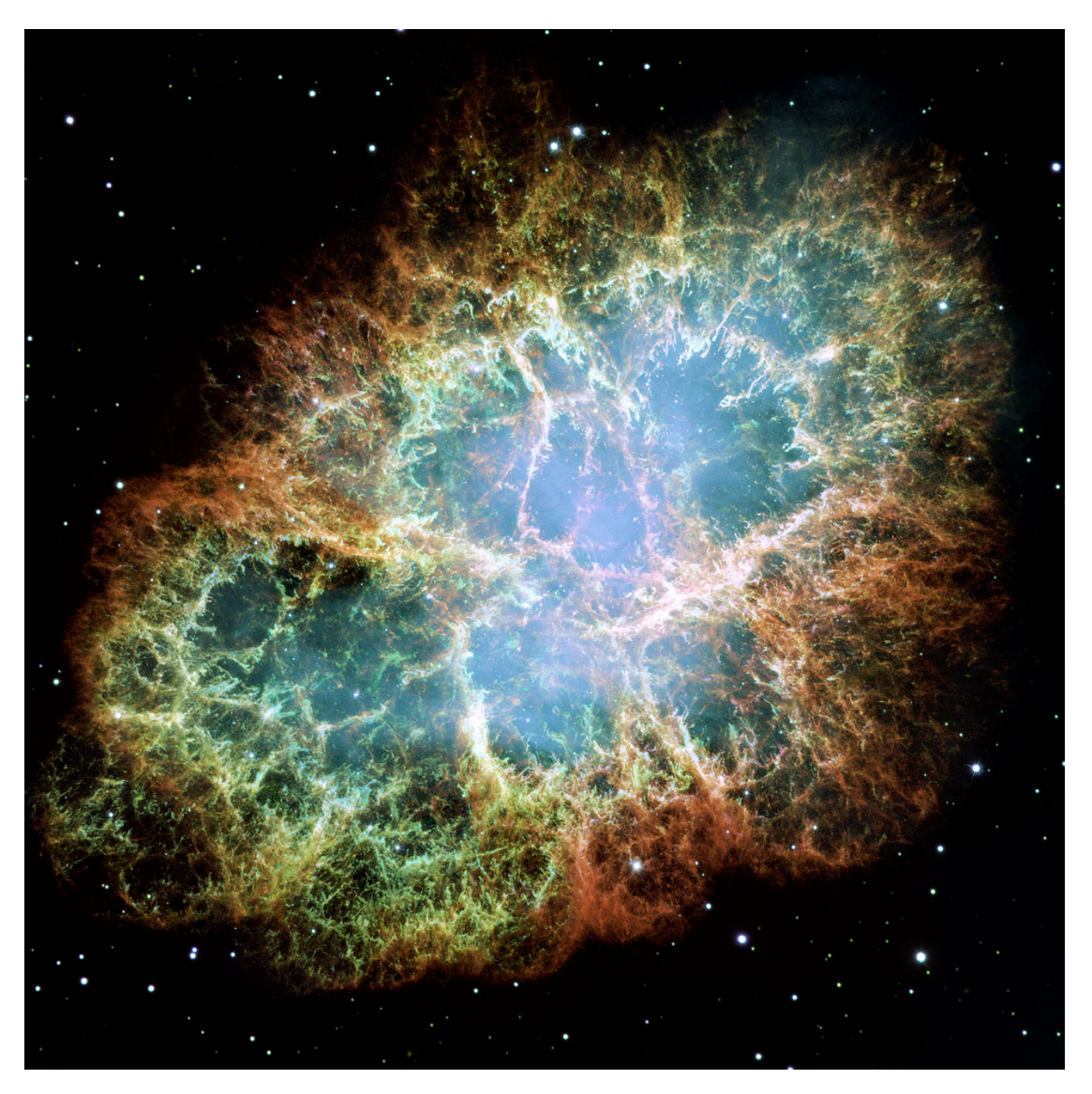


FIGURE 1.1: An image of the Crab Nebula in optical wavelengths (Emission from OI, [SII], [OIII]) taken by the Hubble Space Telescope. Credit:NASA, ESA and Allison Loll/Jeff Hester (Arizona State University).

As a result of this carbon burning, lighter elements are fused together into heavier and heavier elements. This fusion results in the production of iron-group elements, such as Nickel-56 (Ni⁵⁶) (Truran et al., 1967). Ni⁵⁶ is unstable, and decays to Cobalt-56 by capturing an inner electron, and releasing \sim 2 MeV per decay. This process has a half life of roughly one week. Cobalt-56 further decays to the stable Iron-56 with a half life of \sim 11 weeks, releasing \sim 3.6 MeV per decay (Colgate & McKee, 1969). This energy is released in the form of γ radiation, which is deposited as heat in material surrounding the progenitor star. This heat is reprocessed and released as optical radiation, the final light that we observe.

Thus, after close to two millennia of observations, theories and calculations, the mysteries of these 'guest stars' began to unravel. They were the result of a stellar explosion so violent that it unbound the star, synthesising a vast quantity of unstable elements, which decayed and heated up the surrounding material to such extremes that it was visible from Earth. However,

determining what caused these bright transient stars was only the first piece of the puzzle; the question of what they could be used for still remained.

1.1.1 The first rungs are set

Distances to objects on Earth are simple, and can be empirically measured. Distances outside of Earth however, are more complex. There exists no universal ruler to measure the distance to the sun or the moon, and distances beyond the solar system are further complicated.

Instead, to measure the distance to nearby stars, such as those within our galaxy, astronomers use the 'parallax method'. This method relies on the fact that objects appear to move relative to the observer from two different lines of sight. Thus, as the Earth orbits the Sun, stars on the sky will shift relative to background sources. This shift however, is small, with an object 31 trillion kilometres away only shifting by 1/3600 of a degree (1 arcsecond). This calculation defines a parsec (pc) - the distance from Earth at which an object will experience a parallax shift of 1 arcsecond.

While useful for stars within our galaxy, further objects experience smaller shifts in parallax, requiring more and more precise measurements of the apparent shift. For example, objects a distance of 10^6 parsecs away would only display a parallax shift of 10^{-6} arcseconds. This is further complicated by observations only showing how bright an object appears to be to the observer, rather than how bright it intrinsically is.

A solution to this problem arrived in 1908, when Henrietta Swan Leavitt discovered a relation between the luminosity of Cepheid variables (Pigott, 1785) and their period (Leavitt & Pickering, 1912). This relation allowed Cepheid variables to be used as the first 'standard candle'. By measuring the distance to nearby Cepheid variables via parallax, how bright it appeared on Earth (the apparent brightness or 'flux') and period, the relation between how bright the object intrinsically was (the luminosity, L) and period could be calibrated. Once this absolute luminosity versus period relation is calibrated, one can infer distances to extra-galactic Cepheid variables by measuring the difference between its apparent brightness, as the measured brightness of a source decreases with distance (Flux $\propto \frac{1}{4\pi d^2} \times L$) and the luminosity (calculated via the above period-luminosity relation).

Thus the first 'rungs' of the ladder to measure distances were set, parallax allowed the calibration of Cepheid variables that could measure distances to nearby galaxies. To push this further, astronomers needed an observable that was much brighter than a Cepheid variable, but still had a known intrinsic brightness.

1.1.2 The climb further

The solution came in the form of the previously discussed type Ia supernovae. While their spectra were similar (Minkowski, 1941), the maximal brightness each one achieved varied. They were first though to be used as 'standard candles' by Kowal (1968) who discovered the average peak brightness of type I supernovae was relatively consistent when the distance from the observer was taken into account.

This standardisation was bettered when it was discovered by Rust (1974) and Pskovskii (1977) that the length of time each event was visible for corresponded to the brightness achieved at peak. Further standardisation was improved with the discovery that the peak brightness of a given SN was directly proportional to the amount of Ni⁵⁶ synthesised in the explosion, which came to be known as Arnett's Rule (Arnett, 1982).

Work continued to attempt to standardise type Ia SNe, with the Philips relation (Phillips, 1993), who characterised faster fading SNe as intrinsically fainter in the B band, and vice versa. Along with this, relations between the difference in measured B and V band magnitudes (B-V) and the peak brightness were also found, with bluer (i.e B < V) SNe being intrinsically brighter than redder (i.e B > V) SNe (Riess et al., 1996; Tripp, 1998a).

Applying these light curve corrections allowed the standardisation of the peak luminosity of all 'typical' type Ia SNe. With these standardised luminosities, type Ia SNe within nearby galaxies that contained Cepheids could be calibrated from these extra-galactic Cepheids (that were in turn, calibrated by Galactic Cepheids and parallax). These calibrated SNe could then be used as a baseline to allow for the measurement of distance to type Ia SNe billions of light years away, providing distances to SN hosts much further than Cepheids could.

At its most basic, the difference between the observed brightness and the absolute brightness (also known as the distance modulus) $\mu_{\text{obs},i}$ of any given SN 'i' is given by

$$\mu_{\text{obs},i} = m_{x,i} + \alpha x_{1,i} - \beta c_{\text{SN},i} - M \tag{1.1}$$

where $m_{x,i}$ is the maximum brightness of the SN 'i' in a given band 'x' (typically the B band), $x_{1,i}$ (also known as the stretch of a SN) encapsulates the decline rate of the SN and $c_{SN,i}$ describes the (B-V) of the SN. α , β are nuisance parameters found to best fit to a given sample, and M is the absolute brightness of the whole sample, typically around -19.5 magnitudes. The distance modulus is empirically linked to distance to by $\mu = 5\log_{10}(d) - 5$, where d is the distance to an object in parsecs.

This allowed empirical measurements of the distance to a given SN, with no assumed model for the underlying mechanics of the Universe. As such, these distances could be used to test the validity of any given cosmological model.

1.1.3 Testing the Universe

The theory that the Universe itself, and objects within the Universe were static was generally accepted for centuries. To counteract the effects of gravity, Einstein introduced a 'cosmological constant', a type of undetectable energy that kept the Universe in a state of balance, neither collapsing nor expanding (Einstein, 1917).

This theory was challenged in the 1920's when Edwin Hubble discovered that not only were galaxies receding from our home galaxy, but that more distant galaxies were receding faster (Hubble, 1929). This measurement of expansion came about from the measurement of the offset of radiation emitted by galaxies being shifted to redder wavelengths when compared to radiation emitted in a laboratory rest-frame (aka redshift, z). In mathematical terms, this is expressed as z = v/c, with v being the recession velocity of a given galaxy, and c being the speed of light.

The measurement of the increasing recession velocity (v, in km/s) of a galaxy with relation to its distance (d, in Mpc) can be also expressed as $v = H_0 d$, where H_0 is the 'Hubble Constant'. For probing dark energy, the exact value of H_0 is not important, instead the relative distance as a function of redshift is. As the redshift of an event is proportional to the distance of the event, the relative distance (and therefore the objects luminosity) can be calculated from the shift in its emission lines.

We now have all the tools in order to investigate the underlying laws governing our Universe. This starts with measuring the redshift of each SN in a given sample, and determining the expected brightness for each SN as a function of its redshift. Then the difference between the observed and absolute brightness for each SN is determined from Eq. 1.1.

Comparing the observed brightnesses of SN to the model brightnesses will allow the testing of cosmological models, probing whether an object is further or closer than predicted for a given cosmological model.

Performing such a test with ~ 50 SNe provided the first evidence for the accelerating expansion of our Universe (Riess et al., 1998; Perlmutter et al., 1999, See Fig. 1.2), where the measured distances to the SNe were 10-15 per cent further than expected in a low mass-density Universe with a cosmological constant consistent with 0. Instead, they found better agreement for a Universe with a positive cosmological constant, where the fate of the Universe is infinitely accelerating expansion, never re-collapsing.

This detection of a cosmological constant was the first of its kind, and confirmed by other probes of cosmological parameters, such as those from the CMB (Planck Collaboration et al., 2020). Future SN surveys would also show agreement with a positive cosmological constant. However, other variables affecting SN brightnesses would shortly be discovered, requiring further standardisation and astrophysical explanations to reduce their effect on cosmological results.

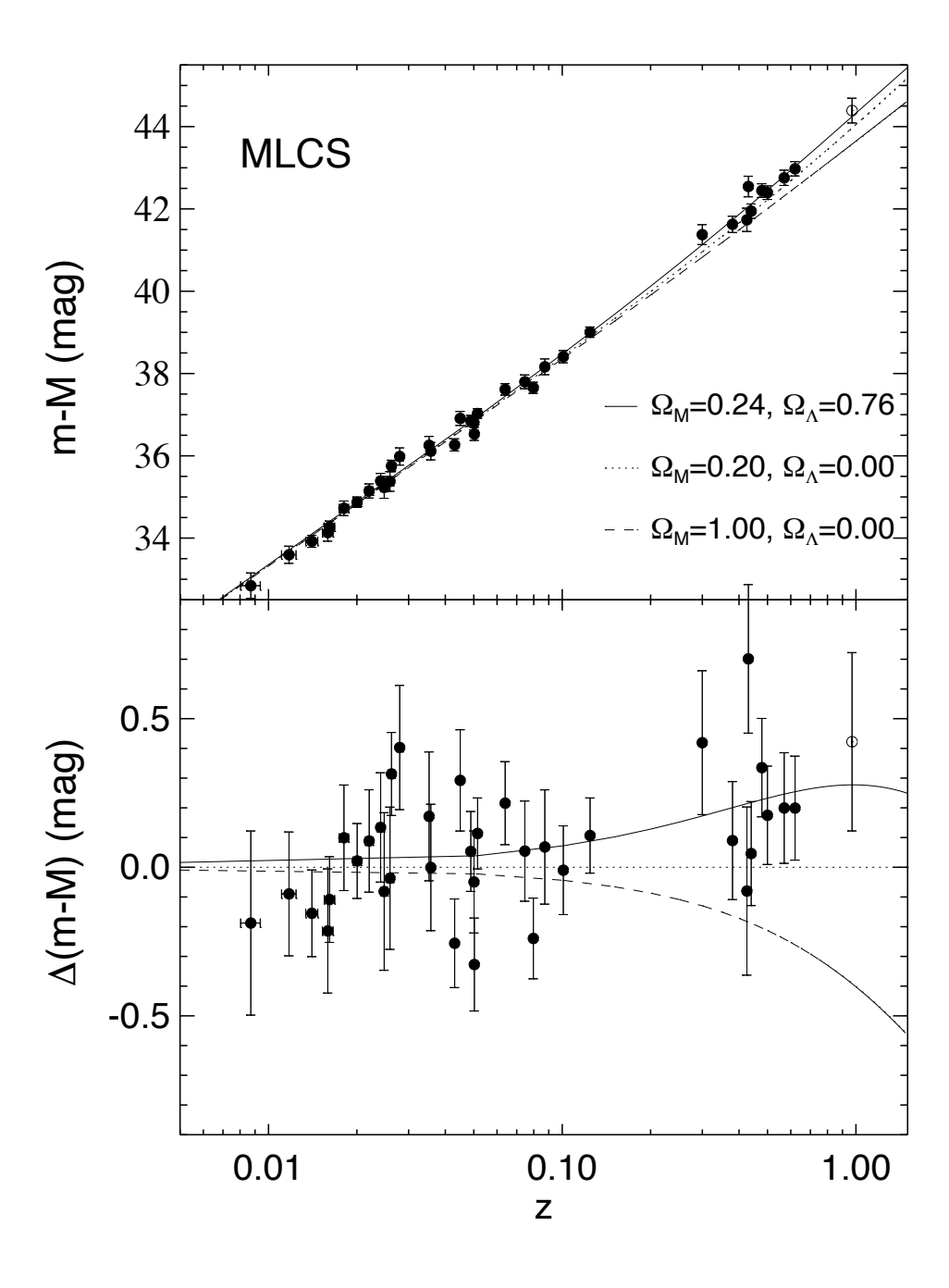


Figure 1.2: Distances to a given SNe as a function of redshift. Over-plotted are 3 different cosmological models, a low-mass Universe with no cosmological constant (dotted), a high mass Universe with no cosmological constant (dashed) and a low-mass Universe with a cosmological constant (solid). The data are in excellent agreement with a Universe that contains a non-zero cosmological constant. Credits: Riess et al. (1998), Figure 4.

1.1.4 Other measurements of H_0

The cosmic microwave background (CMB) can also be used to measure H_0 . These microwaves are formed from photons released after the recombination of the hot plasma formed after the big bang. While a full explanation is beyond this thesis (see Lemos & Shah (2023) for an excellent overview) the 'power spectrum' measured from the CMB can be fit to a given cosmological model and 'forwarded' through time to obtain the current value of H_0 . The benefit of this method is that calibration is relatively easy, however its detriment is that it is very sensitive to the cosmological model it is fit to.

Additionally, rather than calibrate SN using cepheids, main sequence stars at the tip of the red giant branch on the Hertzsprung-Russell diagram are relatively equal in their brightnesses. These instead can be used to calibrate distances to type Ia SNe, provided one is locatable within the SN host (Freedman et al., 2019).

1.1.4.1 Progenitors of type Ia supernova

The exact progenitor system of a type Ia supernova has yet to be identified (see Maoz et al., 2014, for a review). Leading models include a single white dwarf that accretes matter from a companion main sequence star (Whelan & Iben, 1973) or two white dwarfs that in-spiral due to the emission of gravitational wave energy before a period of common envelope sharing, leading to a cataclysmic explosion (Tutukov, 1981) (see Fig. 1.3 for an artistic impression). These two progenitor channels have different periods of time between the formation of white dwarf to the resulting type Ia supernova, called the 'delay time'. Theory of the distribution of the delay time (Ruiter et al., 2009) and measurements of the delay time (Castrillo et al., 2021; Wiseman et al., 2021) predict that most, if not all type Ia supernovae result from the in-spiralling of two white dwarfs.

However, more 'exotic' models exist, in both mass growth and detonation.

Some have proposed that in dense stellar environments, white dwarfs may collide head on, rather than in-spiral. The collision may be fully head on (in which much of the mass is converted to nuclear energy) or grazing, which more resemble main sequence collisions (i.e no SN produced) (Benz et al., 1989).

Other propose that if the density of unstable heavy metals (such as Thorium-232 or Uranium-235) within a galaxy is high enough, white dwarfs can form with a significant nuclear fraction present. These nuclides can crystallise and begin fission reactions, heating the surrounding Carbon and Oxygen hot enough to begin fusion (Deibel et al., 2022), thus leading to a supernova.

Accreting Helium from a companion star may lead to a Helium shell around the white dwarf. This, if heated sufficiently, can ignite helium fusion on the surface of the white dwarf. The

force of this fusion can compress and heat the remaining carbon/oxygen mixture to also begin fusion, unbinding the star. This detonation method is similar to the single degenerate model (in which matter is accreted from a companion star) but rather than a single detonation there is a double detonation (Taam, 1980).

1.1.5 Possible causes of light curve differences

Given that not all white dwarfs will be identical in composition nor mass, along with the detonation model itself being uncertain (Hillebrandt & Niemeyer, 2000), the resulting explosion has a great deal of variation possible. This variation in mass at time of explosion may lead to different masses of Ni⁵⁶ being produced within the supernova, and thus to faster decline rates and fainter supernovae. Indeed, even sub-Chandrasekhar mass explosions yield fainter supernova than close-to Chandrasekhar mass explosions (Shen et al., 2017).

This variation in progenitor, accretion method, detonation method and even mass at time of explosion may explain some of the differences observed within light curves. However, it is likely that direct observation of many progenitor system of type Ia SNe will be required to provide a definitive answer to this problem. However, direct observation remains a challenge due to the resolution required to resolve individual binary systems (and whether accretion is occurring!) in galaxies outside of our own.

1.2 Environments of type Ia supernovae

Type Ia SNe were now proven useful as calibratable standard candles, where, after correcting for the decline rate and B-V variations in their light curves, scatter in their peak brightnesses could be reduced to ~ 0.15 magnitudes (mag) (Guy et al., 2007). However, while uncertainties on cosmological parameters could be reduced with an increase in sample size (to reduce the statistical uncertainty), only by understanding and correcting for the remaining peak brightness scatter could the systematic uncertainties be reduced.

SNe Ia were observed to be intrinsically fainter and faster evolving in passive elliptical galaxies when compared to galaxies with ongoing star formation (Hamuy et al., 1995). Additionally, the rate of type Ia supernova is decreased in passive systems compared to active systems (Mannucci et al., 2005; Sullivan et al., 2006). The rate of supernovae decreases as a function of time after white dwarf binary formation (Wiseman et al., 2021), typically with rate evolving proportional to a $t^{\sim -1}$ power law. However, younger galaxies can contain orders of magnitude less stellar mass than older galaxies, which means that a typical 'older galaxy' may have many more binary systems that are Gyrs old. Convolving these two relations between age and stellar mass typically leads to a 'prompt' population, of young binary systems, and a 'delayed' population of older binary systems (Scannapieco & Bildsten, 2005; Sullivan et al., 2006). This can be

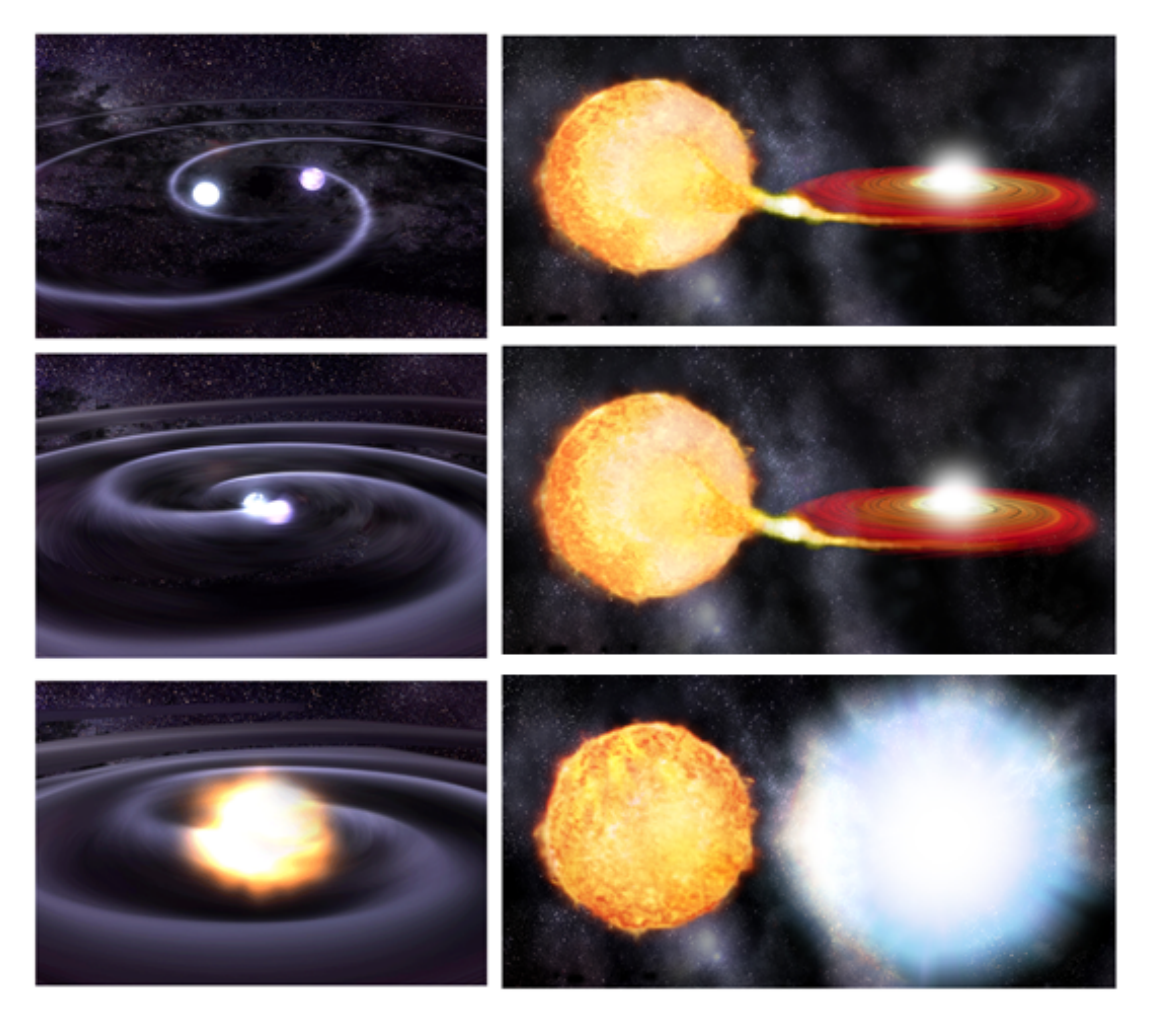


FIGURE 1.3: Artists impression of the double degenerate (left) and single degenerate (right) progenitor systems of type Ia SNe. Credit: Wikipedia Commons, Discover Magazine, Astrobites.

achieved by two different explosion mechanisms (such as single or double degenerate systems) or by a single double degenerate path.

Further complications arise in the still ongoing uncertainty with separating the intrinsic colour of a supernovae from the reddening caused by line-of-sight dust between a transient and observer. While redder SNe appear fainter than blue SNe, the colour correction slope β is inconsistent with a dust law slope (R_x) due to the Milky Way dust alone (Tripp, 1998a; Astier et al., 2006).

With these observed differences in SNe light curve properties and rates, the search to understand the underlying astrophysics causing these differences, or to correct for their effects began.

1.2.1 Effect of environment on the light curve properties of type Ia supernovae

It is now known that photometric properties of SNe Ia vary according to the host galaxy properties of the SN. Hamuy et al. (2000) used a sample of 62 type Ia SNe and found that

brighter and slower declining SNe preferentially preferred bluer environments. They attribute this bluer environment to be caused by a younger age of the stellar population.

Curiously however, while bluer environments typically host only slow declining (and therefore brighter) SNe, the older, redder environments are bi-modal, and host both slow declining and fast declining SNe Ia (Hamuy et al., 2000; Rigault et al., 2020; Wiseman et al., 2022a). This bi-modality further hints to two separate channels for the creation of a SNe Ia, and is in agreement with rate measurements (Mannucci et al., 2005; Scannapieco & Bildsten, 2005; Sullivan et al., 2006). Here, younger environments have not evolved long enough for the delayed channel to dominate, and almost solely host prompt explosions, while older environments may have ongoing prompt explosions, while being aged enough that delayed detonations can occur.

However, determining the age of a host is non-trivial, and often inferred from other measurements, such as its colour (as in Hamuy et al. (2000) or from spectroscopic measurements that indicate ongoing star formation (as in Rigault et al. (2020).

While the effects of star formation rate have already been discussed above, with galaxies with low star-formation rates host faster-declining and fainter SNe Ia than similar mass galaxies with more vigorous star-formation rates (Hamuy et al., 1995; Sullivan et al., 2006; Lampeitl et al., 2010), these analyses used the overall star formation rate of the host, not the star formation only around the SN itself.

Rigault et al. (2013) (Furthered in Rigault et al. (2020)) measured the local specific star formation rate (LsSFR) in a 1 kpc aperture around the supernova. The LsSFR was calculated from the strength of the H α line, which can be used as a tracer of the underlying star formation (Kennicutt, 1998). Rigault et al. (2013) investigated ~80 SNe Ia, split evenly between locally passive and locally star forming regions.

With the furthering of this study and a larger sample size, Rigault et al. (2020) found that the decline rate of a SN Ia's light-curve correlated with LsSFR to 6.5σ , with more star forming regions (or younger) hosting SNe with high stretch values, and vice versa. This relation was not unexpected, however, Rigault et al. (2013) found that $\sim 50\%$ of the SNe found in locally passive environments were located in globally star forming galaxies. This result added further correlations, and hinted that the local properties of the host may be of greater importance to their standardisation than the global properties.

On the opposite end, the presence of large scale structure around the SN, such as galaxy clusters (see Fig. 1.4 for one such cluster) may also have an effect. Galaxies located within galaxy clusters are often older, and with less ongoing star formation than similar mass galaxies located in the field (Bower et al., 1990). Within these structures, stars torn from their hosts by tidal forces float freely within the intracluster medium. These stars have then evolved to the point of detonation and been observed as type Ia SNe (Gal-Yam et al., 2003). These SNe could be used as a powerful tool to measure the intrinsic colour distribution, as they should not be affected by host galaxy extinction.



FIGURE 1.4: Hubble Space Telescope image of the galaxy cluster eMACS J1823.1+7822. Credit: ESA/Hubble & NASA, H. Ebeling

However, even cluster SNe within a host have been observed to have differing light curve properties than those outside clusters. Those within clusters decline faster, and are fainter than non-cluster based SNe (Xavier et al., 2013). This correlates with the distance from the centre of the cluster, with those closer to the centre of the cluster having even faster decline rates (Ruppin et al., 2024), while their colour remains unaffected. This trend remains when limiting both cluster and non-cluster SNe to passive galaxies, pointing to the older stellar population in clusters driving the observed decline rate difference (Ruppin et al., 2024).

The colour of a given SN also depends on its host properties, although this manifests in a different way to the decline rate. It shows no strong evolution with local nor global specific star formation (Sullivan et al., 2010; Rigault et al., 2020), nor with host stellar mass (Sullivan et al., 2010; Lampeitl et al., 2010). It has been noted however that the intrinsic colour distribution takes the form of a Gaussian, (mean μ_c , width σ_c), with reddening due to line-of-sight dust modelled as an exponential tail (of scale τ_E) (Jha et al., 2007; Mandel et al., 2011; Brout & Scolnic, 2021). The strength of this reddening (R_v) and the physical amount of extinction depends both on the composition of the dust within the host, and the amount of dust present in the line-of-sight. There are some indications that the strength of the reddening in the SN

line-of-sight varies between high and low mass hosts (Brout & Scolnic, 2021; Popovic et al., 2021a).

1.2.2 Effects of environment on distance measurements

Previously we discussed how type Ia SNe allowed the first evidence for the accelerating expansion of the Universe, due to their measured distances disagreeing with a model with no cosmological constant. This difference between measured distance and model distance is referred to as a 'Hubble Residual'. For testing cosmological models, the model that reduces these residuals the most is preferred, as it would provide the best fit to the observed SN distances. Variations within these models can also be tested, such as varying the fraction of matter, Ω_M (composed of both observable and 'dark' matter), within the Universe which will affect the expected distance of a given SN, along with equation of state of the Universe, w, describing the ratio between the pressure of the Universe and its energy density (w = -1 describes no evolution of energy density of cosmic time, equal to a cosmological constant).

However, the measured brightness of a given SN (and thus the measured distance, and residual from a given cosmology) depends on the properties of the SN host. Should the galaxy make-up evolve with redshift, the variation in measured brightness may mimic the effects of dark energy, or variations in other cosmological parameters.

As a quick side note, while measurement of the Hubble parameter (H_0) can be inferred from these medium to high redshift SNe, the calibration of this relies on using SNe close enough that the absolute distance to them can be measured from lower rungs on the distance ladder as calibrators (such as Cepheid variables or stars at the tip of the red giant branch) (e.g., Freedman et al., 2001; Riess et al., 2009, 2022)

An example of the measured brightnesses of SNe varying due to their host is the fact that after the light curve standardisation from Eq. 1.1, the brightnesses of SNe Ia (and thus the distances inferred to them) in massive, passive, older galaxies are brighter, and those in low-mass, younger, star-forming galaxies are fainter. Simplistically, this manifests as a step in SN Ia post-standardisation luminosity at a host galaxy stellar mass close to $10^{10} M_{\odot}$ (Kelly et al., 2010; Sullivan et al., 2010; Lampeitl et al., 2010, see Fig. 1.5). This so-called 'mass step' is observed or routinely modelled in all large SN Ia surveys or compilations of datasets (e.g., Betoule et al., 2014; Brout et al., 2022; DES Collaboration et al., 2024b) and has a typical size of about 0.06–0.15 mag (or three to seven per cent in distance) depending on the details of the sample. Similar trends are seen when replacing host stellar mass with other global host galaxy properties such as star-formation rate (SFR; Rigault et al., 2013), rest-frame colours (Roman et al., 2018) or gas-phase/stellar metallicity (Childress et al., 2014), and when considering these properties measured locally in a small aperture at the SN position (Rigault et al., 2013; Roman et al., 2018; Kelsey et al., 2021). The origin of the mass step is controversial and has implications that extend beyond SN Ia cosmology. Explanations include changing properties of

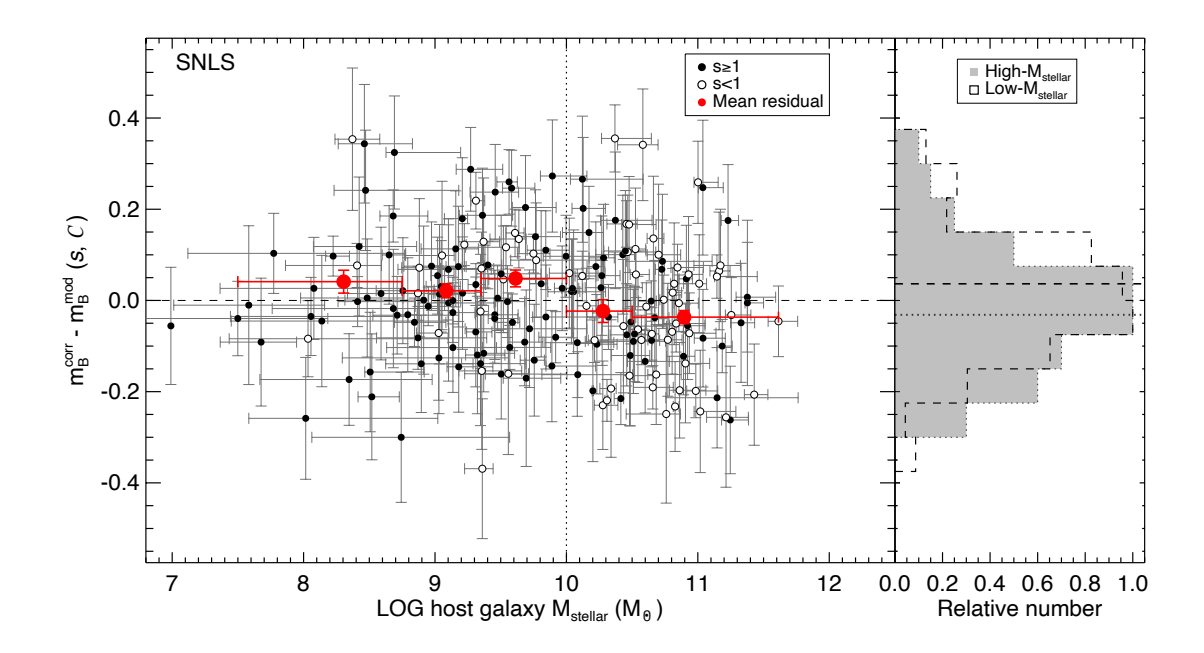


Figure 1.5: Manifestation of the 'mass step', where SNe Ia in massive galaxies are ~ 0.06 -0.09 mag brighter than those in less massive galaxies. Credit Sullivan et al. (2010), Figure 4.

the progenitor star, e.g., age (Rose et al., 2019; Rigault et al., 2020) or metallicity (Hayden et al., 2013), differing progenitor systems themselves, or dust properties that change with galaxy stellar mass (Brout & Scolnic, 2021).

The explanation of the age of the progenitor star came from measurements of the local specific star formation rate, and was found to reduce the significance of the host mass step. However, it instead introduced a step with the local specific star formation rate at a higher significance, indicating a stronger dependence of SN brightnesses on star formation than on host mass.

Indirect measurements of dust indicates that the ratio of total-to-selective extinction R_V is different in low and high-mass galaxies. Accounting for this variation in R_V reduced the significance of the host mass step, and also accounted for the variation of the step size with SN colour, with redder SNe appearing to show a larger step (Brout & Scolnic, 2021).

While a complete astrophysical explanation of the host mass step remains unknown, this step may be accounted for in cosmological analysis with the introduction of a γG_{host} term in Eq. 1.1 (see DES Collaboration et al., 2024b, and references therein). However, understanding of the changes in SNe brightnesses as a function of host galaxy properties remains a key area of research in order to reduce uncertainties and account for potential biases within a given sample of SNe.

In this Thesis I aim to investigate some of the outstanding problems introduced here, such as the difference observed in light curve properties between large scale environments such as the field and cluster. Additionally, while the effect of age upon rate measurements is fairly well modelled, there exists an enhanced rate of type Ia supernovae in cluster environments compared to the field (Freundlich & Maoz, 2021), which goes against this school of thought. I also aim to further the investigation of host galaxy properties affecting the post-standardisation brightnesses of type Ia supernovae, as current consensus as to the cause of the host mass step varies between differing dust parameters and galaxy/local age.

The layout of this Thesis is as such: Chapter 2 introduces the survey and instrumentation used to obtain data used. Methods to reduce and analyse the data are also outlined. Chapter 3 discusses the difference in light curve properties between type Ia supernovae found within clusters compared to the field. Chapter 4 builds on this work, presenting a calculation and discussion of the respective rates of type Ia SNe. Chapter 5 describes the dependence of the host mass step on the projected galactic distance between host and supernova. Conclusions of the thesis are then presented.

Chapter 2

Data and Methods

Okay. Look. We both said a lot of things that you're going to regret. But I think we can put our differences behind us. For science. You monster.

GLaDOS, Portal 2, Chapter 1: The Courtesy Call

2.1 The Supernova Sample

Before one can begin working on the science of supernovae, they must first obtain data. Many supernova surveys exist, such as the Zwicky Transient Facility (ZTF, Graham et al., 2019), which scans the entire northern sky every two nights from a single camera. The All-Sky Automated Survey for Supernovae (ASAS-SN, Shappee et al., 2014) consists of scanning the entire sky once a night down to ~ 18 mag, using 24 telescopes. These high-cadence surveys contain a great deal of fantastic data, but lack depth, and sensitivity to longer wavelengths to observe red-shifted optical light. For further away (or 'deeper') transients, sacrifices are made in cadence, as observations take longer. The Dark Energy Survey (DES) and its supernova program had finished their observations, and reduced much of the data by 2019, with a wealth of simulations to help interpret the data also available. As such, I elected to use DES data, to probe high depth type Ia supernovae and their host galaxies.

2.1.1 The Dark Energy Survey

The Dark Energy Survey was an imaging survey that started in 2013 and ran over the next 5 years for five-month seasons each year. The primary goal of this survey was to investigate the nature of dark energy. To do so, four complementary probes were used. The main probe I focus

on is type Ia supernovae, of which DES identified thousands photometrically. Over this 5 year period DES also measured and correlated the shapes of over 100 million galaxies in order to analyse Weak gravitation Lensing (Gatti et al., 2021), looked at the excess number of galaxies in clusters (Porredon et al., 2022) and measured the peak of the Baryonic Acoustic Oscillation from the clustering of galaxies (DES Collaboration et al., 2024a). These probes can be used individually, but are often combined to give tighter constraints on the cosmological parameters that govern our Universe (e.g. Brout et al., 2022).

The primary instrument was the Dark Energy Camera (DECam, Flaugher et al., 2015) mounted on the 4m Victor M. Blanco telescope at the Cerro Tololo Inter-American Observatory (CTIO). This 570 megapixel camera was designed to survey $5000 \, \text{deg}^2$ of the southern sky with high signal to noise (S/N \geq 5) at depths of \sim 23-24 mags while being sensitive to near-infrared wavelengths (750 nm-1450 nm, Flaugher et al., 2015). DECam observes with 70 charge coupled devices (CCDs), of which 62 were for scientific purposes. Due to instrumentation issues however, only 59 of these were operational throughout the whole survey.

The DES field overlaps with parts of the South Pole Telescope survey area, specifically the SZ cluster survey area (Lueker et al., 2010), along with part of Stripe 82 from the Sloan Digital Sky Survey (Ahn et al., 2012) which provides additional constraints on cluster measurements. The camera has a field of view of 2.7 deg² and used five photometric filters, *grizY* spanning a wavelength range from 400 to 1065 nm. The relative transmissions of these filters (including atmospheric transmission) is shown in Figure 2.1. While a *u*-band filter was contributed by CTIO, it is not of primary interest to DES, and thus was not used in the wider survey.

Before full DES operation, exposures were taken to verify that the camera was working to the survey requirements. This science verification (SV) 'mini-survey' was conducted in order to ascertain if any adjustments were required to survey strategy, and identify any undiscovered issues with the DECam prior to full survey use. It went to the depth of the full wide-field survey and, crucially for SN science purposes, covered the future DES SN fields. It is a well-tested data set (Bonnett et al., 2016; Jarvis et al., 2016; Jeffrey et al., 2018) ¹.

The SV data encompasses 250 deg², and was collected between November 2012 and February 2013. Over this time period, 10,000 exposures were taken and the images were reduced by an early version of the DES Data Management (DESDM) pipeline (Sevilla et al., 2011; Mohr et al., 2012; Desai et al., 2012, See 2.1.2 for further details on DESDM).

2.1.2 The DES Supernova Program

The Dark Energy Survey Supernova Program (DES-SN) was a separate observing mode of DES optimised for SN Ia cosmology. The survey was conducted over 10 fields, 8 'shallow' and 2 'deep', with limiting AB magnitudes of 23.5 and 24.5 respectively. Accounting for field

http://des.ncsa.illinois.edu/releases/sva1

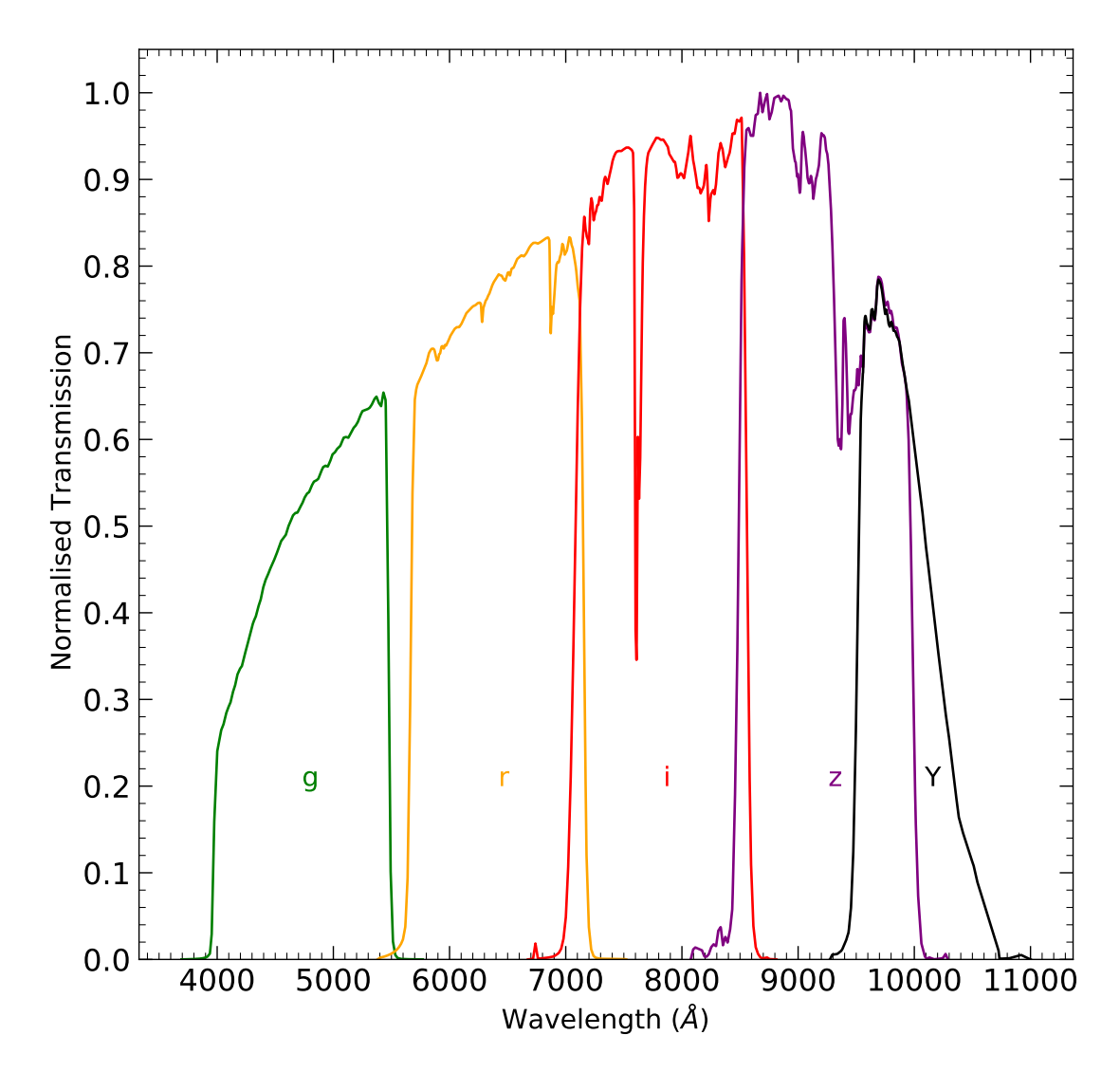


FIGURE 2.1: A figure showing the relative transmission for each of the DES photometric passbands *grizY*.

overlaps, the total observing area was roughly 23 deg². These 10 fields are located in four regions of the sky, each of which is previously well observed by various other surveys. A summary of the locations of the DES-SN fields and their respective legacy observations may be found in Table 2.1.

DES-SN was run in 'sequences' for observation scheduling purposes. A summary of the total exposure times, number of exposures and achieved depth per filter in the shallow and deep fields per sequence is given in Table 2.2 (Smith et al., 2020a). While DES has the ability to obtain observations in the Y band, the simulated signal-to-noise of a typical median redshift ($z \sim 0.4$ -0.5) SN Ia (simulated within the SuperNova ANAlysis framework (SNANA), see Kessler et al., 2009, absolute magnitude of \sim -19.5) in the Y band rarely exceeded 5, even with a total exposure time of 1800 s which is half of the z band deep field exposure time. At deeper redshifts ($z \sim 0.7$), this is further reduced and drops below the signal-to-noise selection for DES SNe. For reference, typical signal-to-noise values for simulated SNe in the griz bands range

Legacy Survey	DES Field	R.A. (deg)	Decl. (deg)	Type
Chandra Deep Field—South	C1	54.2743	-27.1116	Shallow
(Giacconi et al., 2001)	C2	54.2743	-29.0884	Shallow
	C3	52.6484	-28.1000	Deep
Elais-S1	E1	7.8744	-43.0096	Shallow
(Rowan-Robinson et al., 2004)	E2	9.5000	-43.9980	Shallow
SDSS Stripe 82	S1	42.8200	0.0000	Shallow
(Adelman-McCarthy et al., 2007)	S2	41.1944	-0.9884	Shallow
XMM-LSS	X1	34.4757	-4.9295	Shallow
(Pierre et al., 2004)	X2	35.6645	-6.4121	Shallow
	X3	36.4500	-4.6000	Deep

TABLE 2.1: A summary of the 10 DES-SN fields, including the location of the field centre and the legacy surveys that observed them.

TABLE 2.2: The total exposure time, number of exposures and typical median limiting magnitude for each filter, per visit, used in the DES-SN program

Filter	Shallow Field		Deep Field			
Tillel	t _{exp} (s)	N _{exp}	Depth (mags)	t _{exp} (s)	N _{exp}	Depth (mags)
g	175	1	23.7	600	3	24.6
r	150	1	23.6	1200	3	24.8
i	200	1	23.5	1800	5	24.7
z	400	2	23.3	3630	11	24.4

from ~ 500 at $z \sim 0.1$ to 10 at $z \sim 1$. Due to the time required to get signal-to-noise that would pass selection cuts in the Y band compared to the griz bands, DES-SN elected to not use this filter in their observations (Bernstein et al., 2012).

These exposures were then processed by the DES Data Management (Morganson et al., 2018) pipeline nightly to assess image quality. For DES-SN, the first quality check is the ratio between the actual exposure time and the exposure time required for similar S/N of a point source in normal conditions. This ratio, defined as $t_{\rm eff}$ is 1 under normal conditions, and decreases with worsening sky quality. It is calculated as,

$$t_{\text{eff}} = \left(\frac{\text{FWHM}_{\text{fid}}}{\text{FWHM}}\right)^2 \left(\frac{B_{\text{fid}}}{B}\right) F_{\text{trans}}$$
 (2.1)

where FWHM is the measured point spread function (PSF) full width half maximum, B is the measured sky background and F_{trans} is the atmospheric transmission relative to an almost clear night. fid denotes a historical measurement of that parameter, previously observed at CTIO. Exposures in the g band must have a calculated t_{eff} above 0.2, while those in the riz bands have a minimum t_{eff} of 0.3. Should any exposure fail this initial requirement the sequence containing it is rejected and rescheduled (Morganson et al., 2018).

2.1.3 Transient Detection

To detect transients, DES-SN used difference imaging. First, a template image was constructed using previously taken exposures, for example the template for the first season (Y1) was built on the science verification data. Several exposures were coadded to reduce sky-noise and increase depth, and this template used as a reference image.

On a given night, sky conditions will vary compared to the template image. As such, the template image is distorted to better reflect the observational conditions. The template is then convolved with the science images to match reference stars between the two, and outputs the difference between the convolved template image and science image. Doing such matching should remove all non-transient detections, however many of the remaining transient detections will be spurious. Detection efficiency is measured via the insertion of simulated transients to each CCD. Isolated sources at a brightness of 20th magnitude are inserted in order to assess image depth, and helps check if an observation needs to be re-taken. Additionally, sources that imitate SNe Ia, spanning the whole redshift and host-separation distributions, are inserted to estimate detection efficiency versus signal-to-noise. These detection efficiencies are vital as they allow rigorous simulations of DES-SN to be constructed, which allows inherent biases in the survey to be estimated. These biases then allow the more accurate standardisation of SNe, providing tighter constraints on cosmological parameters.

Image artefacts from the difference imaging are removed via various brightness, signal-to-noise and PSF cuts. Those that pass these basic cuts are sent to an automatic machine learning algorithm (Goldstein et al., 2015), to further determine if they are a 'true' transient. This machine learning algorithm uses many techniques to distinguish between fake and real transients, but there are 3 main features it uses: the ratio of PSF-fitted flux to aperture flux, magnitude difference between the object and its closest static neighbour, and consistency with a point source PSF. The algorithm then assigns each potential transient a value between 1.0 (perfect confidence the object is not an artefact) and 0.0 (no confidence the object is not an artefact). Should an object have two detections ranked above 0.3 (either on different nights or different bands) and be separated by less than 1 arcsecond it is labelled as a transient candidate. This left around 30,000 candidate transients that were then matched to a host galaxy using the directional light radius (DLR; Sullivan et al., 2006, see 2.2.1 for more information) method.

Initial DES-SN were matched to hosts identified in the first annual release of the SV data (henceforth SVA1). However, recent analyses match the DES SNe to hosts identified in 'deep image co-adds' provided by Wiseman et al. (2020). For a given transient, Wiseman et al. (2020) selected all exposures passing an effective exposure time cut, and excluding the seasons in which the transient occurred. Exposures passing the quality cuts were stacked using swarp (Bertin et al., 2002). Outliers in the co-adds, introduced by the stacking of different depth images, were removed via a clipping procedure. The magnitudes of the co-adds were then calibrated via the use of reference stars. After calibration, these stacked co-adds had a limiting magnitude of 0.6-1.2 mag deeper in the shallow field, and 1.7–2.1 mag deeper in the deep field,

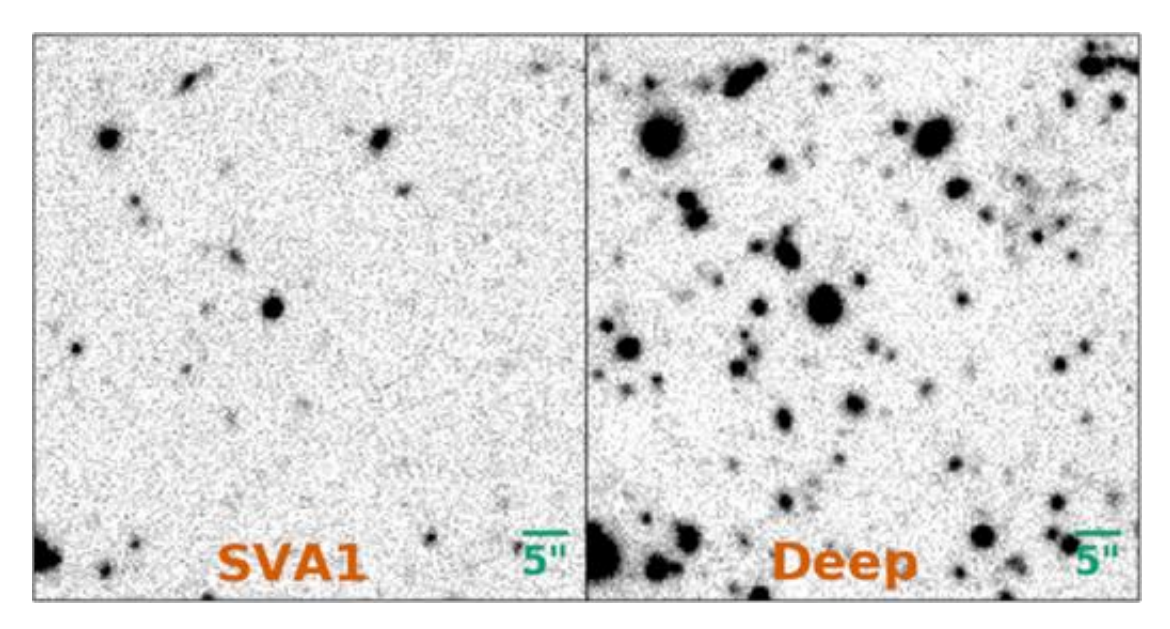


Figure 2.2: A comparison of the co-adds in the r band between the SVA1 and deep images. There is a clear increase in the number of sources detected in the deep images. Figure from Wiseman et al. (2020)

when compared to the SVA1 data. Figure 2.2, from Wiseman et al. (2020), shows the improvement on the source detection, with a clear increase in the number of sources detected in the deep images compared to the SVA1 images.

2.1.4 Spectroscopic Data

These reduced images from DES-SN allow for science in four photometric bands. At its most basic, this provides at most four data points per pointing, containing the time of pointing and the flux values from each source. While useful, this does not provide any data from emission lines, adding error onto both classification of sources and the distance to each source. Spectroscopic follow-up of likely transients can allow for clear classification, and provided a source has known emission lines (such as $H\alpha$ or $H\beta$), redshifts can be constrained with little uncertainty (on the order of $\bar{\sigma}_z \sim 0.002$).

Much of the spectroscopic data for DES came from OzDES (Yuan et al., 2015; Childress et al., 2017; Lidman et al., 2020), which targeted the 10 SN fields in DES over 6 years. This programme used the 2dF robotic fibre positioner on the 3.9-m Anglo-Australian Telescope. For the purposes of SNe, OzDES performed two tasks - real time spectroscopic classification and measuring host galaxy redshifts. For the real time spectroscopic classification, OzDES was guided by the use of the photometric classifier PSNID (Sako et al., 2011). This photometric classifier flagged likely Type Ia SNe based on their initial light curves, which were predominantly followed up by OzDES (Smith et al., 2020a). Such follow-up provided a spectroscopic classification for the transient. This sample, along with DES SNe classified by

other follow-up surveys such as the Very Large Telescope (VLT), were combined and presented in Smith et al. (2020a).

Compared to spectroscopic classification, the measurement of a given host's redshift can be much more efficiently scheduled. Due to the lack of time sensitivity, as the galaxy will not significantly change on a human timescale, sources can be visited seasons after a transient has occurred. If the initial exposure was unable to obtain a redshift, sources can be revisited to provide additional signal-to-noise and depth. During its 6 year run time, OzDES measured host galaxy redshifts for around 7000 transient hosts, using 68,000 fibre hours. Data from the 3rd observing season of OzDES (Y3) had redshifts measured using MARZ (Hinton et al., 2016) while prior data had redshifts measured by Runz, developed by Will Sutherland. OzDES was magnitude limited down to the \sim 24th mag in the r band. The fraction of usable redshifts decreases with dimmer sources, with the efficiency of obtaining a redshift dropping to \sim 20 percent at 24 mag in the r band (Vincenzi et al., 2021).

Thus, after 5 years of observing and consequent spectroscopic follow-ups, DES-SN had ~ 500 spectroscopically classified Type Ia SNe, along with ~ 7000 transient light curves with usable host galaxy redshifts.

2.1.5 SN Classification

With \sim 7000 candidate transients with light curves from the DES 5 year pipeline, getting a spectrum with high enough signal-to-noise to determine transient type for each candidate would be incredibly time consuming. For example, classifying one SN Ia at z \sim 0.05 with a single slit, 4m telescope, takes on the order of 15 minutes of exposure alone (Toy et al., 2022, see SN2022qye), ignoring slew time and other various observational calibrations. OzDES spent over 4000 fibre hours to classify transients spectroscopically, with 2164 individual spectra taken. Of this, \sim 500 transients were positively classified, while the remainder were either unclear in their classification or simply not observed due to time or brightness constraints.

With the Vera C. Rubin Observatory conducting the Legacy Survey of Space and Time (LSST) expected to begin observations in the near future, this problem is further exacerbated. Rubin expects to discover 400,000 Type Ia SNe over its lifespan (Ivezić et al., 2019). Even though telescopes such as 4MOST will follow up transients discovered by LSST with fibre based spectroscopy, at best performance only ~ 3% of the SNe discovered by LSST will have a spectroscopic classification (Frohmaier et al 2024, in prep). Further issues arise as 4MOST only reaches ~22.5mag in ~ 40 minutes, while LSST will reach depths of ~25mag (The LSST Dark Energy Science Collaboration et al., 2018), limiting the maximal redshift it may spectroscopically classify SNe at.

We therefore examine alternate methods, such as photometric classification. Modern classifiers typically use machine learning to classify transients, such as SuperNNova (SNN; Möller & de Boissière, 2019) or Supernova Classification with a Convolutional Neural Network

(SCONE; Qu et al., 2021). This allows surveys to sort their transients based on the evolution of their multi band light curves. SNN for example, can discern between Type Ia SNe and non Type Ia SNe with accuracies of 99.55 ± 0.06 per cent, provided redshift information is available. Such a high accuracy is achieved by the lump classification of "anything that isn't a type Ia SNe", along with including host galaxy and redshift information. For a singular 'whole' light curve, accuracies decrease to closer to 95 per cent.

SNN uses a recurrent neural network to take an input light curve, and its most basic output is the probability of said light curve being a type Ia SN. Previously, negative classifications of type Ia SNe were rejected from cosmological samples. However, the probability of being a type Ia SN can be used instead as a weight, where a given events contribution to a SN Ia based cosmological analysis is weighted by its probability of being a type Ia SN, e.g. (DES Collaboration et al., 2024b).

The final DES release contains 1499 'cosmologically useful' type Ia SNe, after light curve and classification cuts. However, after relaxing requirements on obtained host galaxy redshift and light curve quality cuts, DES discovered 3,547 type Ia SNe, classified with SNN (Möller et al., 2024).

2.1.6 SN Light Curve Fitting

After identifying which candidates are likely SNe Ia, we obtain parameters to describe the evolution of the light curve. To do this, candidates are fit with the SALT3 spectral energy distribution (SED) model (Guy et al., 2007; Guy, J and Sullivan, M et al., 2010; Kenworthy et al., 2021) in the SuperNova Analysis framework (SNANA; Kessler et al., 2009).

A singular SN Ia typically shows two main types of variability in their light curves: a variation in their broadband colours that is time independent ($c_{\rm SN}$) and the rate of decline in a given band from its peak (x_1). SALT3 models the behaviour of SN Ia light curves using these variabilities and one additional parameter: x_0 which models the amplitude of the light curve. With these parameters, the spectral flux for a given SN, at a rest frame phase p (relative to the B band maximum) and wavelength λ is given by

$$F(p,\lambda) = x_0[M_0(p,\lambda;m_0) + x_1M_1(p,\lambda;m_1)] \times \exp(c \times CL(\lambda;cl)). \tag{2.2}$$

Here $M_{0,1}(p,\lambda;m_{0,1})$ are flux surfaces (see Fig 2.3) that represent the SED of a reference SN (0) and the time-dependent variability of the total population fitted. These flux surfaces have 2520 free parameters that are determined by the training for the SALT3 model. $CL(\lambda;cl)$ defines how SN $c_{\rm SN}$ affects its light curve, combining the effects of the variation in colour over a population of SNe and extinction from the dust within its host galaxy.

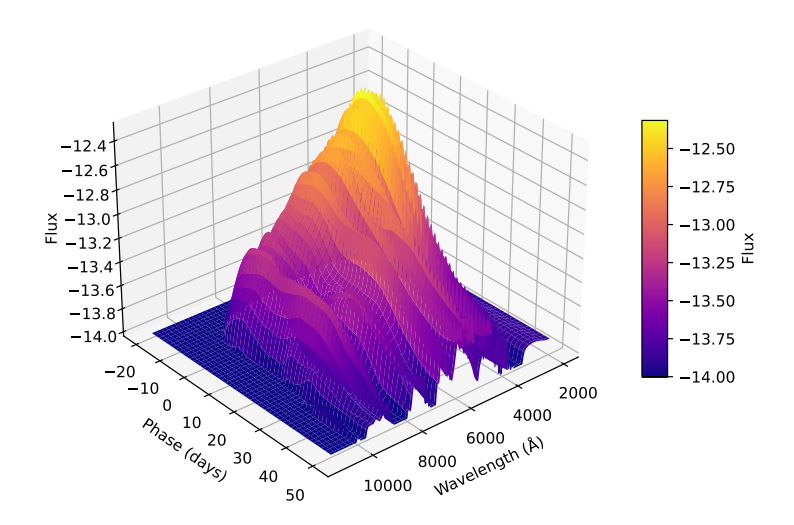


FIGURE 2.3: A 'Flux Surface' for a type Ia SN at z=0.01, with $x_0=0$, $c_{\rm SN}=0$

SALT3 is trained using the light curves and spectra from 1083 SNe. While initially 2520 free parameters appears greater than the amount of training data, each single SN will have many parameters describing its light curve and spectral evolution. The training alternates between fitting the flux surfaces and colour law, along with the parameters $x_{0,1}$ and c_{SN} , while keeping the output model uncertainties fixed. It then fits for the output model uncertainties while keeping the flux surfaces and colour law fixed. For the purposes of training, the light curve parameters $x_{0,1}$ and c_{SN} of the training set (which describe and vary between individual SNe) are of little concern. Instead the converging of the flux surfaces is the main goal of the training, as these may be used to calculate the light curve parameters of newly discovered SNe Ia.

Once the fit for the flux surfaces, colour law and output model uncertainties has converged, training is complete. The result is the best fit flux surfaces and colour law that describe a population of SNe, along with their uncertainties. While it is computationally expensive to obtain these flux surfaces and colour law, once done they may be applied on a different sample of SNe. Doing so allows surveys to calculate the light-curve parameters $x_{0,1}$ and c_{SN} , which are used to standardise the brightnesses of SNe Ia, and thus to constrain cosmology.

For most of the work within this thesis, we apply a similar light curve selection to those described in Vincenzi et al. (2021), and used in Wiseman et al. (2021), on SN light-curve width (SALT3 x_1) and SN rest-frame colour (SALT3 c_{SN}): $-3 \le x_1 \le 3$ and $-0.3 \le c_{SN} \le 0.3$. These selections aid machine learning in reducing contamination from core-collapse SNe (Vincenzi et al., 2021). Additionally, the SALT model functions such that the average light curve width of a given sample is Gaussian, with a mean of 0 and standard deviation of 1. As such these light curve cuts also serve to remove outliers above 3σ from the mean.

2.1.7 Supernova Standardisation

After light curve parameters are calculated, we are able to obtain distances to each SN. Distances to the i'th supernova are calculated for a given sample via the Tripp equation:

$$\mu_{\text{obs},i} = m_{x,i} + \alpha x_{1,i} - \beta c_{i,\text{SN}} - M$$
 (2.3)

where x_1 and $c_{i,SN}$ are the SALT3 light curve parameters described above, m_x is the magnitude of the SN flux in a given pass band and M is the absolute magnitude. α and β are global parameters determined from a minimisation over the sample to a given cosmology.

Provided a redshift for the SN or its host is available, model cosmologies may be tested and discerned between. An example is shown in Figure 2.4 where our corrected SN distances are plotted alongside the expected distance assuming a universe described by a flat Λ CDM model with parameters of $H_0 = 70 \text{km/s/Mpc}$ and $\Omega_M = 0.3$. We additionally include models with different values of Ω_M , described in the legend. Of note is that the average residual ($\mu - \mu_{\text{model}}$) over the full redshift range is close to 0 compared to the model with $\Omega_M = 0.3$. This showcases the ability of SNe Ia to discern between differing cosmological parameters, while requiring only a redshift and a light curve.

2.1.8 Galaxy Clusters

After this stretch and colour standardisation, there remains a luminosity difference between SNe in high and low mass hosts (Kelly et al., 2010; Sullivan et al., 2010; Lampeitl et al., 2010). There still exists debate as to the underlying astrophysical phenomena that causes these luminosity differences, with no clear consensus. Current explanations involve a range of ages for the progenitor star (Childress et al., 2014; Rose et al., 2019; Rigault et al., 2020), varying dust properties between hosts (Brout & Scolnic, 2021), metallicity (Hayden et al., 2013) or even different explosion models and mechanisms.

Due to this unknown astrophysical cause, one of the interesting environments for type Ia SNe studies is clusters of galaxies. Ages of stars and galaxies within clusters are typically old, with most of the galaxies and stars within clusters forming at least a few Gyrs ago (Guglielmo et al., 2015). Furthermore, when compared to similar mass galaxies outside of clusters (field galaxies), cluster galaxies often have little ongoing star formation (Balogh et al., 1997; Haines et al., 2015). There is also evidence that the quenching of star formation in galaxies within clusters depends more strongly on the radial distance from the cluster centre (with cluster centres being the most efficiently quenched) than on the galaxy stellar mass (van der Burg et al., 2018), leading to a greater number of lower mass galaxies with extinguished star formation (van der Burg et al., 2013) than the field. This leads to an overall reduction in star formation rates within clusters compared to the field, across all galaxy masses.

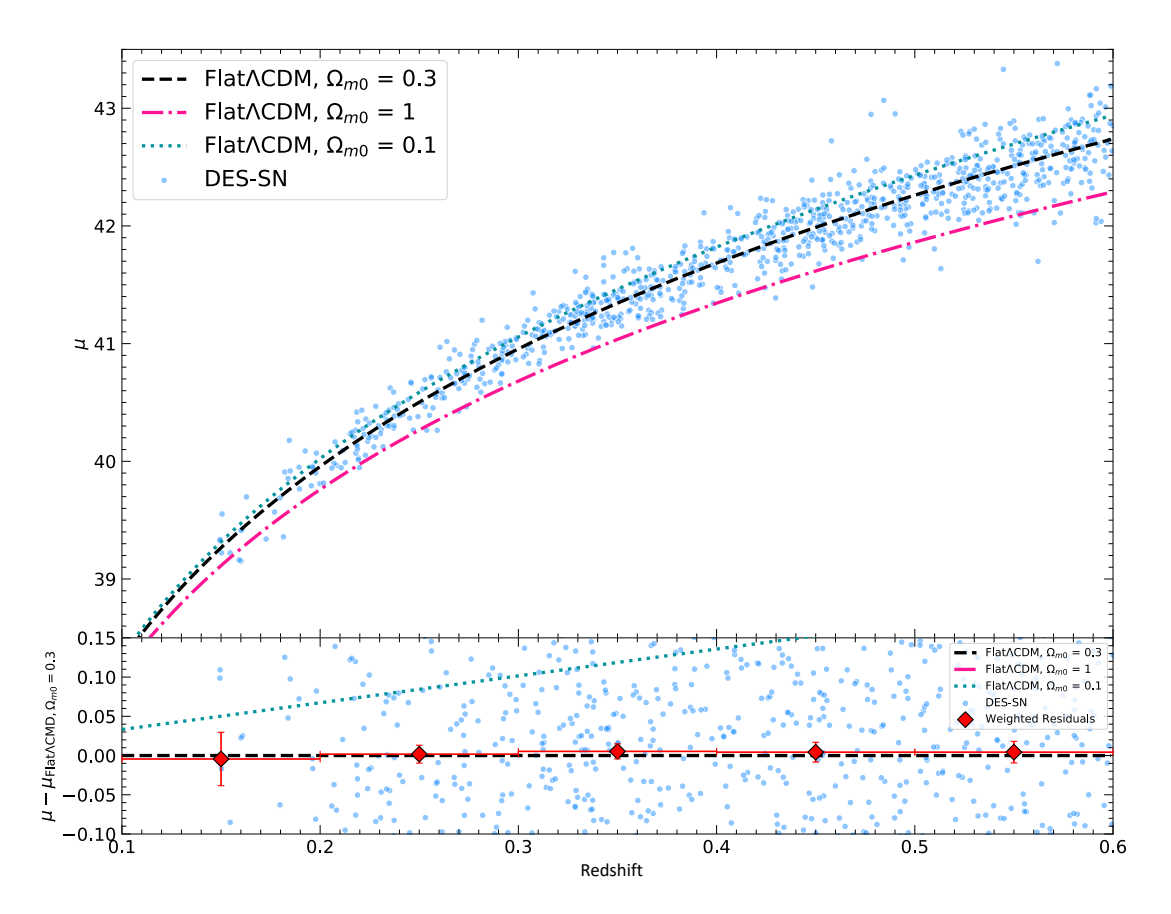


FIGURE 2.4: Upper Panel: Corrected distances to the DES 5 year photometric sample, along with an assumed Flat Λ CDM cosmology with parameters of $H_0 = 70 \text{km/s/mpc}$ and $\Omega_M = 0.3, 0.1$ and 1.0. Lower Panel: The difference between the corrected distances and the assumed cosmology, along with the weighted average in equally spaced redshift bins of 0.1.

DES based clusters were identified within the first annual reduction of the SV data (SVA1; Rykoff et al. 2016) using the red-sequence Matched-filter Probabilistic Percolation (redMaPPer, RM) cluster finding algorithm (Rykoff et al., 2014).

redMaPPer is a photometric red-sequence cluster finder, designed specifically for large scale surveys such as DES (Rykoff et al., 2014). First, a training sample of clusters is constructed from red spectroscopic galaxies. These are used to look for similar colour galaxies, and for over-densities of these types of galaxies. These over-densities are then used as training clusters themselves, giving a sample of probable cluster members that are consistent with the red sequence.

For each possible cluster from this initial finding, the cluster candidates are sorted by richness (the sum of the membership probabilities over all galaxies within a given radius of the likely cluster centre, λ) and centring likelihood (likelihood a given galaxy is the central cluster galaxy). The sorted list is then filtered to assign cluster members correctly and to not double-count potential clusters. For each cluster, it starts by recomputing the richness and photometric redshift of the cluster based on the filtered catalogue (in the first run this will simply be the input catalogue). It then determines the cluster centre and the probability of this

centre, and again re-calculates richness and photometric redshift based on this new central galaxy.

Galaxies are then removed from the list of possible central galaxies if they have a probability of membership to that cluster of less than 50 per cent. These galaxies are however, still allowed to be members to other lower ranked clusters.

This process is repeated for the next cluster galaxy from the sample, until completion. After this process, RM will have filtered all possible cluster galaxies, and assigned them to a potential cluster candidate (should they be associated with an actual over-density), along with the central galaxies.

For each cluster candidate, RM provides a richness estimate λ , and a scaling factor S that accounts for survey incompleteness. These parameters are calculated such that each cluster with richness λ has λ/S galaxies brighter than the limiting magnitude of the survey within the geometric survey mask.

This red-sequence technique is built around richness estimators that have been optimised in Rozo et al. (2009); Rykoff et al. (2012). RM handles broad ranges of redshift well, and is ideal for use on DES data (Rykoff et al., 2016).

For work contained in this thesis involving clusters, we selected all clusters with $\lambda/S \geq 5$ from the SVA1 Gold 1.0.2 catalogue. While this catalogue is less reliable for analysis than other RM catalogues with more stringent richness cuts, it gives us a higher space density of clusters. Using the more stringent catalogues could cause us to attribute SNe that occurred within less rich clusters as field SNe. The $\lambda \geq 5S$ catalogue contains roughly 1000 clusters within the DES-SN fields and spans a redshift range of $0.1 \leq z \leq 0.95$.

2.2 Methods

In this section I outline the various methods employed either by myself or others within the DES collaboration to calculate the various data used.

2.2.1 Host Galaxy Matching

SN hosts in DES were matched to their galaxy via the directional light radius (DLR) method, first proposed by Sullivan et al. (2006). This method not only takes into account the angular separation of a SN from a potential host, but also the radius of each potential host in the direction of the SN.

To calculate the value of DLR for galaxies in our sample, we run Source Extractor (Bertin & Arnouts, 1996; Bertin, 2011, SEXTRACTOR) on the deep galaxy images described in Wiseman

2.2. *Methods* 29

et al. (2020). Galaxies are typically well modelled by an ellipse, and for each source we use the SEXTRACTOR OUTPUTS A_IMAGE, B_IMAGE and THETA_IMAGE, being the semi-major axis (a), semi-minor axis (b) and positional angle (relative to the positive right ascension, R.A. axis, ϕ) of the source. We transform both A_IMAGE and B_IMAGE out of pixel units into arcsecs, by measuring how many arcsecs per pixel there are in the DES images.

DLR for each source is calculated as follows, (Qu et al., 2024)

$$DLR = \frac{ab}{\sqrt{(a\sin\phi)^2 + (b\sin\phi)^2}}.$$
 (2.4)

DLR allows for the normalisation of the angular separation between a given transient and its host across all types, sizes and inclinations of galaxies. The scale of the semi-major and semi-minor axis are set by the second order moments of the galaxies profile along their respective axis. With the galaxies profile accounted for, roughly 68 per cent of the galaxies light is contained within a $d_{\rm DLR}$ of 1, and a $d_{\rm DLR}$ of 3 is roughly the galaxy's isophotal limit.

The normalised separation of SN to host d_{DLR} , is then calculated as follows:

$$d_{DLR} = \frac{\Delta \theta}{DLR},\tag{2.5}$$

where $\Delta\theta$ is the angular separation, in degrees, of the SNe and a potential host, and DLR is the directional light radius for that given galaxy, also in degrees. As such d_{DLR} is unit-less.

The galaxy with the lowest value of $d_{\rm DLR}$ is then selected to be the transient host. As mentioned above, the matching of transient to host for all 30,000 DES transient candidates was performed in Wiseman et al. (2020).

2.2.2 Calculating host galaxy properties

Once a SN is matched to a given host, we calculate various host properties. As the spectra for each galaxy were primarily taken to obtain an estimate of the host galaxy redshift, these are relatively low signal-to-noise. As such, we rely on the photometry of host galaxies obtained via the deep galaxy images, described above, to estimate the properties of each SN host.

As we only have the *griz* bands, we follow the method of Sullivan et al. (2006) and Smith et al. (2020b). *griz* data, while useful for SN science due to much of the emitted light being within these bands, does not typically encompass the light emitted by star formation (Kennicutt, 1998) or dust (Nersesian et al., 2021). These studies used the PÉGASE.2 (Fioc & Rocca-Volmerange, 1997; Le Borgne & Rocca-Volmerange, 2002) spectral synthesis code in order to generate synthetic galaxy spectral energy distributions (SEDs). For a given initial scenario, and various time based parameters such as the in-falling of gas, PÉGASE.2 will provided SEDs over the

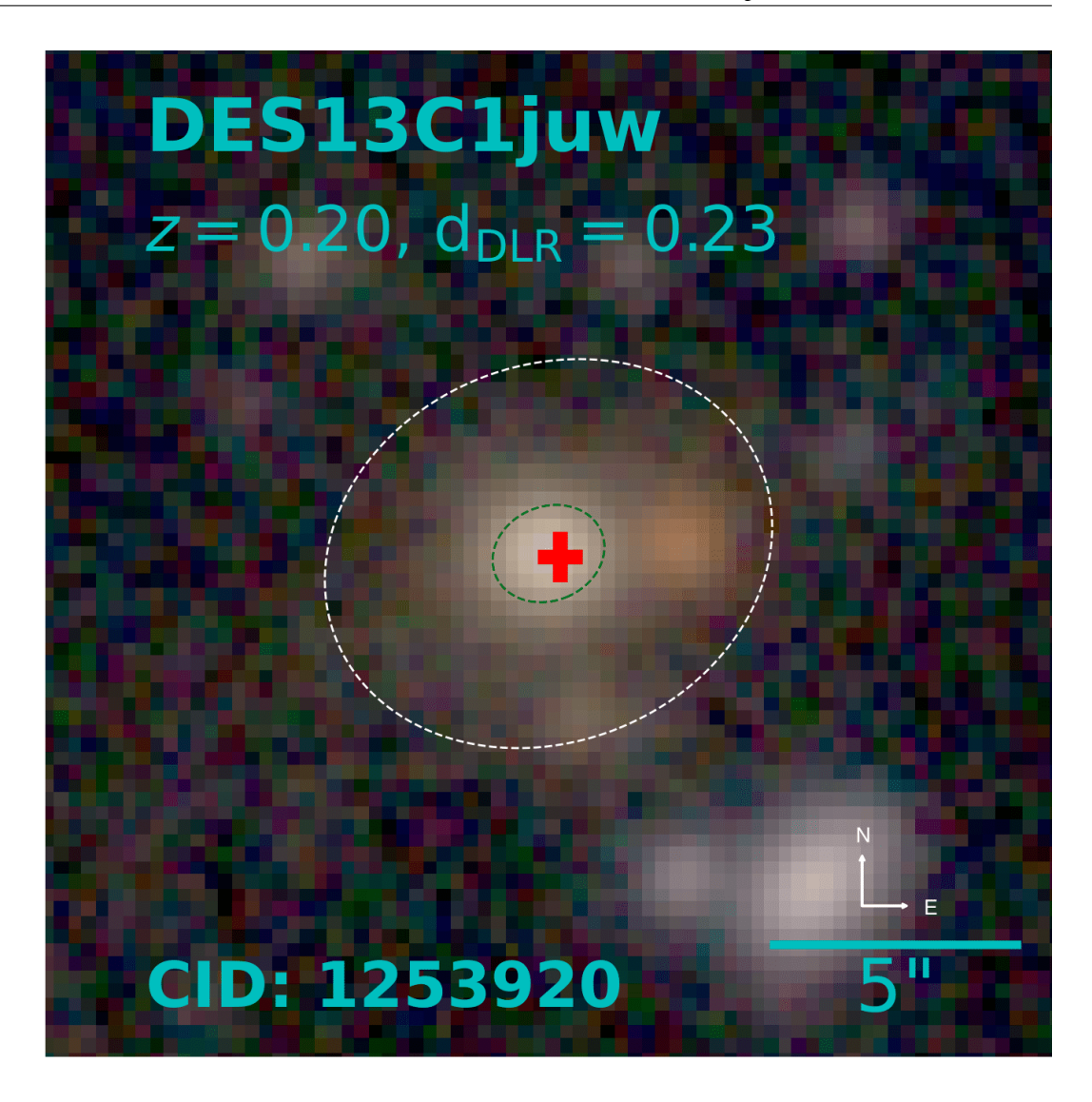


FIGURE 2.5: A stamp of DES13C1juw. Shown are the location of the SN (red cross) along with a $d_{\rm DLR}$ of 1.0 (green ellipse) and 4.0 (white ellipse). Note that as $d_{\rm DLR}$ is directional it is ellipsoidal, and takes the shape of the host galaxy.

total evolution of the galaxy, along with various other parameters, such as the stellar mass (M_*) and star formation rate (SFR). We generate DES griz photometry for each generated SED, and fit that to the obtained photometry from the deep galaxy images in order to determine the best fitting SED. Thus, for each host we obtain a best fitting stellar mass and star formation rate. This SED fitting will also allow us to determine the total formed mass of each galaxy over its lifetime.

We additionally force the best-fitting template SED to exactly match the observed galaxy *griz* photometry using a wavelength dependent multiplication function. This allows accurate estimation of the galaxy rest-frame *UBVR* magnitudes, a process referred to as 'mangling' (e.g., Kelsey et al., 2021). For host NIR data, we make use of VISTA images in the *J*, *H*, *K* bands from the VIDEO survey that have been combined with DES for a subset of the DES-SN survey area (Fields C3, X3 and E2, Hartley et al., 2022).

2.2. *Methods* 31

To calculate local properties around a SN's location we employ similar methods. We first place a 4 kpc radius circular aperture about the SNe within the deep galaxy images. Such an aperture, translated to angular size, remains larger than the smallest useful aperture (0.55 arcsec) out to a distance of z=0.6. 0.55 arcsec is approximately the smallest possible standard deviation on the point spread function (PSF, FWHM = $2\sqrt{2\ln(2)}*\sigma$) of the DECam in the best possible sky conditions (Kelsey et al., 2021). Aperture photometry was then performed within the PHOTOUTILS Python Module, using the APERTURE_PHOTOMETERY function. We then perform SED fitting as above using this local photometry to obtain local stellar masses and star formation rates. As a galaxy's apparent size decreases with redshift, the smallest useful aperture increases. As such, the smallest useful aperture past $z \sim 0.6$ increases to \sim 5 kpc. Such an increase in required aperture radius with redshift encompasses more and more of the host galaxy, 'blurring' the local data with non-local light. As such we do not calculate local properties for SNe further than $z \sim 0.6$.

2.2.3 Bias Corrections

While the previously described light curve standardisation performs well to obtain distances to SNe, there are still inherent biases that affect individual or groups of SNe. Such biases include the 'Malmsquist bias' (Malmquist, 1922, 1925), where dimmer SNe may be missed at higher redshifts in magnitude limited surveys such as DES. Additionally, I previously mentioned that the post-standardisation brightness of a given SN depends on various host properties, such as total stellar mass, with more massive hosts containing brighter SNe (even after the stretch and colour standardisation from 2.3, see Kelly et al., 2010; Sullivan et al., 2010; Lampeitl et al., 2010). To account for this so called 'host mass step', and bias dependencies, and to better standardise a set of SNe, additional terms are added to the standardisation equation, becoming

$$\mu_{\text{obs},i} = m_{x,i} + \alpha x_{1,i} - \beta c_{i,\text{SN}} - \gamma G_{\text{host},i} - M - \Delta \mu_{\text{bias},i}$$
 (2.6)

where x_1 , $c_{i,SN}$, m_x M, α and β are the same as in 2.3.

 γ is an additional global parameter determined from a minimisation over the sample to a given cosmology. G_{host} refers to the relation between SN Ia luminosity and their host properties. $\Delta\mu_{\text{bias}}$ accounts for selection biases in the sample.

These biases are calculated from simulating DES-SN within the SNANA framework (Kessler et al., 2009) using the BEAMS with Bias Corrections (BBC; Kessler & Scolnic, 2017) method. Explaining the inner workings of BBC is beyond the scope of this thesis, but simply, it first simulates a large range of SNe. This simulation models the SN rest frame SED, SN and host galaxy correlations, along with instrument noise, survey strategy, cadence, filters used and redshift effects. The biases then are recovered from interpolation over the parameters within

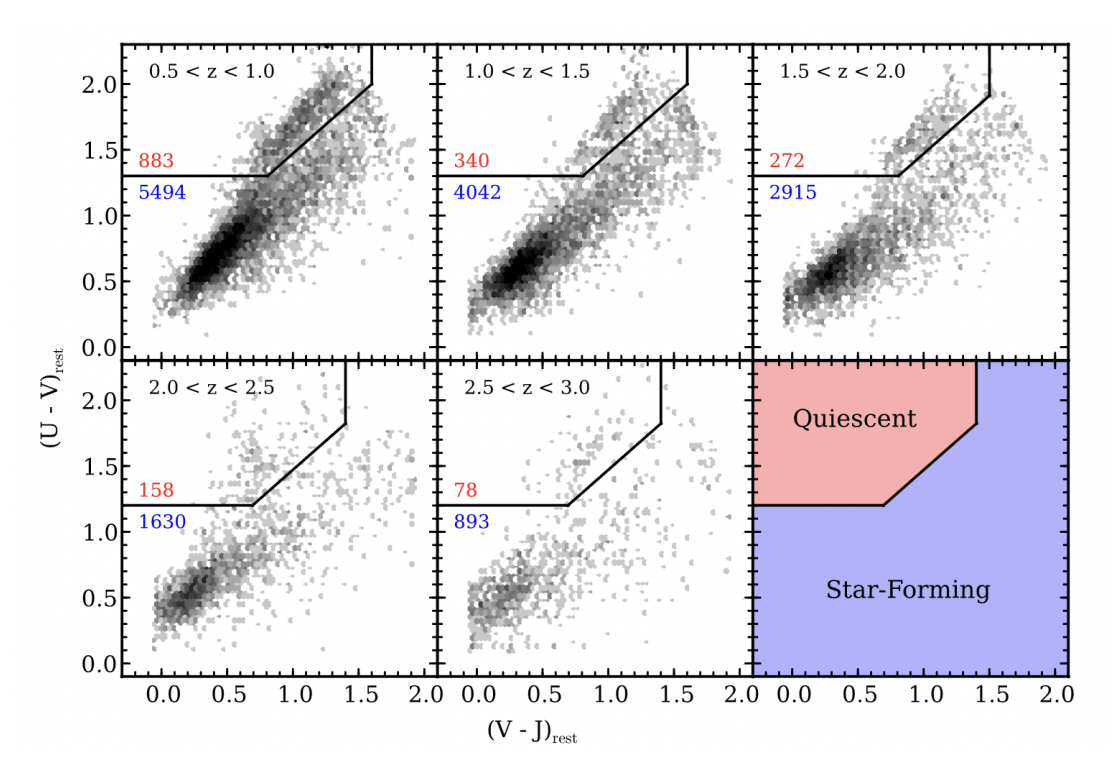


FIGURE 2.6: The UVJ diagram for the zFOURGE sample from Tomczak et al. (2014).

this simulation. This allows us to correct for the differences between observed and simulated SNe brightnesses.

Two types of bias corrections are utilised in this thesis - a '1D' bias correction, which simply accounts for the Malmsquist bias above, and a '4D' bias correction. The 4D bias correction, formalised in Popovic et al. (2021b), adds an additional 3 bias terms. This splits the solely redshift bias into a redshift bias, a stretch bias, a colour bias and a bias based on the host galaxies stellar mass. It additionally swaps the SALT2/3 model for SNe colour (a singular $c_{\rm SN}$ term) for an intrinsic colour distribution, modelled by $c_{\rm SN}$ and β and a colour reddening due to dust term from Brout & Scolnic (2021). This method attempts to better model the effect of dust on SNe.

2.2.4 Identification of Passive Galaxies

griz data, as previously mentioned, is not perfect for the identification of galaxies. As such, to select only passive galaxies within DES we elect to use the UVJ selection method, described in (Tomczak et al., 2014). This method effectively separates galaxies into star-forming or passive (Quiescent) based on their U - V and V - J colours. Figure 2.6, from Tomczak et al. (2014) shows an example of this method.

While this method requires near-infrared data, it is crucially insensitive to the extinction brought about by dust. This extinction will typically act along the same vector as the UVJ cut, preventing galaxies from crossing the boundary between star-forming and passive. UVJ bands

2.3. *Summary* 33

are calculated as in Section 2.2.2, with the addition of infrared data from the VISTA images provided by the VIDEO survey (Hartley et al., 2022).

2.3 Summary

In this chapter I have outlined the workings of the Dark Energy Survey, how the type Ia supernova and galaxy cluster data were obtained, reduced and standardised. How SN data have been matched to hosts, and their host properties calculated, should now be well understood. Furthermore I have mentioned how we further reduce the scatter on SN distances, allowing for precise cosmological parameters to be obtained.

Critically however, while these host dependencies and biases may be accounted for, they are not fully understood. Debate has settled some in recent years, but still lurks in many a cosmologist's mind - what exactly causes the mass step?

In the remaining chapters of this thesis, I aim to probe the environments of type Ia supernovae. I investigate from the overarching environments of clusters in Chapters 3 and 4 to the individual galaxy parameters in Chapter 5. I toss into the ring of cosmology another tracer of the mass step and find rates of SNe that don't quite agree with established literature.

Get yourself a coffee and strap in. I hope you enjoy the ride as much as I have.

Chapter 3

Properties of Type Ia SNe within Clusters

Let me take stock. My equilibrium is askew, my vision is partially impaired, and I'm clearly slurring my words. To put a fine point on it, your boy is turnt.

Captain Holt, Brooklyn 99: A Tale of Two Bandits

3.1 Supernova within Clusters

Galaxy clusters are some of the largest gravitationally bound structures within the known Universe. One of the most massive cluster systems, 'El Gordo', contains a mass of 2 quadrillion suns within a radius of roughly 2.0 Mpc (Kim et al., 2021). These massive structures typically contain older populations of stars, with around two-thirds of their stellar populations being formed before $z \ge 2$, compared to less than fifty percent of the stellar populations in the field being formed before this time (Guglielmo et al., 2015).

This disparity in stellar population may arise from an increase in the fraction of quenched galaxies within clusters compared to the field. Here, quenching is the shut-off or reduction of star formation, either due to non-environmental causes, such as feedback from SNe or galactic winds (Oppenheimer et al., 2010) or environmental causes, such as the removal of cold gas due to ram pressure (Gunn & Gott, 1972) or galaxy mergers (Moore et al., 1996). While all galaxies are effected by non-environmental based quenching, cluster galaxies are more susceptible to environmental quenching due to the density of galaxies within the cluster. The efficiency of this environmental quenching increases with respect to the centre of a given cluster, with those in the centre more quenched than those in the outer regions (van der Burg et al., 2018).

Interestingly, this environmental quenching doesn't appear to be dependent on galaxy mass, with even low mass cluster galaxies also turning from the 'blue star forming' phase to the 'passive red' phase of galaxy evolution sooner than field galaxies (Wilman et al., 2005).

Curiously, while the rate of type Ia per stellar mass SNe positively correlates with the star formation rate of the host they are in (Sullivan et al., 2006), the rates of supernova per stellar mass within clusters appears to be increased with respect to the field (Freundlich & Maoz, 2021). Additionally, the SN stretch parameter x_1 , which parameterises the rate of decline of a given SN's light curve, is on average lower for SNe within clusters than those in the field. However, there appears to be no difference between the colour (c_{SN}) distributions of cluster based SNe compared to field based SNe (Xavier et al., 2013). While the difference in star formation rate could drive the different x_1 distributions (Rigault et al., 2013), the apparent similarity of their colour distributions, when the environments between field and cluster are so different, is peculiar. Dust reddens SNe, and the mass of dust within a galaxy increases with star formation rate and stellar mass (Lianou et al., 2019). With this increase in dust, one might expect that massive star forming galaxies within the field to have more reddened SNe than those in clusters, especially if mergers have stripped cluster based galaxies of their dust content. With these colour distributions being the same, the likelihood that the dust content is different is low.

With these differences in both galaxy composition and hosted SNe in mind, we investigated first the light curve properties within clusters, and their dependence on any host properties. We compare these to the field, and try to find the causes of some of these differences. To do this, we use the DES-SN5YR type Ia SN sample, and the redMaPPer (RM) SVA1 Gold 1.0.2 catalogue cluster catalogue. First however, cluster based SNe must be identified.

3.1.1 Finding Supernovae Within Clusters

To identify if a SN event occurred within a cluster, we followed the procedure outlined in Xavier et al. (2013). Firstly, we checked if any given SN was projected onto a cluster in the RM catalogue. For a given SN s to be projected onto a cluster k it must obey

$$\cos \delta_s \cos \delta_k \cos(\alpha_s - \alpha_k) + \sin \delta_s \sin \delta_k \ge \cos \left(\theta_{\max}^{(k)}\right),\tag{3.1}$$

where

$$\theta_{\text{max}}^{(k)} = \frac{1.5 \text{ Mpc } (1 + z_k)}{c \int_0^{z_k} \frac{dz}{H(z)}}$$
(3.2)

is the angular radius of cluster k, which we limit to a maximum value of 1.5 Mpc, c is the speed of light, $\alpha_{s(k)}$ and $\delta_{s(k)}$ are the right ascensions and declinations of the SN and cluster respectively, z_k is the cluster redshift and H(z) is the Hubble parameter.

We limited the maximum angular radius of a given cluster to be 1.5 Mpc to be consistent with other cluster SN rates in the literature (Mannucci et al., 2008). Additionally, a significant

over-density of galaxies are still present at these radii (Hansen et al., 2005), and such SN on the edge of our limit will still be contained within an over-dense environment compared to the field.

This matching identifies SNe that are projected onto the cluster, but this only takes into account 2D projection on the sky, not if they are at compatible distances from earth. To find if they are at the same distance, we next compared their redshifts. As galaxies within clusters are gravitationally bound, any measured redshift differences between cluster member galaxies arise from peculiar velocities and measurement uncertainties in the redshifts themselves.

As each redshift measured is never exact, with measurement uncertainties from instruments and methods, we cannot say for certain if two objects are at exactly the same distance. Thus, we find the probability, p, for the redshift difference between a projected SN (with spectroscopic redshift) and cluster (with a photometric redshift) to be consistent with the SN being within the cluster. We assume the SN and cluster have a redshift that is described by a Gaussian probability distribution centred on the measured redshift, with standard deviations (uncertainties) σ_s and σ_k respectively. The probability for compatible redshifts is then

$$p = \frac{1}{\sqrt{2\pi \left(\sigma_s^2 + \sigma_k^2\right)}} \int_{-z_d}^{z_d} e^{-\frac{\left[z - (z_s - z_k)\right]^2}{2\left(\sigma_s^2 + \sigma_k^2\right)}}.$$
 (3.3)

For the SN sample, the typical value of σ_s is $\simeq 0.0001$. These redshifts come from the SN host, and were measured spectroscopically via follow-up surveys such as OzDES (see Section 2.1.4 for further information). However, RM does not have a follow-up spectroscopic program, and instead measures its redshifts photometrically. The performance of the photometric redshifts for the clusters using RM is $\sigma_k/(1+z_k) \sim 0.01$ (Rykoff et al., 2016). As our cluster sample uses photometric redshifts, we set the maximum redshift difference, z_d , at 0.03 following Xavier et al. (2013), who found this value to maximise the statistical difference between the cluster and field samples for photometric redshifts. Additionally, they calculate their contamination of field SNe in the cluster sample for their photometric sample at 42 per cent, with a combined photometric and spectroscopic contamination of 29 per cent. Using a similar calculation, we find our contamination to be ~28 per cent, comparable to the combined contamination found in the Xavier et al. (2013) analysis, but smaller than their photometric sample's contamination by 14 per cent.

The purity of our cluster sample is the probability that any given cluster is classified correctly, i.e., the probability that any cluster identified by RM is real. We refer to these purities as q. As measurements of purity are not available for the SVA1 RM catalogue, we instead used estimates based on cluster richness from a similar cluster catalogue (Hao et al., 2010), and apply these to our sample. These purity estimates vary with richness, and are shown in Table 3.1. We then make our final selection on the data. SNe that are projected onto a given cluster, with a combined probability of matching that cluster's redshift and the cluster itself being correctly identified of above 50 per cent (pq > 0.5), are considered as cluster SNe. This value of 50 per

Richness	Purity
5-10	0.60
10-15	0.75
15+	1.00

Table 3.1: The purity of a given cluster in a richness bin, estimated using Hao et al. (2010).

cent was chosen in line with other SN analyses, that typically require the probability of a given transient being a type Ia SN (using SNN or similar classification methods, see 2.1.5) to be above 50 per cent (e.g. Wiseman et al., 2021).

While we previously discussed a significant over-density of galaxies at 1.5 Mpc, beyond this limit the density (and thus if the environment in this region is truly 'cluster') will rely heavily on the richness of a given cluster. Due to this richness-based total radius, it is unclear if SNe Ia that are located within $1.5 \,\mathrm{Mpc} \le r \le 2.5 \,\mathrm{Mpc}$ truly belong to nearby clusters they are projected onto. This effect could contaminate our field sample with possible cluster SNe, and vice versa. To reduce such uncertainty, and possible contamination of cluster SNe within the field, we remove these SNe from both our samples if they pass the pq test outlined above.

Due to the potential for misattribution of cluster SNe as field SNe when using a more stringent cluster catalogue (described in Section 2.1.8) we elect not to use the more conservative richness selection. Doing such a selection and restricting our cluster catalogue to $\lambda \geq 20S$ only identifies 15 SNe within clusters. We investigate the effects of using a more strict richness cut on our results in Appendix A.1, where we find that our results are broadly unchanged (barring a reduction in sample size) when using a richness cut of $\lambda \geq 15S$.

Fig. 3.1 shows the redshift distribution of our two samples, together with the stellar masses of the identified SN Ia host galaxies. We find a lack of SN Ia hosts in both field and clusters around and below $\log(M/M_{\odot}) = 10$ at $z \ge 0.7$. This lack of lower mass host galaxies is likely a selection effect (the lower mass galaxies are fainter and therefore harder to measure a spectroscopic redshift for) and we thus make a selection in redshift of z < 0.7 for both samples. This leaves 66 SNe Ia located within clusters, and 1024 SNe Ia located in the field. Table 3.2 shows how many SNe are removed at each stage of our selection.

Previous studies (e.g., Xavier et al., 2013) have found that SNe within clusters have differing light curve properties than those located within the field. As the light curve properties of SNe correlate with the properties of their host galaxy (Hamuy et al., 1995; Sullivan et al., 2006), this effect may be due to differing host make-ups within cluster and the field. We show our U - R vs stellar mass distribution in Fig. 3.2. It is evident that cluster and field SNe inhabit different galaxy populations, which is not suprising given the differences in age and quenching (e.g., Wilman et al., 2005; Guglielmo et al., 2015; van der Burg et al., 2018)

In order to fairly compare the samples like-for-like, we select a sub-sample (which we call the 'cluster comparison sample') of cluster and field SNe Ia with similar host properties, and investigate any host dependencies. We select SNe with a host galaxy rest-frame U - R colour of

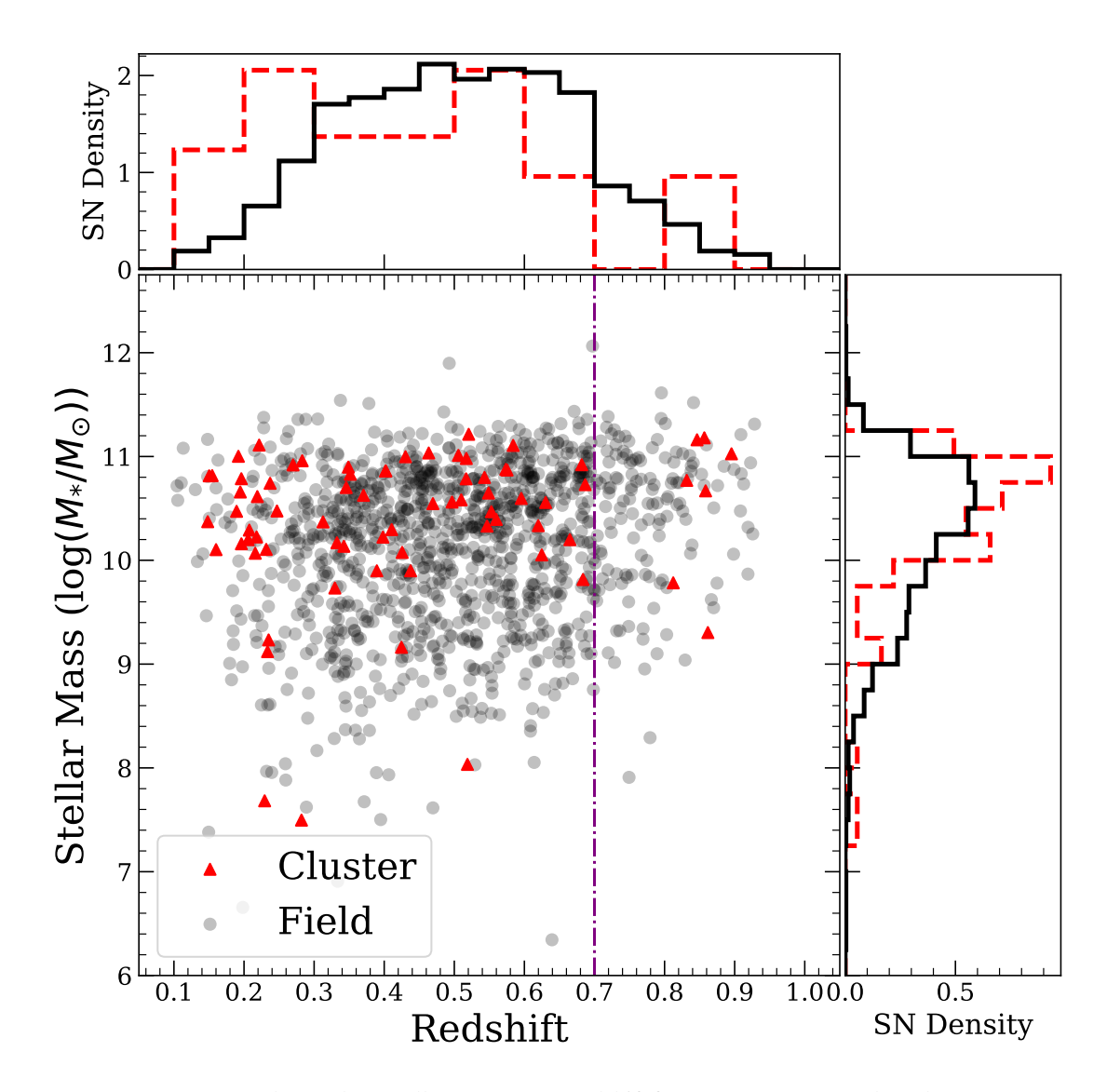


FIGURE 3.1: SN Ia host galaxy stellar mass versus redshift for our two SN Ia samples (cluster SNe as red triangles, and field SNe as grey circles). Average uncertainties on the host masses are $<\sim 0.04$ dex. We note a lack of SNe Ia in field and cluster galaxies at z>0.7 and $\log{(M/M_{\odot})}<10$. As such we make a redshift selection of z<0.7, shown by the dashed line.

> 1 and a host stellar mass $\log(M_*/M_\odot)$ > 10. This is intended to select SNe in older, massive, and passive hosts. Such a selection reduces our sample sizes to 48 (27 per cent removed) SNe Ia located within clusters and 516 (49 per cent removed) SNe Ia located in the field.

3.1.2 SN Ia properties in field and cluster galaxies

Having defined our cluster and field SN Ia samples, we next compare their light curve properties, $c_{\rm SN}$ and x_1 , as well as properties of their host galaxy. SALT3 x_1 is a measure of how quickly a SN's light curve evolves, with faster evolving events having lower values of x_1 . The SALT3 $c_{\rm SN}$ of a SN is how red or blue the event is and encapsulates both intrinsic SN colour

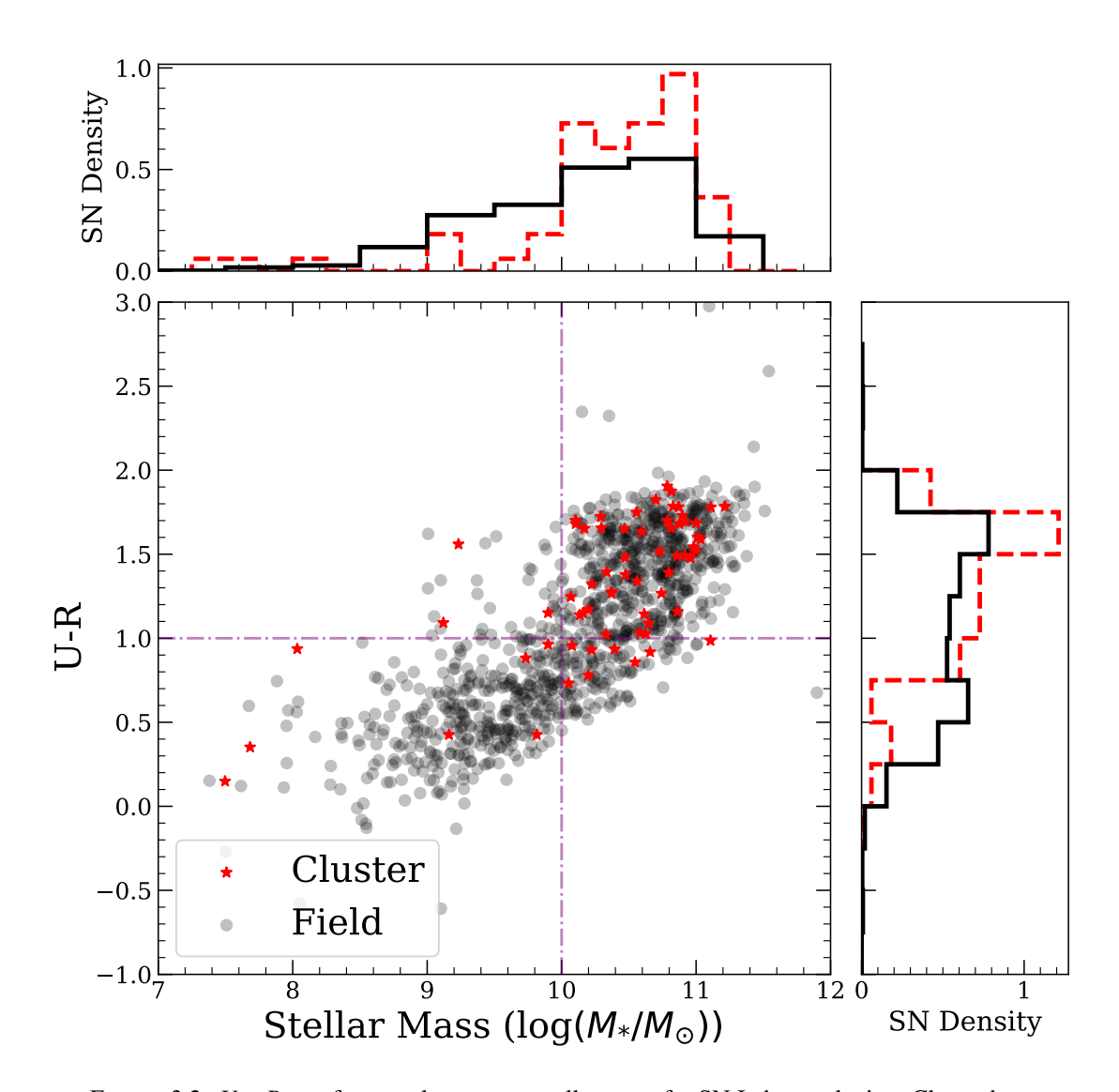


Figure 3.2: U-R rest-frame colour versus stellar mass for SN Ia host galaxies. Cluster host galaxies are redder and more massive on average than those in the field. The horizontal and vertical lines indicate our selection of red, massive galaxies, with masses $\log{(M/M_{\odot})} > 10$ and U-R > 1.

Table 3.2: The number of SNe that are removed from our sample at each stage of selection.

Selection	Number remaining	Number removed
SNe pre-light curve cuts	2802	
(see Möller et al., 2022)	2002	
SALT3 & P(Ia) selection	1306	1496
Redshift selection $(0.1 \le z \le 0.7)$	1154	152
'Exclusion zone' cut a	1090	64
Cluster SNe	66	
Field SNe	1024	
'Cluster comparison' selection		
Cluster SNe	48	18
Field SNe	516	508

^a SNe within $1.5-2.5\,\mathrm{Mpc}$ of a given cluster that also match the pq limits described in Section 3.1.1 are excluded from the sample.

and reddening by host galaxy dust. SN c_{SN} and x_1 are empirically related to luminosity, via the linear 'bluer-brighter' relationship and the 'faster-fainter relation'.

3.1.2.1 SN Ia light-curve width

The x_1 distributions for the full sample of cluster and field SNe, together with the cumulative distributions, are shown in Fig. 3.3. The cluster distributions are shifted slightly to more negative x_1 values when compared to the field. A two-sided Kolmogorov–Smirnov (K-S) test returns a p-value of 0.023, indicating that the two distributions are not drawn from the same parent distribution with a 97.7 per cent confidence level. A two-sided Anderson-Darling (A-D) test returns a value of 0.0039, implying a confidence level of 99.61 per cent.

This is a tentative confirmation of what we might expect to observe: cluster galaxies are typically more massive and passive than those in the field, and these galaxies typically host fainter, faster SNe Ia than galaxies with stronger star formation (Hamuy et al., 1995).

Previous results have found more significant differences in the x_1 parameter between cluster and field samples (Xavier et al., 2013). Their result however uses different light curve quality cuts. Furthermore they only consider rich galaxy clusters, while we make no such distinction.

The same analysis performed on our cluster comparison sub-sample of cluster and field SNe Ia in older, massive and passive galaxies is shown in Fig. 3.4. The x_1 distribution is still shifted to the more negative values, but the significance is reduced with a K-S test p-value of 0.068. We attribute the change in significance due to a smaller sample size. We confirm the effect of sample size via bootstrap resampling of our whole sample, selecting the same sample size (but not the same sample) as in our cluster comparison sub-sample. Re-calculating the p-value of the above K-S test we calculate a p-value higher than 0.068 33 per cent of the time, and above 0.023 66 per cent of the time.

3.1.2.2 SN Ia colour

The SN colour distributions and cumulative distributions are shown in Fig. 3.5. The field and cluster distributions are consistent, with a K-S test p-value of 0.801. A two sided A-D test returns a p-value of 0.274. While reduced in confidence that the distributions are drawn from the same parent distribution compared to the K-S test, this is still far below the typical 3σ confidence for a detected difference in the samples. Comparing the samples after the U-R and host mass selection gives a similar p-value of 0.827.

Thus, we see no evidence in our sample for SN colour distributions that differ between cluster environments and the field.

These results are consistent with previous analyses between field and cluster environments (e.g. Xavier et al., 2013) and between passive and star forming environments (e.g. Rigault et al.,

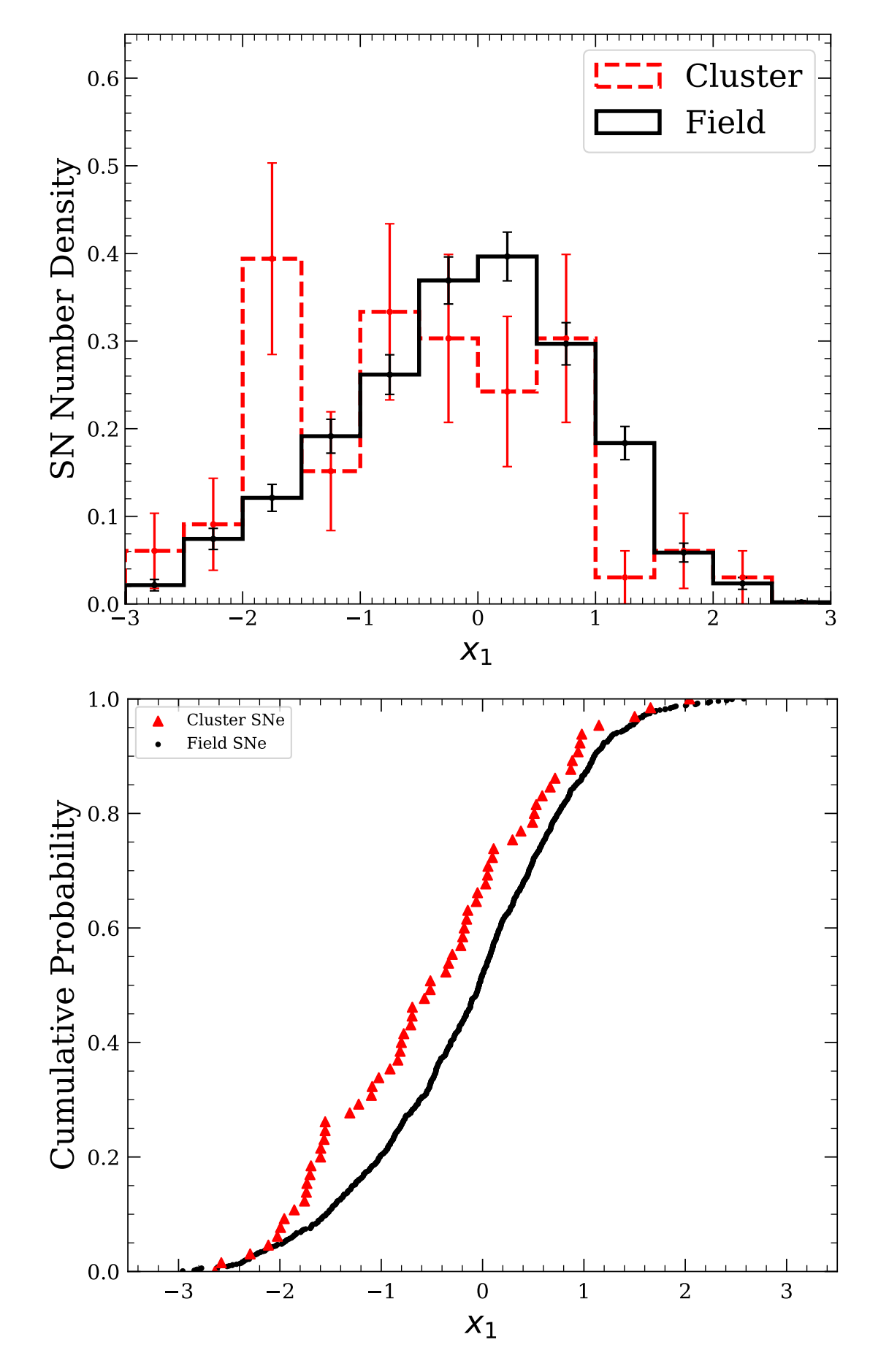


FIGURE 3.3: SN Ia x_1 distributions for events located in clusters versus those in the field. Upper: x_1 values in bins of width 0.5. Lower: CDFs of the x_1 data. A K-S test measures a 0.023 probability that the distributions are drawn from the same parent distribution.

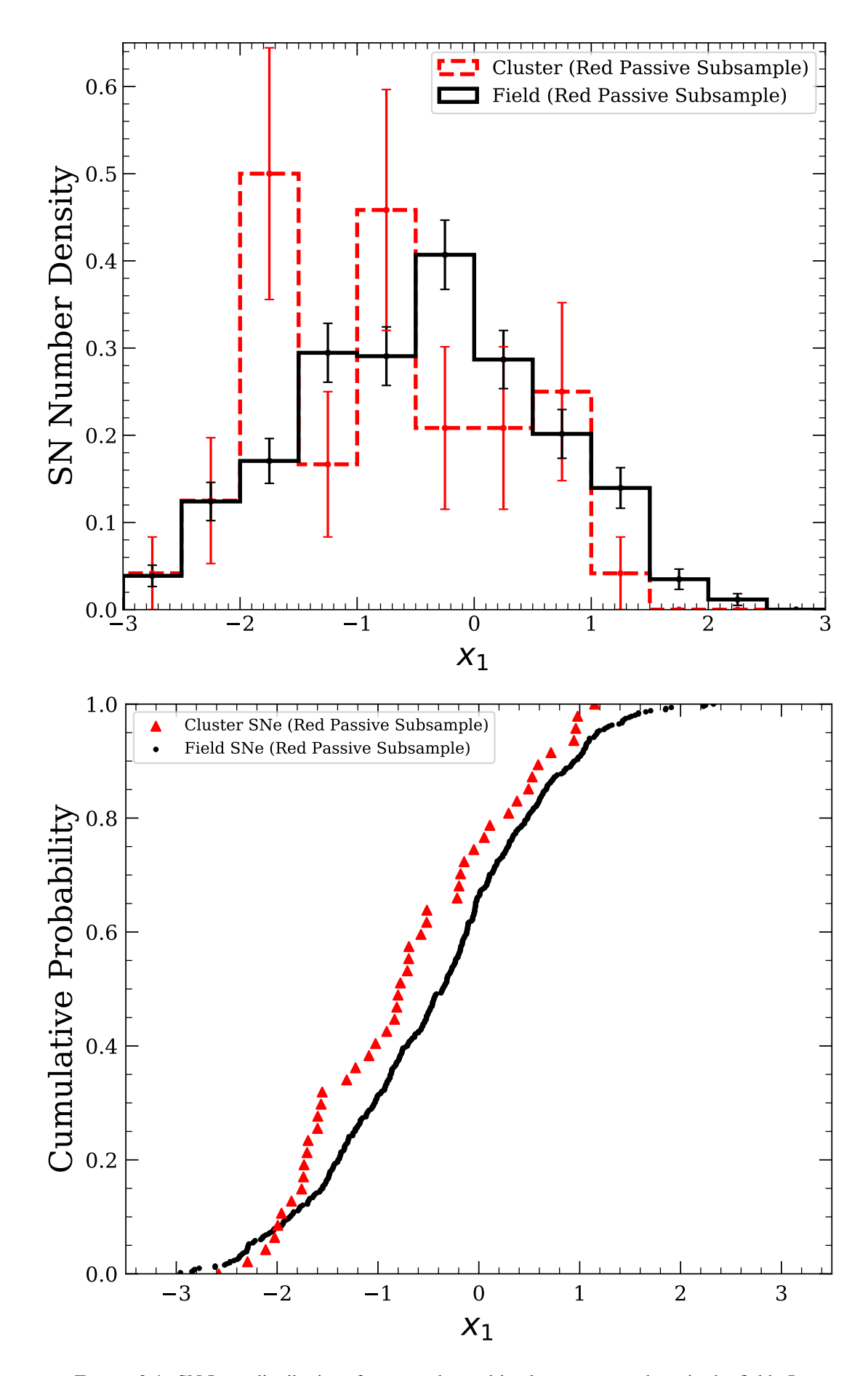


FIGURE 3.4: SN Ia x_1 distributions for events located in clusters versus those in the field. In these plots, both samples have been selected to be only red and massive host galaxies (i.e., U-R>1 and $\log(\mathrm{M_*/M_\odot})\geq 10$) as described in Section 3.1.1. A K-S test measures a 0.068 probability that the distributions are drawn from the same parent distribution.

2020). However, this result remains curious. The amount of dust, which will redden an 'unblemished' sample of SNe, increases with the amount of ongoing star formation (Orellana et al., 2017). As such, in the more passive galaxies within clusters compared to the field we may expect to see less reddened SNe than those in the passive and star forming galaxies that populate the field. However, it is possible that the reddening we see in cluster based SNe is not from host galaxy dust extinction, but instead from dust within the intracluster medium (ICM), which, can survive and be shielded from the hot, ionising gas present the centre clusters (Shchekinov et al., 2022). However, measurements of dust in the ICM are difficult and often indirect, and would require follow-up observations of the RM clusters to verify this claim.

3.1.2.3 SN Ia host galaxy stellar masses

We show the distributions and cumulative distributions of SN Ia host galaxy stellar mass M_* in Fig. 3.6. As expected from Fig. 3.1, there is a deficit of hosts with stellar masses of $\log(M_*/M_\odot) \le 10$ in clusters, with a K-S p value of 6×10^{-4} , i.e., the two distributions are drawn from different parent distributions with a significance of 3.6 σ . As expected after selecting host mass and U - R to probe similar galaxies, a two sided K-S test returns a p value of 0.715, meaning statistically the two populations are drawn from the same parent distribution, reassuring us that our host mass and colour cut successfully facilitates a fair comparison of the SNe in these galaxies.

Possible explanations for the difference in stellar mass distributions for field and cluster SN host galaxies include: a different stellar mass function of cluster and field galaxies; a different rate of SNe Ia as a function of stellar mass in cluster and field galaxies, or a combination of the two. Such SN rate differences could be caused by the difference in age and star-formation activity between cluster and field galaxies. We examine these possibilities in the next chapter.

Fig. 3.7 shows the SN Ia x_1 versus host stellar mass, where we recover the expected relationship: the average SN x_1 across both field and clusters is smaller in more massive hosts than in less massive hosts. With the exception of the low mass bins (which as we know are not present in high numbers in the cluster data) both cluster and field mean x_1 are equal at equivalent host masses.

3.1.2.4 SN Ia host specific star formation rates

While we have found that cluster-based SNe predominately prefer higher mass hosts than SNe within the field, we also identified that cluster SNe typically are not found within blue galaxies (e.g. Fig. 3.2). This is not surprising, as we have already mentioned that galaxies within galaxy clusters are typically more passive than similar mass galaxies in the field. However our U - R measurements take into account the whole galaxy and it is possible that these are heavily skewed to redder colours due to very red, passive cores.

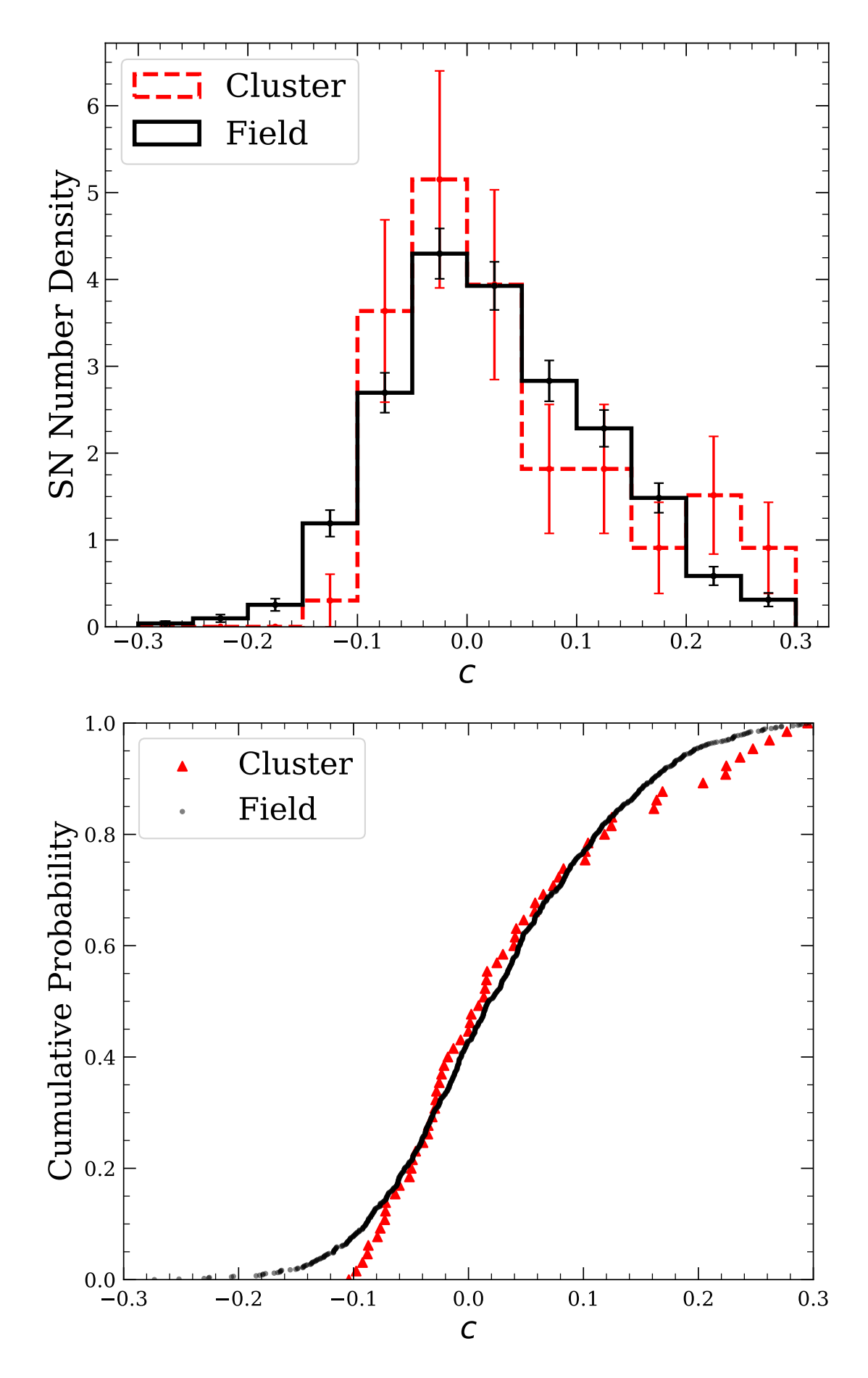


FIGURE 3.5: SN Ia colour distributions for events found in clusters and those found in the field. Upper: Histograms binned in steps of 0.05. Lower: CDFs of the colour distributions. A two sided K-S test gives a *p*-value of 0.801, indicating no statistical evidence that the CDFs are from different parent distributions.

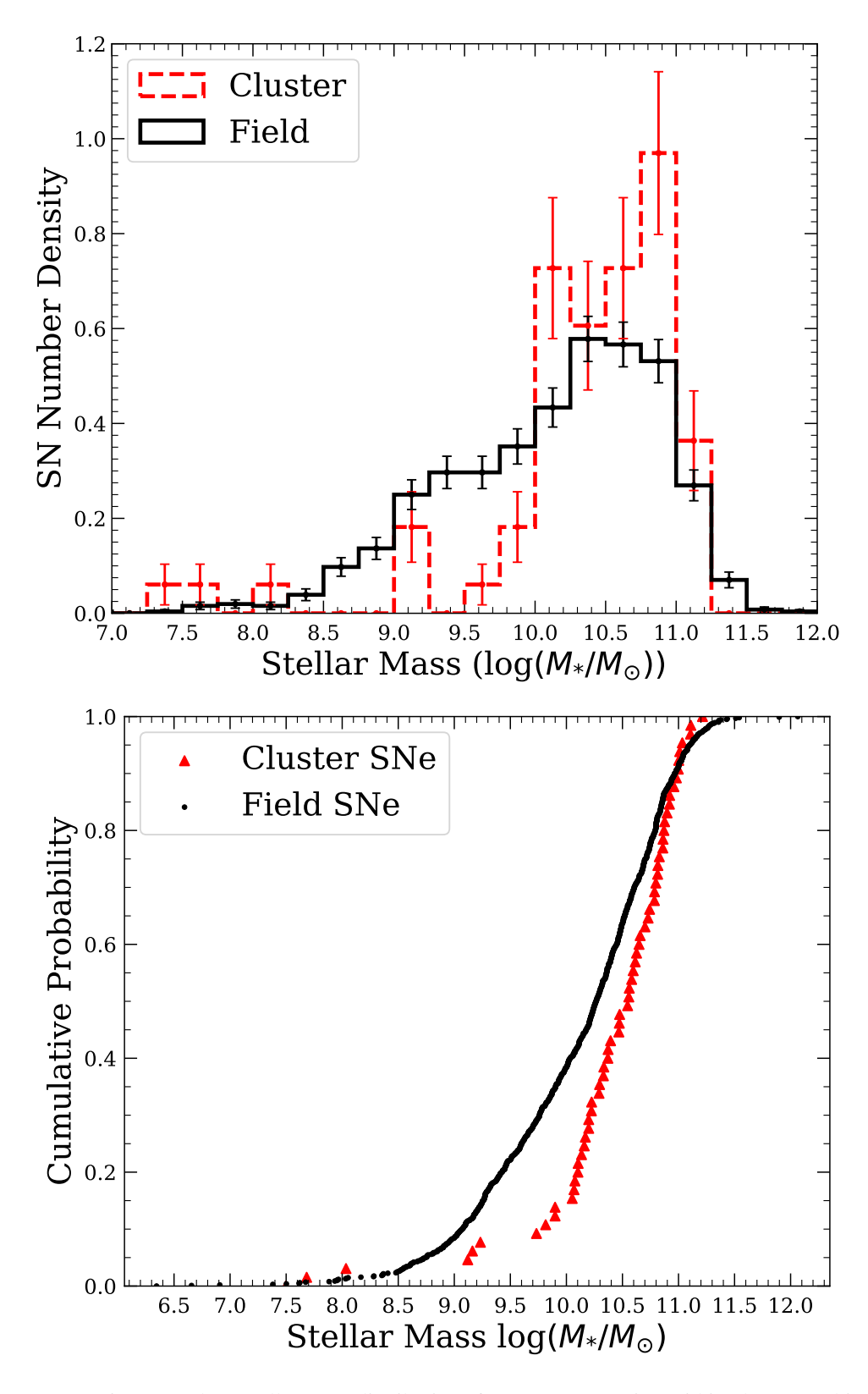


FIGURE 3.6: Host galaxy stellar mass distributions for SNe Ia occurring within clusters and in the field. Upper: Cluster and field data binned in steps 0.25. There is a lack of cluster hosts with stellar masses between $9 \le \log(M_*/M_\odot) \le 10$, skewing the distribution to the more massive end. Lower: CDFs of the host stellar masses. A two-sided K-S test performed on the CDFs returned a p-value of 0.0006, indicating strong evidence that the two distributions are drawn from different base distributions.

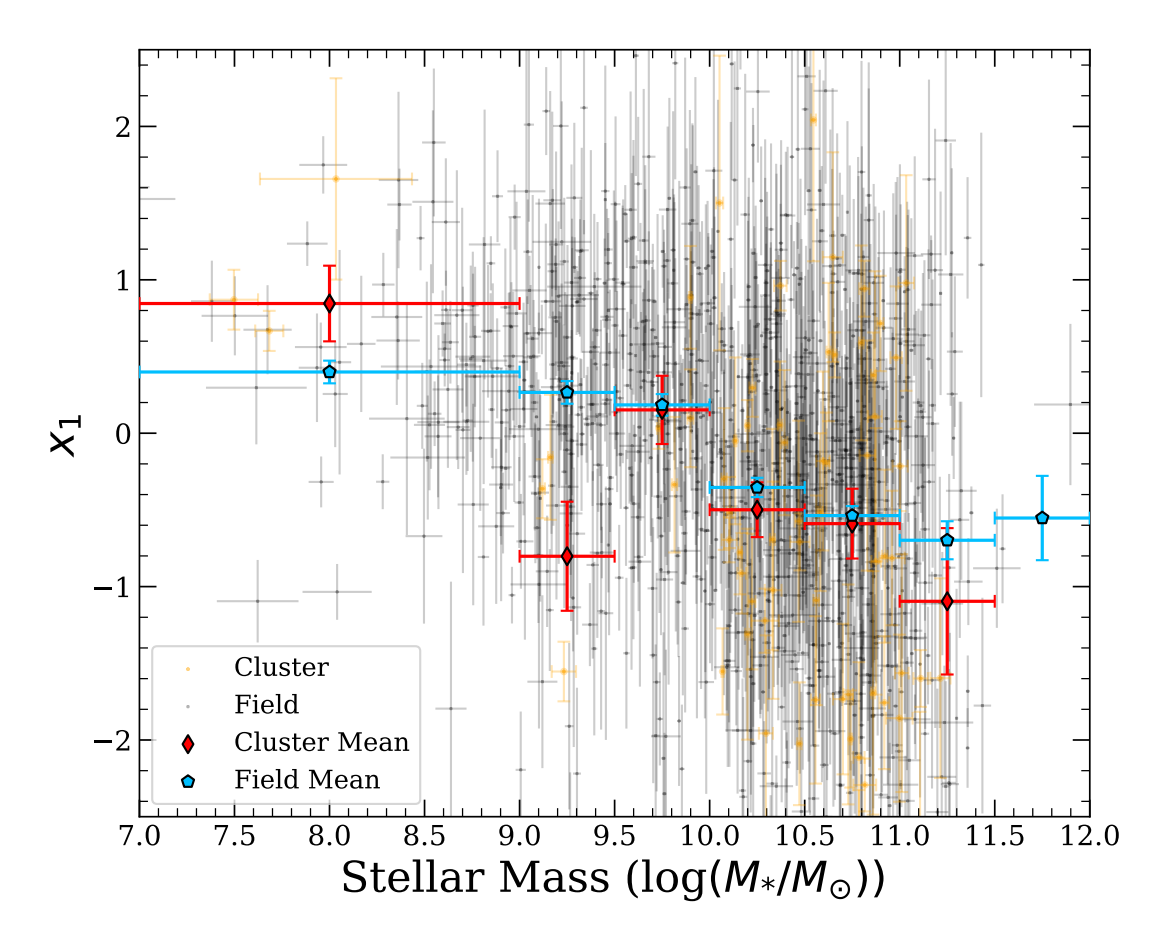


Figure 3.7: SN Ia x_1 versus host galaxy stellar mass for SNe Ia in clusters and the field, shown both as individual points (yellow stars/grey crosses) and as weighted means (red diamonds/blue pentagons). We recover the expected trend of higher mass hosts containing SNe Ia with smaller values of x_1 .

Additionally, it also has been observed that the rate of type Ia SNe positively correlate with respect to the star formation rate of the host they are in. It may be that SNe Ia in galaxy clusters are predominately found within the few hosts with ongoing star formation in their outer regions within these environments.

As such we calculate the star formation rate of each host in both the field and clusters, and normalise this rate by the stellar mass of each galaxy, to calculate the specific star formation rate of each host,

$$sSFR = \frac{SFR}{M_*}. (3.4)$$

Here, SFR is the star formation rate of the host, in solar masses per year, and M_{\ast} is the stellar mass of the host, in solar masses. This calculation provides the specific star formation rate in units of per year. This normalisation should help to offset any effect from the still growing lower mass field hosts (which are not present in clusters in great numbers), and allows us to more fairly compare the two samples.

We present the specific star formation rates of our cluster and field samples in Fig. 3.8. We can see that SNe within clusters are shifted to less vigorously star forming galaxies. This is consistent with the fact that cluster galaxies are less star forming overall than similar galaxies within the field, but against a possible cause for the previously measured increase of the rate of type Ia SNe per stellar mass in clusters. A two sided K-S test performed on the two samples returns a p-value of $0.0009~(\sim 3.5\sigma)$ giving strong evidence that the two samples do not come from the same parent distribution.

However, we know our cluster and field samples do not occupy the same distribution in host stellar masses. To investigate the effect this may have, we only use the host mass selection from Sec. 3.1.1, and only select massive galaxies. Using our full cluster comparison sub-sample would yield little difference between the two samples sSFR, as we would only select passive, massive galaxies. The resulting distributions are shown in Fig. 3.9. It is plain to see that the two samples are near identical at higher masses, with a two sided K-S test returning a p-value of 0.77. It appears that any differences between the two samples specific star formation rate is driven by low mass, star forming field galaxies.

Additionally, we previously recovered the known relation between x_1 and host stellar mass, with a decreasing average x_1 with increasing galaxy mass. As we have found that high mass hosts in both cluster and field environments have similar sSFR distributions, we additionally investigate how the light curve width of our SNe varies with sSFR. The relation is shown in Fig. 3.10, and we reconfirm previous results that hosts with higher star formation contain longer lived and brighter SNe than passive hosts. Furthermore there is little distinction between SN x_1 for SNe in cluster or field hosts with similar specific star formation rates. This, combined with the similar distributions found in Fig. 3.7 and Fig. 3.4 gives evidence that the differing x_1 distributions we find in the overall cluster and field sample is caused by a lack of low mass, star forming galaxies within the cluster environment.

3.1.2.5 The Effect of Progenitor Age

Galaxies in clusters have been found to be older than their similar-mass field counterparts (Saracco et al., 2017), with much of their stellar populations formed at z > 2 (Guglielmo et al., 2015). Furthermore, stars near the centre of galaxies, regions with lower specific star formation rate, tend to be older (Zheng et al., 2017).

For SNe Ia, Ivanov et al. (2000) and Galbany et al. (2012) find that SNe Ia in the centres of galaxies are fainter, and Howell (2001) find that older progenitors lead to fainter SNe Ia. Rigault et al. (2020) provides an updated analysis, showing that x_1 correlates with specific star formation rate measured within a projected distance of 1 kpc from each SN location (local sSFR, or LsSFR), and therefore progenitor age. Additionally, regions of high surface brightness lead to increased scatter in their fluxes, increasing the uncertainty of SN brightnesses in the bright centres of galaxies (Kessler et al., 2015).

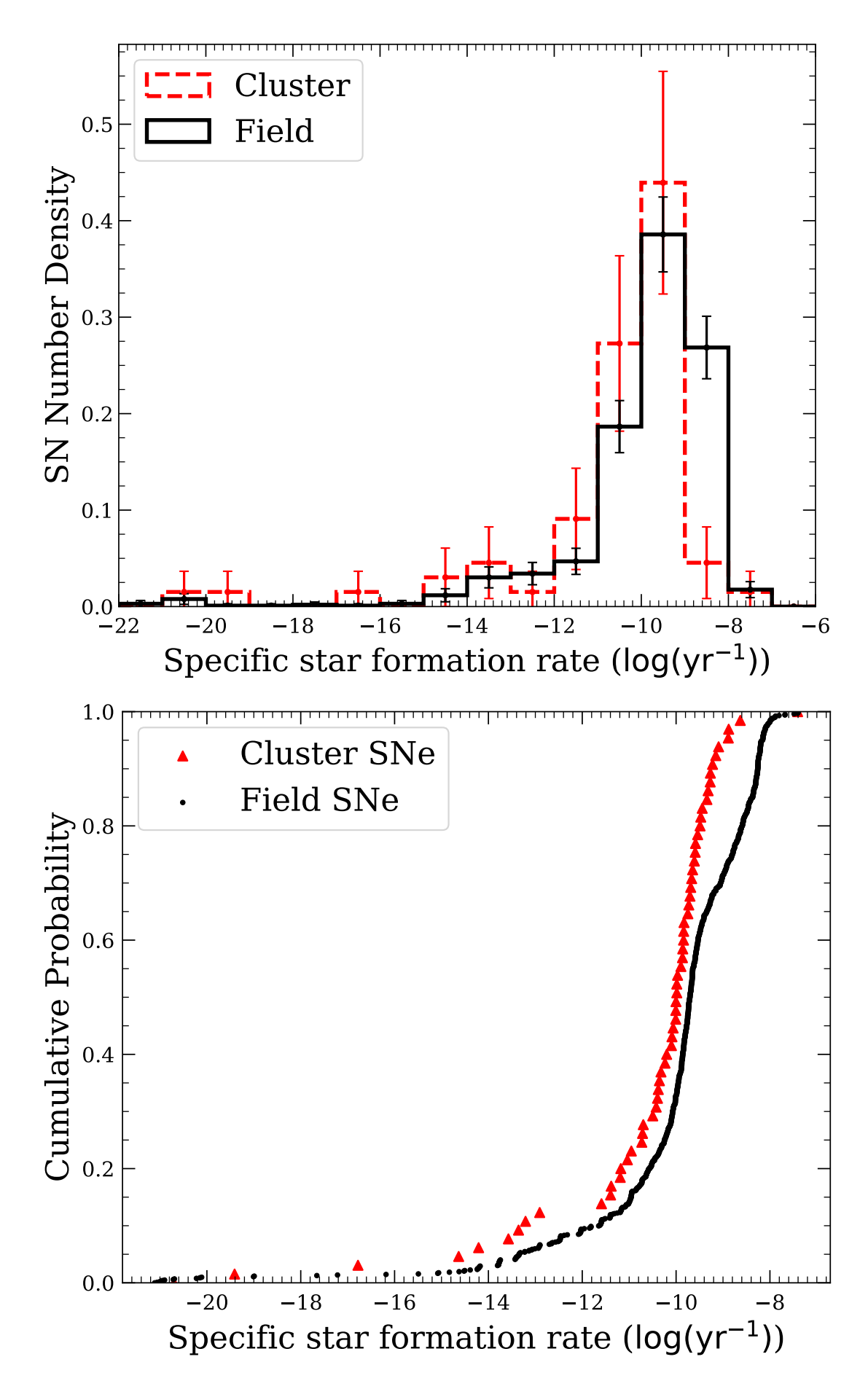


FIGURE 3.8: Upper: SN Ia host specific star formation rate distributions for those location in clusters verses those in the field. There are a higher proportion of hosts with more vigorous star formation in the field than in clusters. Lower: A CDF of the above distributions. The cluster SN hosts have a clear shift to lower specific star formation rates. A two sided K-S test returns a p-value of 0.0009, giving strong evidence for two separate populations.

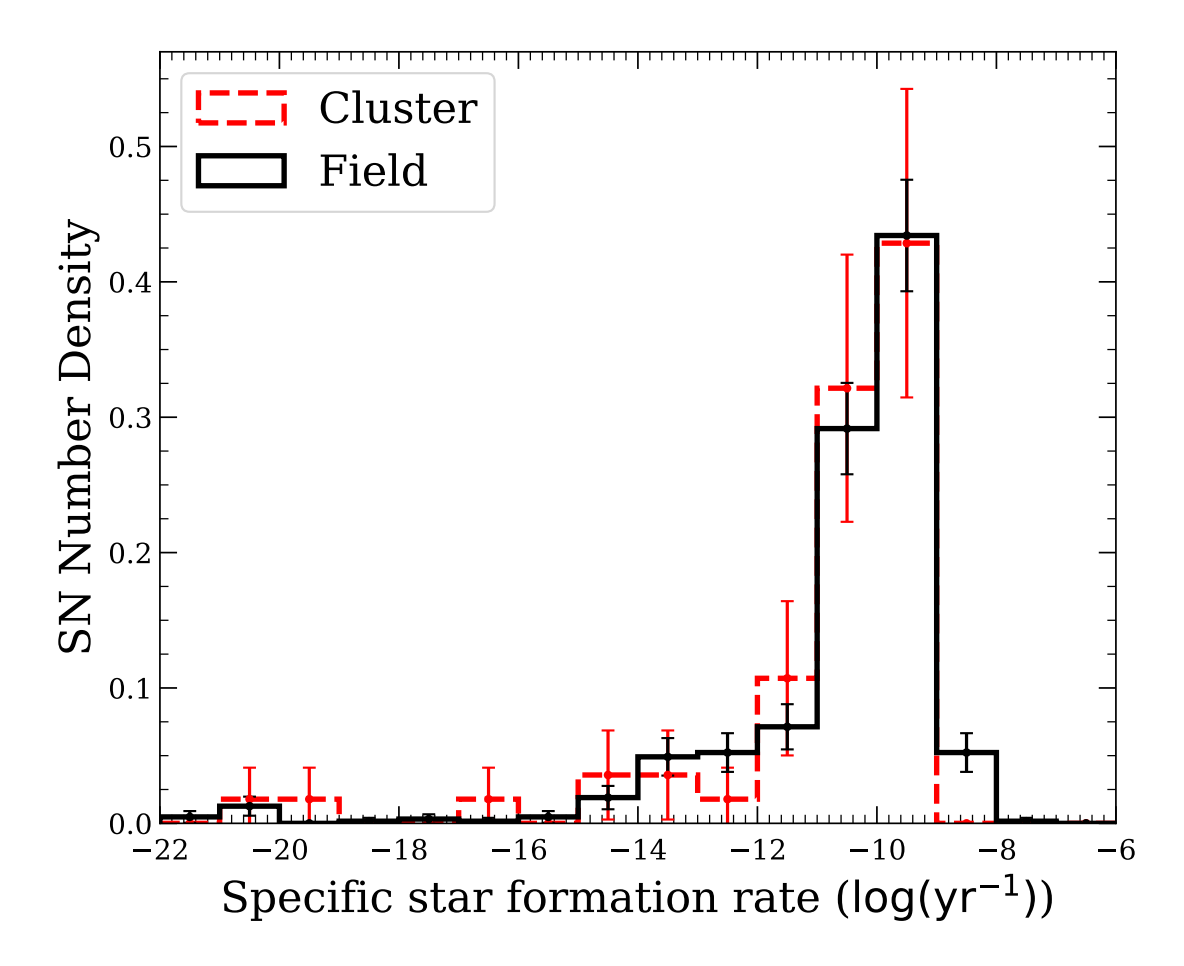


Figure 3.9: Distributions of the specific star formation rates of high mass hosts within clusters and the field. The two distributions are nearly identical, with a two-sided K-S test returning a p-value of 0.77.

In Fig. 3.11, we show x_1 versus d_{DLR} , a measurement of the effective distance of the SN from the galaxy centre (Sullivan et al., 2006). With the exception of the lowest d_{DLR} bin, in the field there is no trend between x_1 and d_{DLR} ; the weighted mean values for the cluster sample are broadly consistent (average difference between the two is $\sim 1\sigma$) with those of the field sample. We confirm this visual lack of a trend by fitting a straight line to the data, which has a gradient consistent with zero, and a Spearman correlation coefficient of -0.12, with an associated p-value of 0.68.

In the lowest $d_{\rm DLR}$ bin, there is a decrease in the error-weighted mean x_1 for SNe in both field and cluster galaxies (i.e., intrinsically fainter SNe Ia are preferentially located in these region). The SNe in this $d_{\rm DLR}$ bin are closest to the host galaxy centres, where increased surface brightness would bias *against* detecting fast, faint SNe. Similarly, increased dust extinction in these regions is unlikely to drive the absence of the intrinsically brighter / larger x_1 events. Thus, it is likely that the age gradient present in star-forming galaxies, strongest for $d_{\rm DLR} < 0.5$ (González Delgado et al., 2015; Ibarra-Medel et al., 2016), drives the effect that we see.

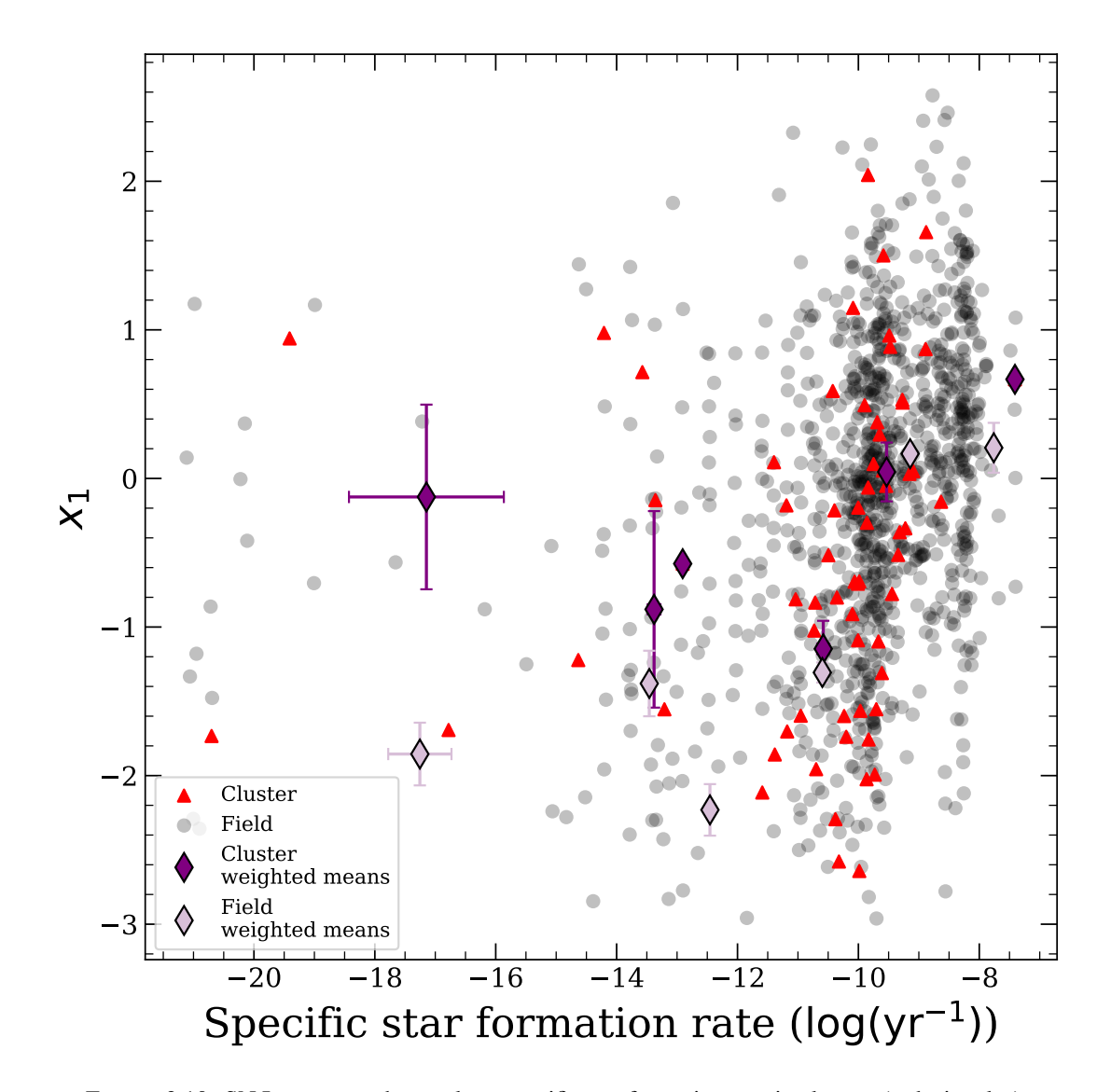


Figure 3.10: SN Ia x_1 versus host galaxy specific star formation rate in clusters (red triangles) and the field (black circles). Weighted means are shown in purple (cluster) and thistle (field). We confirm previous results that more vigorously star forming galaxies (in both the cluster and field environments) host longer lived SNe.

3.1.3 Other causes of host distribution differences

The main difference between type Ia SNe light curves and host properties within cluster environments is in their host galaxy stellar masses and specific star formation rates. These differences drives the observed x_1 distributions, as in similar galaxy makeups few differences are observed. However, clusters are inherently messy environments. With so many galaxies in a tight space, it is possible that these host property differences are not inherent to cluster based SNe, but instead due to observational difficulties. To investigate if this effect is driving the host galaxy stellar mass differences, we probe the likelihood that a given SN is assigned to the wrong host.

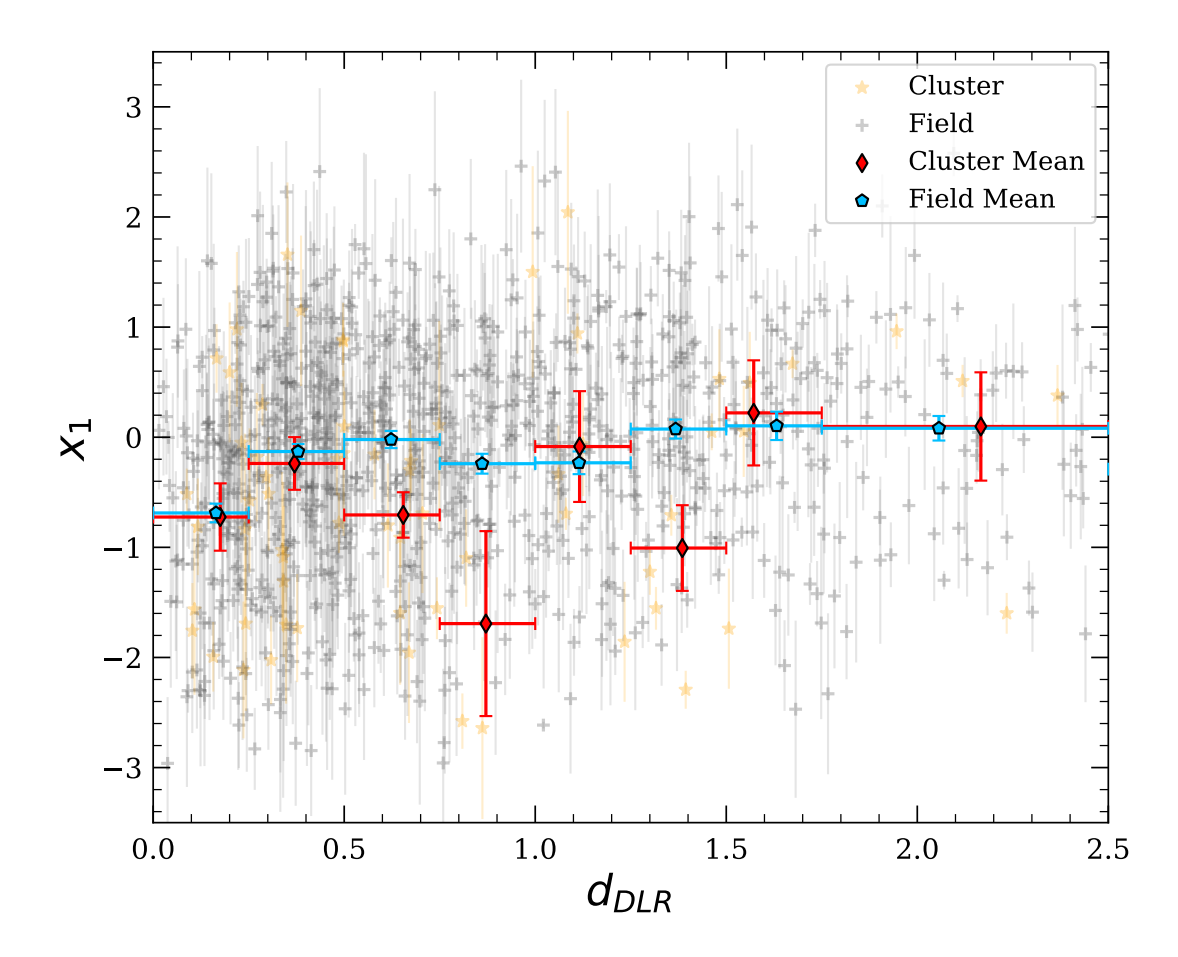


FIGURE 3.11: SN x_1 vs fractional host galaxy distance (d_{DLR}) for SNe Ia in clusters and the field, with the mean values for x_1 within d_{DLR} bins of width 0.25 plotted. Due to few SNe Ia at these distances, we use one bin between $1.75 \le d_{DLR} \le 2.5$.

3.1.3.1 Host Confusion

Our SNe are matched to hosts via the $d_{\rm DLR}$ method, which selects the galaxy with the minimum normalised angular separation between host and SN. However, the $d_{\rm DLR}$ method on occasion will select hosts that are further from the SN in angular separation than a secondary host, but larger on the sky (and thus have a larger normalisation factor). To parameterise the possibility that an assigned host is chosen simply due to a larger size on the sky, Gupta et al. (2016) defined a 'Host confusion' parameter, where larger values indicate a higher level of 'confusion' in correct host selection.

For a given SN with N galaxies with a calculated $d_{DLR} \le 4$, host confusion (HC) is defined as:

$$HC = \begin{cases} -99 \text{ if N} = 1\\ \log_{10} \left(\frac{D_1^2/D_2 + \epsilon}{D_2 - D_1 + \epsilon} \sum_{i=1}^{N-1} \sum_{j>1}^{N} \frac{D_i^2/D_j + \epsilon}{i^2(D_j - D_i + \epsilon)} \right) \text{ if N} > 1 \end{cases}$$
(3.5)

Here D_n is the galaxy that is the n'th closest (in terms of d_{DLR}). ϵ is chosen as 10^{-5} , but the HC is not sensitive to this exact value. This parameter weights higher the contribution from the two

3.2. *Summary* 53

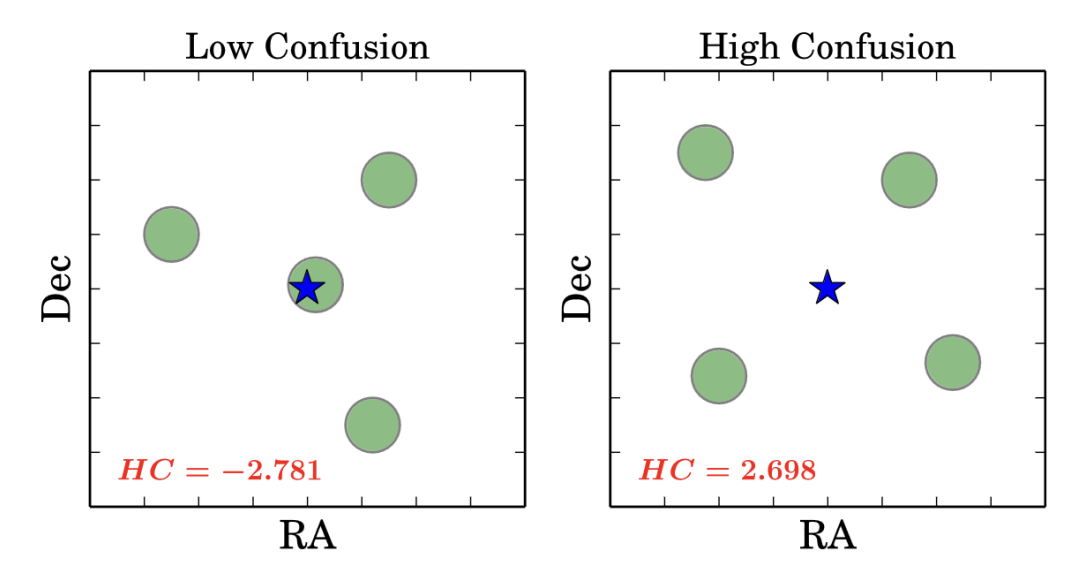


FIGURE 3.12: A cartoon showing the behaviour of the host confusion parameter. Regions of space where the SN is close to or within a specific host having a low degree of confusion, while regions with SN spread more equally between several potential hosts have a higher degree of confusion. From Gupta et al. (2016).

closest galaxies $D_{1,2}$ and down weights each successive galaxy (from the i^2 term in the summation denominator. Figure 3.12, from Gupta et al. (2016), shows the behaviour of the HC parameter, regions of space where the SN is close to or within a specific host having a low degree of confusion, while regions with SN spread more equally between several potential hosts have a higher confusion.

We present our host confusion values in Figure 3.13. As can be seen, there is no significant difference between hosts in cluster or field environments. A two sided K-S test returns a p-value of 0.94, meaning there is no significant difference between our two distributions, and that it is likely both come from the same 'parent distribution'.

We can thus conclude that even with the over-density present in cluster environments, there likely to be no more mismatching of hosts present in these environments than in the field. This allows us to say with confidence that our host stellar mass distributions for clusters, where fewer SNe are observed in lower mass hosts, is a real effect of the cluster environment, rather than an observational mismatch. This is likely due to these low-mass galaxies being quenched within clusters, and thus the rate of SNe within these low-mass galaxies is damped compared to the field.

3.2 Summary

Using the DES 5 year photometrically identified SN catalogue, we identified 66 type Ia SNe located within cluster galaxies. We analysed both their light curve properties and their host properties. Our main findings are:

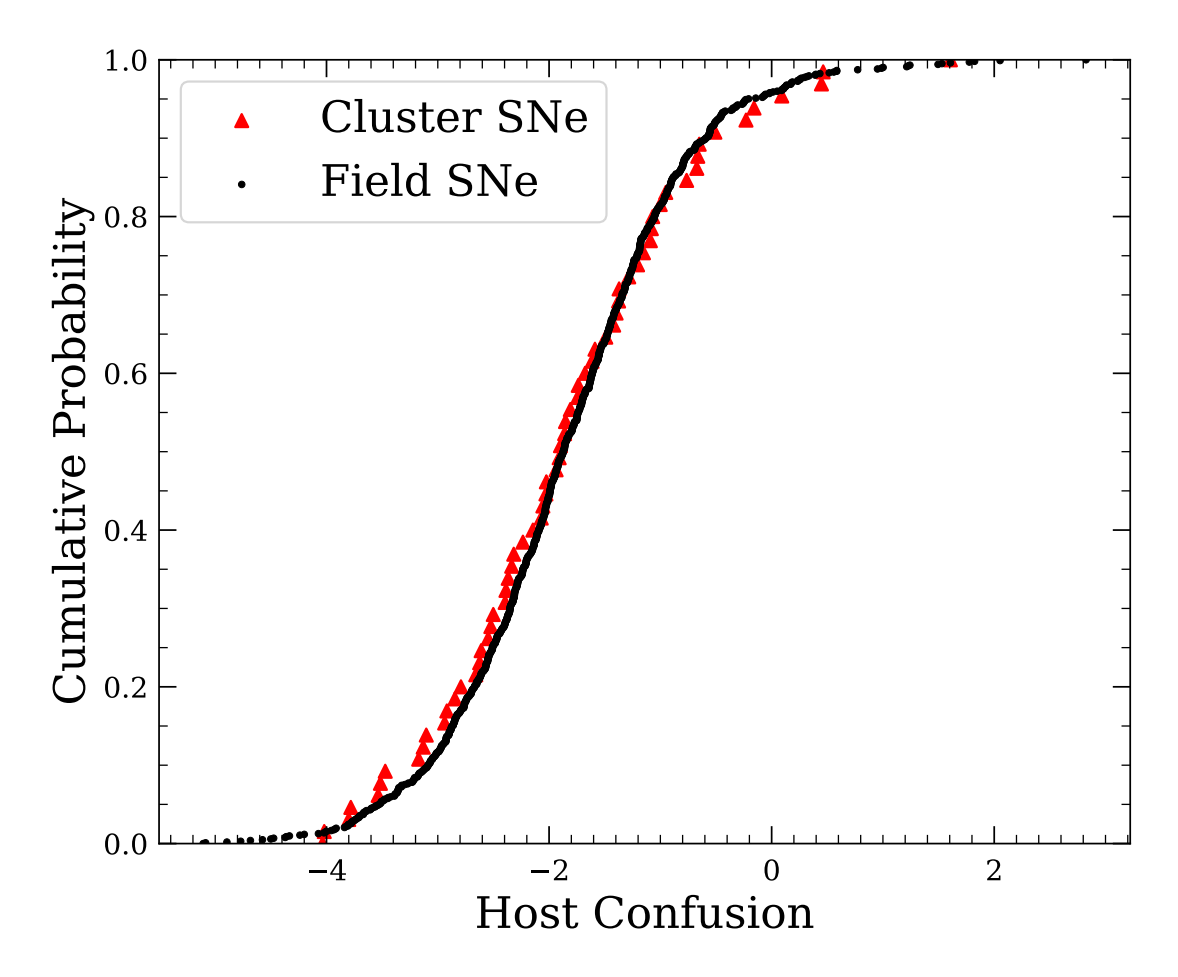


Figure 3.13: Host confusion distributions for cluster and field based hosts. There is no significant difference between the two samples, with a two sided K-S test returning a p-value of 0.94.

- We find a tentative indication that the light curve widths, x_1 , of cluster SNe Ia are, on average, more negative (i.e., fainter and faster evolving) than their field counterparts. Although this is an expected result, as x_1 has a known dependence on galaxy stellar mass and age, the evidence is not strong in this sample. When just comparing galaxies with similar host masses and colours, the significance drops further, perhaps implying that any differences we see are due to the lack of low-mass, young cluster hosts. We find that the colours of cluster SNe Ia statistically match those of the field, with very similar distributions.
- There is no clear relationship between a SN's x_1 and its location in its host. The exception is for the innermost SNe Ia, which have smaller values of x_1 for both cluster and field hosts.
- We find that for similar mass galaxies, the specific star formation rate of cluster or field hosts to be near identical. Any differences seen in these distributions can be attributed to a lack of low-mass, star forming hosts within cluster environments, which have likely been quenched due to disruptive events in the cluster environments. Additionally, the known positive correlation of the x_1 parameter and star formation rate behaves similarly

3.2. *Summary* 55

in clusters and the field. This provides further evidence that these large scale environments do not greatly affect a given SN's light curve, instead, it is the host galaxy itself that is the predominant driving factor.

Previous studies have found an increase in the SN Ia delay time distribution within galaxy clusters compared to the field Freundlich & Maoz (i.e. 2021). Motivated by this finding, we will calculate the mass-normalised rate of SNe Ia in the next chapter.

Clusters remain an interesting area to investigate SNe within. The typical galaxy make-up is more homogeneous than the field, with typically only massive passive galaxies hosting SNe. With the current focus in SN cosmology to understand how host properties introduce uncertainty in distance standardisation, they may prove a powerful tool in the era of LSST to understand and account for these effects, with using the cluster based SNe as a 'unblemished' sample.

Chapter 4

Rates of Type Ia SNe within Clusters

The number of hours we have together is actually not so large. Please linger near the door uncomfortably instead of just leaving. Please forget your scarf in my life and come back later for it.

Mikko Harvey, 'For M'.

4.1 Supernova Rates in Clusters and the Field

In Chapter 3.1.2.3 we showed that there is a differing distribution of host galaxy stellar masses between SNe Ia within clusters and those in the field. This produces an obvious question, why are cluster SNe predominately in higher mass hosts than the field?

This question does not have an obvious answer, as the rate of type Ia SNe per stellar mass declines with increasing galaxy mass (Graur & Maoz, 2013), and increases with increasing star formation rate (Sullivan et al., 2006). This decrease is often attributed to the delay time distribution (DTD), often measured as a power law of slope $t^{\sim -1}$ (Graur & Maoz, 2013; Wiseman et al., 2021), where older populations have a lower rate of SNe than younger populations. Curiously however, previous studies have measured a higher normalised DTD within cluster environments (Freundlich & Maoz, 2021). While this helps explain the excess of high mass hosts within clusters, it does not explain the lack of low mass hosts.

In fact, based on this higher normalised cluster DTD, and assuming that most galaxies within a given cluster are of a similar age, we would expect an excess of cluster SNe at all host galaxy masses.

To investigate this lack of low mass SN hosts, in this Chapter we measure the rate of SNe Ia per unit stellar mass, also called the mass-normalised SN Ia rate, or the specific SN Ia rate, as a function of the stellar mass of their host galaxies for the two samples.

4.1.1 Calculating the SN Ia rate per unit stellar mass

The rate of SNe Ia per unit stellar mass is calculated from the number of SNe Ia ($N_{\rm SNe}$) detected per unit time, divided by the total surveyed stellar mass. This rate can be further calculated as a function of stellar mass by repeating the calculation, but segregating events into bins based on the stellar mass of their host galaxies. The total amount of stellar mass for SN hosts is a simple sum of the masses of each individual host. However, this disregards the galaxies surveyed by DES that did not host a SN Ia. As such we must account for all the mass surveyed by DES in both cluster and field environments. For the field, we estimate the total stellar mass by multiplying a stellar mass function (SMF) by the volume surveyed by the DES-SN survey over 0.1 < z < 0.7. We elect to use the ZFOURGE/CANDELS SMF measured over measured over 0.2 < z < 0.5 (Tomczak et al., 2014). This SMF is complete from $8 \le \log(M_*/{\rm M}_{\odot}) \le 11.25$), (~ 1 dex deeper than previous SMFs over 0.2 < z < 3) encompassing 97 per cent of our SN hosts. While not covering our full redshift range, the SMF measured over 0.2 < z < 0.5 is near identical to the SMF measured over 0.5 < z < 0.75 (Tomczak et al., 2014), and thus well describes our data.

The ZFOURGE SMF, $\phi(M)dM$, is described by the double Schechter function (Schechter, 1976)

$$\phi(M)dM = \phi_1(M)dM + \phi_2(M)dM$$

$$= \ln(10)e^{-10^{(M-M^*)}}10^{(M-M^*)}$$

$$\times [\phi_1^*10^{(M-M^*)\alpha_1} + \phi_2^*10^{(M-M^*)\alpha_2}]dM,$$
(4.1)

where $M = \log(M/\mathrm{M}_{\odot})$, (α_1, α_2) are the slopes and (ϕ_1^*, ϕ_2^*) are the normalisations of the two Schechter functions, and M^* is the characteristic mass. The product of the SMF and the field volume results in the galaxy numbers as a function of stellar mass that DES surveys, from which the total stellar mass in each mass bin can be calculated. For the cluster SN Ia sample, instead of calculating the volume encompassed by our clusters (which is uncertain as clusters are unlikely to be perfect spheroids) and multiplying by a cluster SMF, we instead use the relation between a cluster's richness, λ and its total stellar mass, M_{\star} , i.e.,

$$\ln\left(\frac{M_{\star}}{\tilde{M}_{\star}}\right) = \pi_{M_{\star}|\lambda} + \alpha_{M_{\star}|\lambda} \ln\left(\frac{\lambda}{\tilde{\lambda}}\right),\tag{4.2}$$

where \tilde{M}_{\star} is the median M_{\star} of the sample, and $\tilde{\lambda} = 40$, $\tilde{z} = 0.35$ are the median richness and redshift used in McClintock et al. (2019). Values for $\pi_{M_{\star}|\lambda}$, $\alpha_{M_{\star}|\lambda}$ and \tilde{M}_{\star} are taken from Palmese et al. *in prep* and Palmese et al. (2020), which measured the stellar-to-halo mass relation for DES redMaPPer clusters.

This gives the total stellar mass for each cluster, which may be summed to provide the overall mass for the cluster sample. This may then be separated into mass bins by using a SMF for DES clusters presented in Palmese et al. *in prep*. However, this SMF is only valid for hosts with $\log(M_*/\mathrm{M}_\odot) \geq 10$. As such, we discard cluster SNe in hosts less massive than this limit for this rate analysis. Both field and cluster SMFs assume a Chabrier initial mass function (IMF). In SN Ia rate analyses, a Kroupa IMF is often used. As such we shift our IMFs from a Chabrier IMF to a Kroupa IMF, using Eq. 2 in Speagle et al. (2014) which amounts to a difference of 0.01 dex.

 $N_{\rm SNe}$ for both our samples is calculated as detailed in Chapter 3.1.1. We account for the effects of time dilation deeper in the universe via a (1+z) correction on the number of SNe. DES-SN is not a perfect survey, and some SNe will not be detected, nor will the redshift of some hosts be measurable (typically due to the host being too faint or lacking detectable emission lines). As we require a spectroscopic redshift for our SNe, we must account for the efficiency of obtaining this redshift, along with the efficiency of detecting a given SN.

The efficiency of the DES-SN survey in both detecting SNe and in measuring the redshift of the SN host galaxy using host galaxy spectroscopy is calculated following a standard 'efficiency' method (e.g., Perrett et al., 2012; Wiseman et al., 2021).

The SN detection efficiency is estimated by simulating 1.1×10^6 SNe Ia using snana and running a simulation of the DES-SN survey, and is fully described in Wiseman et al. (2021). To obtain the detection efficiency, we divide the number of SNe detected by the simulation of DES-SN (i.e., that pass the light-curve selection described in 2.1.6) by the total number of simulated SNe Ia. These remaining fraction of SNe depend on the sky location, time of explosion, and the light curve properties of the SN themselves. We show these efficiencies in Fig. 4.1. The detection efficiency depends weakly on stretch and strongly on colour and redshift, with the deeper fields (C3, X3) being sensitive to higher redshifts. Some of the efficiencies downturn at lower redshifts, which initially seems counter intuitive. However, as DES was designed to be a median to high redshift survey, SN at these lower redshifts (and their host galaxies) can over-saturate the detector, leading to an inability to identify the SN, expressed as this downturn in efficiency. Typically these downturns are seen in the higher stretch and/or bluer SN, which are inherently brighter.

The efficiency of obtaining a host galaxy redshift was modelled in Vincenzi et al. (2021). To briefly summarise here, Vincenzi et al. measures $\epsilon_{z_{\rm spec}}(m_{r,i}^{\rm host})$ from the data itself, contrary to previous analyses (Jones et al., 2017, 2019) which model the efficiency as a simple function of redshift. The data driven method doesn't guarantee a match between simulation and data, but instead allows measurements of efficiency as a function of galaxy properties. This allows better modelling of the dependency of SN rates on their host properties. Vincenzi et al. calculates the efficiency of obtaining a host galaxy redshift is roughly 100 per cent for bright host galaxies ($m_r^{\rm host} < 21 \, {\rm mag}$), with this decreasing to $\sim 50 \, {\rm per}$ cent for galaxies with $m_r^{\rm host} \sim 23 \, {\rm mag}$. This efficiency varies between each SN field, due to prioritisation of the deep fields (due to increased amounts of SN candidates) and the Elais-S1 (E1/E2) fields (due to an increased

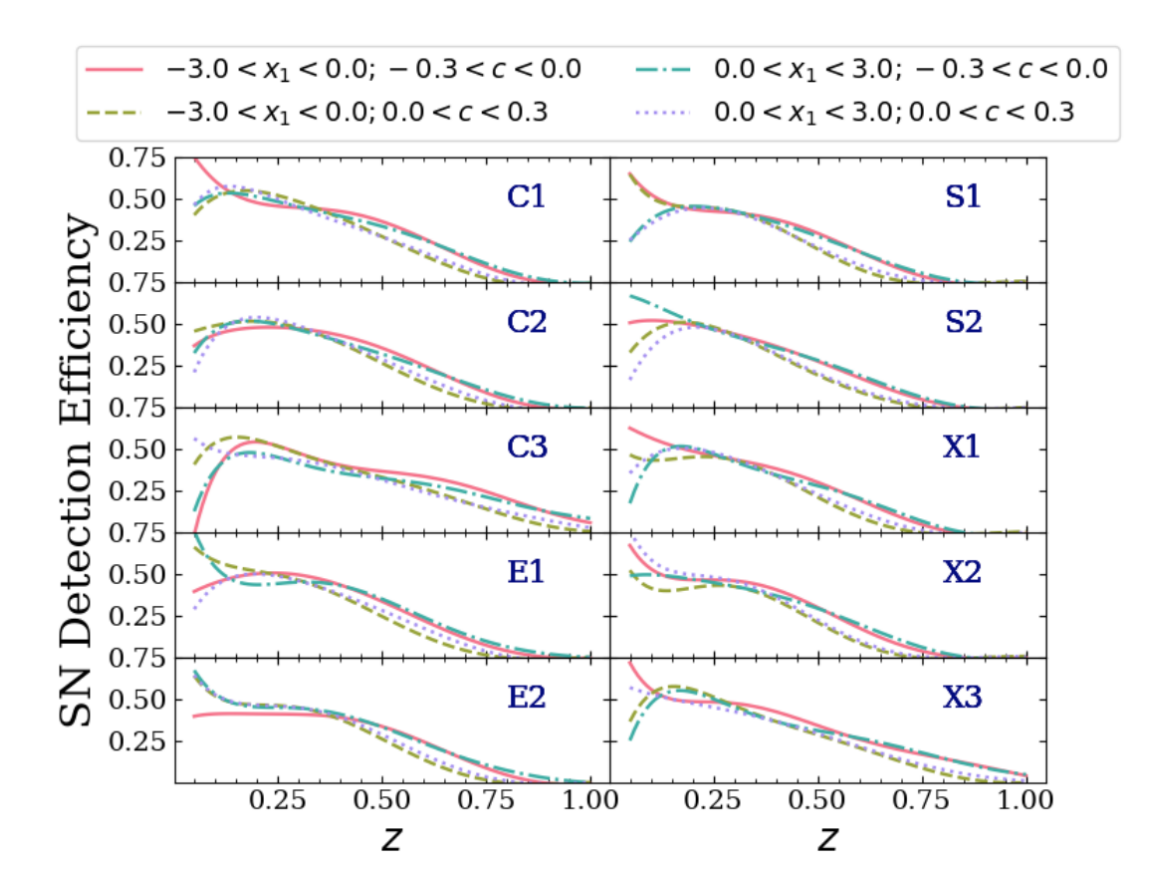


FIGURE 4.1: The efficiency of SN detection as a function of stretch (x_1) , colour (c_{SN}) , field and redshift. Figure adapted from Wiseman et al. (2021).

visibility window for OzDES). Additionally, some of the fields have greater numbers of external surveys that have historically measured galaxy redshifts.

We then compute $\eta_{SN,i}$, the detection efficiency of the *i*th SN, as

$$\eta_{\text{SN,i}} = \eta_{\text{SN,i}}(F_i, z_i, t_{0,i}, x_{1,i}, c_{i,\text{SN}}) \times \epsilon_{z_{\text{spec}}}(m_{r,i}^{\text{host}}),$$
(4.3)

where $\eta_{SN,i}(F_i, z_i, t_{0,i}, x_{1,i}, c_{i,SN})$ is the SN detection efficiency of the *i*th SN exploding in field F, at time t_0 and redshift z, with stretch x_1 and colour c_{SN} and $\epsilon_{z_{spec}}(m_{r,i}^{host})$ is the efficiency of obtaining a spectroscopic redshift for our SN hosts as a function of r-band apparent magnitude. Finally for the rate calculation, the weight (W) of a given SN 'i' is found via:

$$W_i = \frac{1+z}{\eta_{\text{SN,i}}} \tag{4.4}$$

To test the reliability of our detection efficiencies, we calculate a simple average volumetric rate (SNR_{Ia}) for our field sample and compare to other analyses. We take the efficiency-corrected number of field SNe and divide by the co-moving volume (V) within our redshift range.

$$SNR_{Ia} = \sum_{i}^{N} \frac{W_i}{V_{DES}}$$
 (4.5)

We calculate SNR_{Ia}($\langle z \rangle = 0.55$) = 0.406×10^{-4} SNe yr⁻¹ Mpc⁻³, consistent with Neill et al. (2006) who found

 $SNR_{Ia}(\langle z \rangle = 0.47) = [0.42^{+0.13}_{-0.09} \ (syst.) \pm 0.06 \ (stat.)] \times 10^{-4} \ SNe \ yr^{-1} \ Mpc^{-3}$ and Perrett et al. (2012) with $SNR_{Ia}(0.5 < z < 0.6) = [0.48^{+0.06+0.04}_{-0.06-0.05}] \times 10^{-4} \ SNe \ yr^{-1} \ Mpc^{-3}$. Our measurement is also within the 1σ uncertainties of the power-law fit to the evolution of the SNR_{Ia} with redshift (Frohmaier et al., 2019). We also show the volumetric rate, calculated in smaller redshift bins in Fig. 4.2, along with the rate calculated in Perrett et al. (2012) using SNe from the supernova legacy survey. We see that in each redshift bin our calculated rate is contained within the 1σ uncertainties from Perrett et al., and thus conclude that our efficiencies are robust.

We have not performed a full uncertainty analysis on our SNR_{Ia} measurement as this is not the focus of this work, however the errors shown in Fig 4.2 have been estimated as SNRIa_{err} = $\sqrt{N_{\rm SN}}$.

We calculate the rate of SNe Ia per 10^{10} M $_{\odot}$ per century (also know as the SNuM) as a function of host galaxy stellar mass, shown in Fig. 4.3.

$$SNuM_{bin} = \sum_{i}^{N} \frac{W_i * \frac{25}{12} yrs}{M_{bin} * 100 yrs}$$
 (4.6)

Within stellar mass bins that contain detected cluster SNe, the rate of SNe in cluster environments is broadly consistent with the field, with the respective rates mostly being 1σ of each other. The largest outlier is the highest mass bin with cluster SNe detected, which sharply decreases compared to the field, with a difference of 3.6σ . On average however, the rate of cluster SNe per mass is lower than the field, driven by the higher mass bin, with a weighted average ratio of the two of 0.594 ± 0.068 between $(10 \le \log(M_*/\mathrm{M}_{\odot}) \le 11.25)$.

We do not detect any cluster SNe Ia in host galaxies above $\log(M_*/M_\odot) = 11.25$, which is perhaps surprising. This lowers the overall cluster SNuM significantly, as a typical cluster SMF indicates galaxies with these stellar masses exist. For example, if the cluster rate from $11.25 \le \log(M_*/M_\odot) \le 11.5$ was equal to the field rate, 17.8 ± 5.0 SNe would have been expected over the 5-year DES-SN observing period given the total mass observed in that bin, and thus we would expect such objects to occur in our sample. However, cluster environments are also older when compared to the field, which (assuming a DTD that declines with time) also reduces the expected rate in these higher mass galaxies.

By using both SMFs for field and cluster to calculate the total stellar mass of both samples $\log(M_*/\mathrm{M}_\odot) = 10$ for clusters and field, we calculate the integrated SNuM measurement for

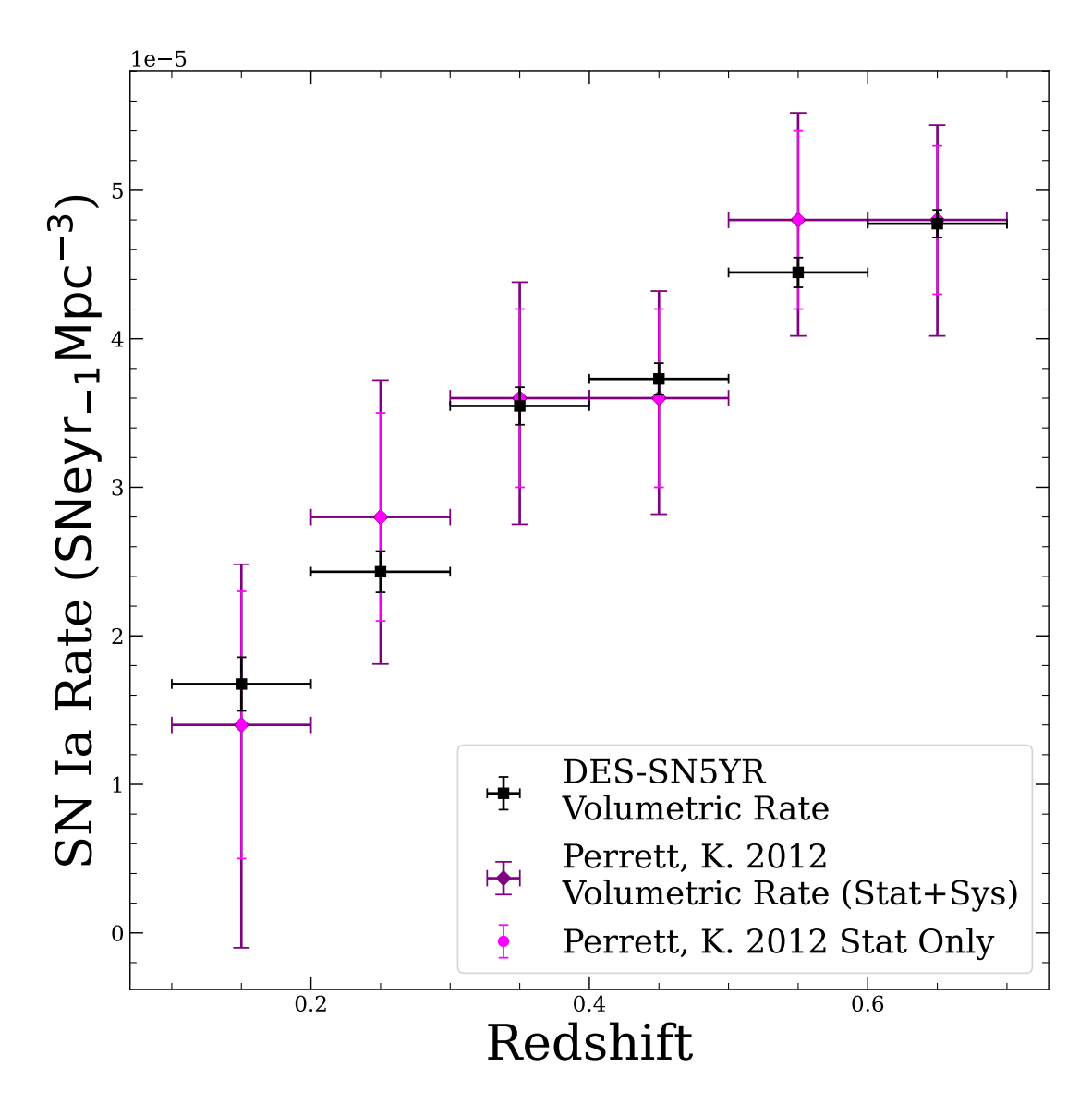


FIGURE 4.2: The number of SNe per year per Mpc³, as a function of redshift. Also shown are the data from Perrett et al. (2012). Our results are consistent within the 1σ uncertainties from Perrett et al..

both environments. SNuM is known to be a strong function of galaxy properties (Mannucci et al., 2005; Sullivan et al., 2006; Smith et al., 2012; Wiseman et al., 2021), and as such this host mass selection is key to making sure our results are a fair comparison, and do not include less massive field hosts, which have a higher SNuM then higher mass hosts. We find the integrated SNuM for clusters to be $0.0332 \pm 0.0040^{+0.0082}_{-0.0044}$ at a efficiency weighted redshift of 0.44, while the field SNuM is $0.086 \pm 0.0069 \pm 0.0062$ at a efficiency weighted redshift of 0.54. Both SNuMs are presented as a function of stellar mass. There exists an evolution of rate with redshift, which will account for some of the difference between our cluster and field rate. We compare our measurements of total SNuM to measurements from the literature in Fig. 4.4 and Table 4.1.

We also calculate the integrated mass of the stars formed (formed mass) in our cluster hosts to

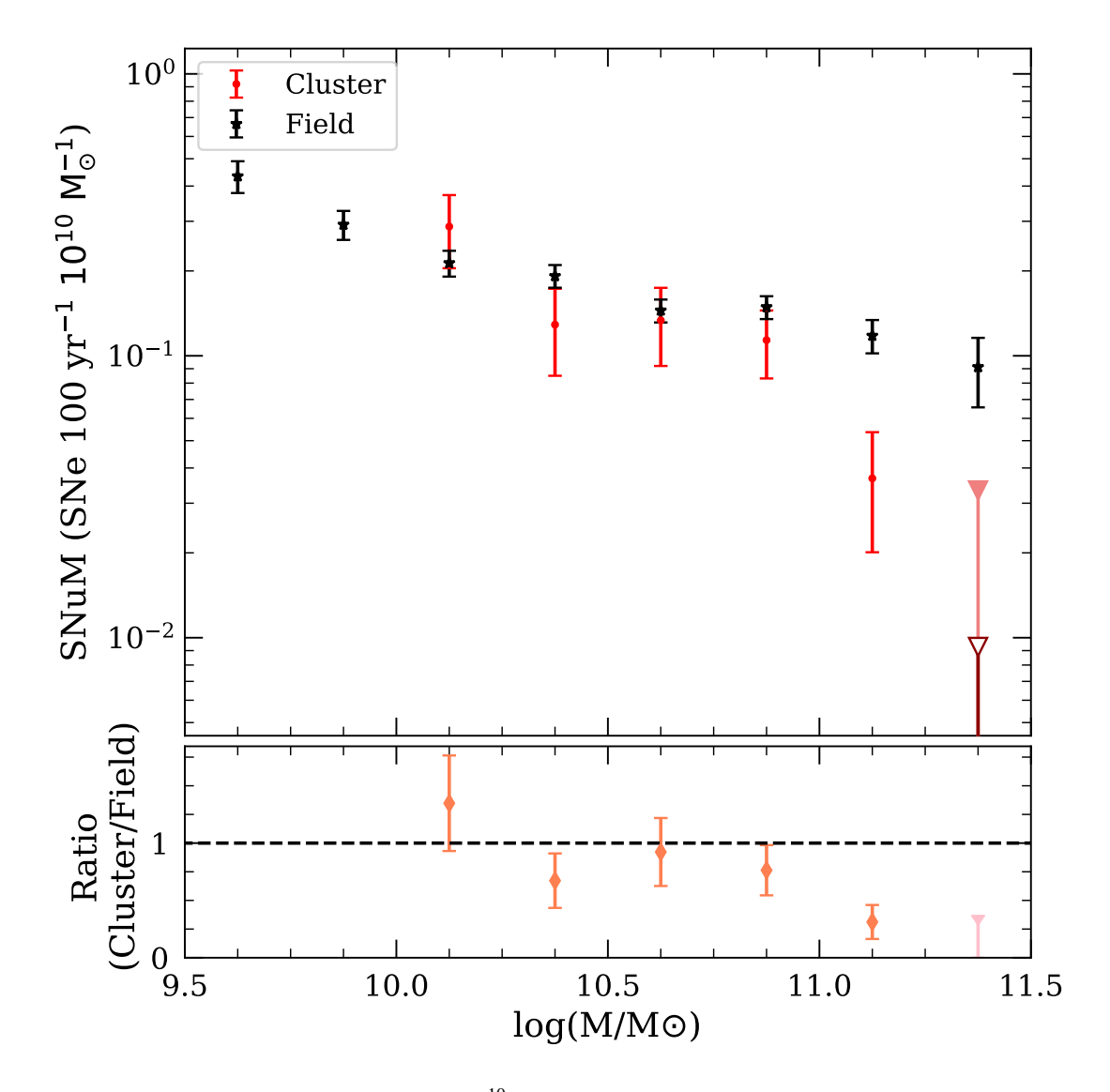


Figure 4.3: The number of SNe per $10^{10}~M_{\odot}$ per century, as a function of stellar mass of the host galaxy for cluster SNe and field SNe. The final cluster data points are the 1σ (dark red) and 3σ (light pink) upper limits for a non detection from Gehrels (1986). The final ratio is the ratio of the 3σ non-detection rate to the field.

compare the production efficiency of SNe Ia between the field and clusters, and for comparison to the literature. For this, for clusters we assume a single burst of star formation at z=3, and a constant metallicity of 0.02, using the Pégase.3 (Fioc & Rocca-Volmerange, 2019) spectral synthesis code as done in Freundlich & Maoz (2021), and present our overall rate as a function of formed mass rather than stellar mass. After cutting low mass galaxies, we assume that the star formation history of the field hosts is the same as the cluster hosts. This allows us to make a simple estimate of the formed mass for the field galaxies, shown as the unfilled black circle in Fig. 4.4.

Our cluster SNuM is the most precise in its redshift range, and is consistent with other measurements at lower and higher redshifts. However, we stress for these overall rates we have removed both cluster and field SNe that are located in low mass galaxies. This would lower our

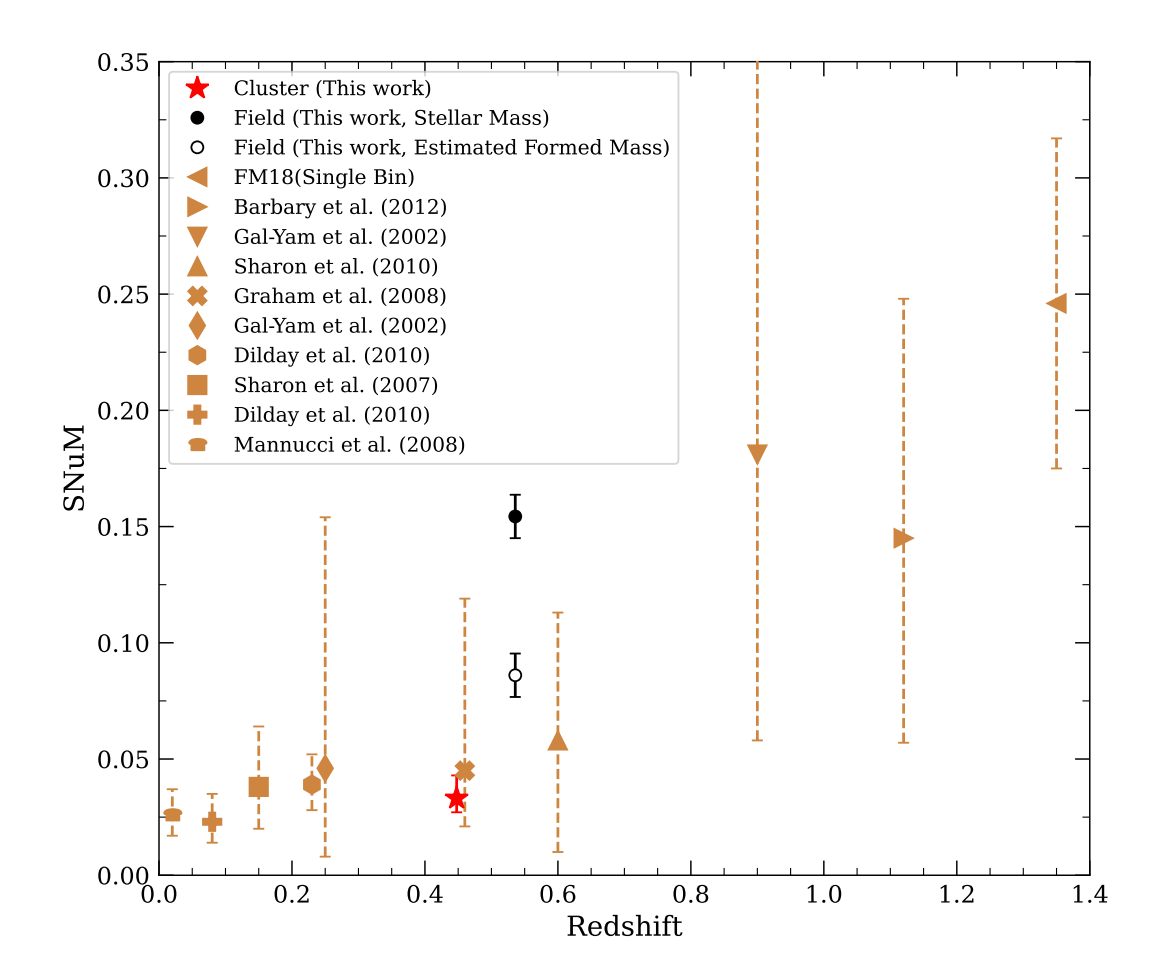


FIGURE 4.4: A comparison of our field and cluster SNuMs, in host galaxies with $\log(M_*/M_\odot) \ge 10$, compared to other literature examples. The gold markers are rates measured in clusters from the literature. The black filled point is the field rate per stellar mass, and the black circle is the estimated field rate per formed mass, assuming a similar SFH to cluster environments, the error of which should be treated as a lower limit. Both cluster and field are presented in terms of formed mass. The redshift range of this work spans $0.1 \le z \le 0.7$. Data are in Table 4.1.

overall rate compared to literature rates. Additionally, due to the cluster SMF being only valid for use in galaxies $\log(M_*/M_\odot) \geq 10$ we have assumed all cluster mass is made up of these galaxies. As we have found cluster SNe Ia hosted in less massive galaxies (Figs. 3.1, 3.2, 3.6, 3.7) we know this to be an over-simplification. As such we estimate the amount of mass below this limit in the cluster using the ZFOURGE/CANDELS passive stellar mass function (measured over 0.2 < z < 0.5). We account for this uncertainty in the mass in the upper error on our cluster SNuM. Our field rate is also consistent with literature cluster rates at similar redshifts.

4.1.2 Discussion of rates

Our SN Ia SNuM in galaxy clusters is lower than that in the field, whether comparing overall values or only rates for SNe Ia in similar mass hosts. Fig. 4.3 also shows that the ratio of the

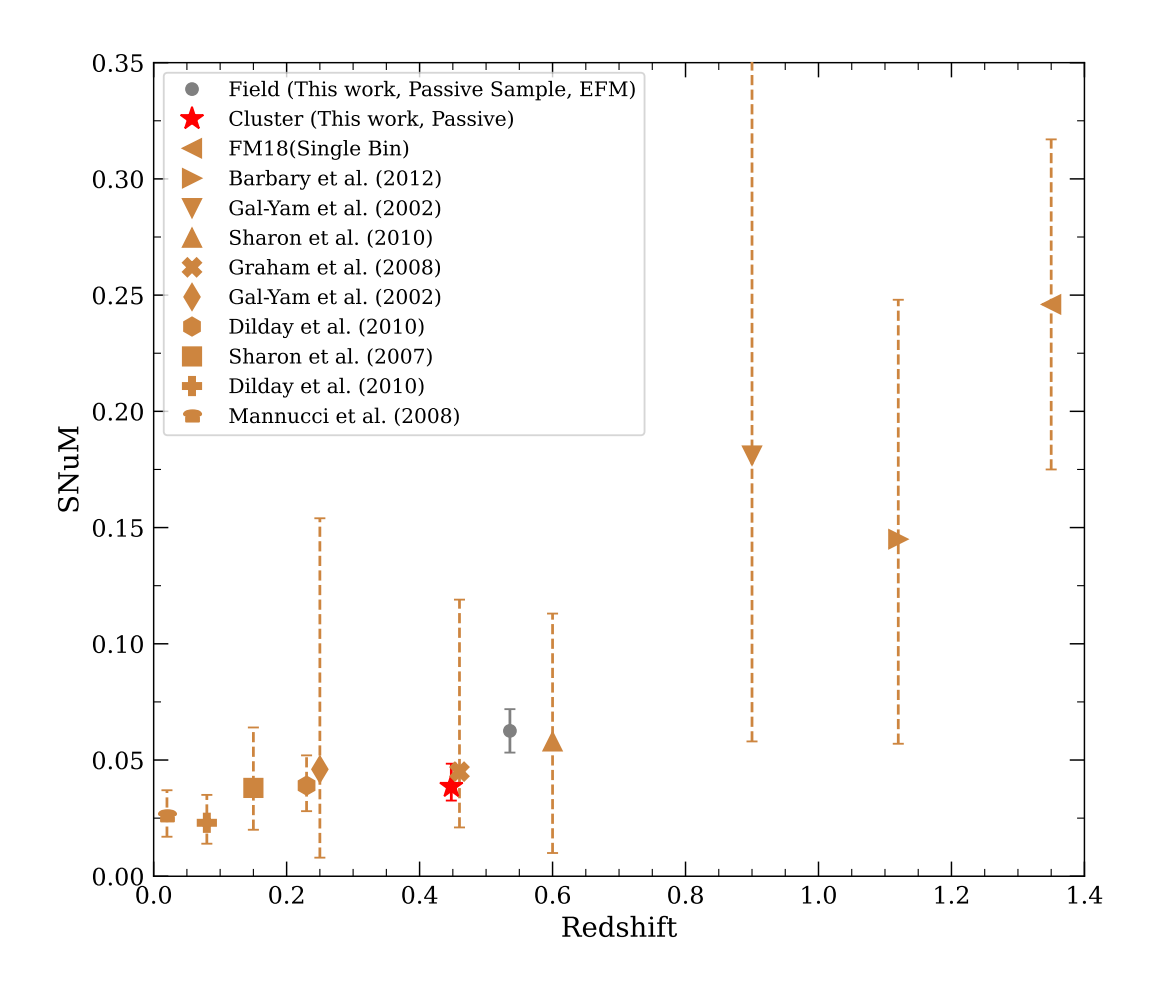


FIGURE 4.5: A similar comparison to 4.4, but instead both field and cluster have been limited to galaxies passing the UVJ cut described in Section 4.1.2.2. Errors on these passive rates should be treated as a lower limit.

cluster rate compared to the field rate tentatively decreases with host stellar mass. We discuss the origin of this trend below.

4.1.2.1 The effect of age on the SN Ia rate

The cluster DTD has been measured to be normalised higher than the field DTD by many studies (Maoz & Graur, 2017; Freundlich & Maoz, 2021). This enhanced DTD could be caused by an excess of white dwarfs (WD), due to a differing IMF, or an enhancement of binary systems within clusters compared to the field (Friedmann & Maoz, 2018). For example, the IMF may be non-universal (van Dokkum, 2008; Davé, 2008) and depend on a galaxy's velocity dispersion, which may in turn lead to an excess of low-mass (0.5 -8 M_{\odot}) stars in the most massive galaxies (Ferreras et al., 2013; Ferré-Mateu et al., 2013). This may lead to cluster galaxies' stellar populations containing a higher fraction of low-mass stars than the field, which, evolved over long enough times could lead to more WDs, causing a higher normalised DTD.

	Rate (SNuM)	Average Redshift
Cluster SNuM (This work)	$0.0332 \pm 0.0040^{+0.0082}_{-0.0044}$ a	0.44
Field SNuM (This work) ^b	$0.086 \pm 0.0069 \pm 0.0062^{b}$	0.54
Field SNuM (Passive galaxies)	$0.0625 \pm 0.0069 \pm 0.0062^{c}$	0.54
Cluster	r literature SN Ia rates	
Friedmann & Maoz (2018) ^d	$0.246^{+0.071}_{-0.071}$	1.12
Barbary et al. (2012)	$0.145^{+0.103}_{-0.088}$	1.12
Gal-Yam et al. (2002)	$0.181^{+0.241}_{-0.123}$	0.9
Sharon et al. (2010)	$0.058^{+0.055}_{-0.048}$	0.6
Graham et al. (2008)	$0.045^{+0.074}_{-0.024}$	0.46
Gal-Yam et al. (2002)	$0.046^{+0.108}_{-0.038}$	0.25
Dilday et al. (2010)	$0.039^{+0.013}_{-0.011}$	0.23
Sharon et al. (2007)	$0.038^{+0.026}_{0.018}$	0.15
Dilday et al. (2010)	$0.023_{-0.009}^{+0.012}$	0.08
Mannucci et al. (2008)	$0.026^{+0.011}_{-0.009}$	0.02

Table 4.1: Overall SN Ia rates (with host mass cuts applied) from this work with comparisons from the literature, as recalculated by Freundlich & Maoz (2021).

One may expect due to this increased DTD, to measure more SNe within clusters than in the field at the same redshift. However we find that the overall rate of SNe Ia per unit formed mass in massive galaxies within the field environments is higher than cluster environments. Assuming a declining DTD, our lower rate in clusters would indicate that cluster galaxies of the same mass have older stellar populations than their field counterparts. This age dependent rate could negate this higher-normalised DTD, and explain the damped cluster rate.

It may be possible to probe the effect of an older stellar population by measuring the U-R colour of SN host galaxies. U-R can be used as a proxy for morphology, and is dependent on the star formation history of the galaxy being studied (Lintott et al., 2008). U-R also correlates with galaxy age (Wiseman et al., 2022a), with redder galaxies being older, and thus we can use U-R to probe the galaxy age. We have shown the U-R colours versus their stellar masses for our two samples in Fig. 3.2. We see a slightly higher proportion of high mass, red galaxies within clusters compared to the field. The increasing U-R with galaxy stellar mass, and the higher proportion of red galaxies in the cluster SNe hosts, may help explain the dampening in the rate as a function of mass in the cluster population.

A possible cause of this older population is that star formation in clusters turned off earlier than in the field. The rate of galaxy mergers within cluster environments compared to the field may be enhanced (Watson et al., 2019), although the significance of this increase is debated, and evidence also exists for a comparable or lower cluster merger rate when comparing the field to

^a Statistical + systematic + SMF Correction

^b This is for a estimated formed mass, assuming a similar SFH as the cluster hosts. Errors presented are for a stellar mass based SNuM, and as such should be treated as a lower boundary.

^c Minimum error, see Section 4.1.2.2.

^d Single redshift bin

the central cluster environment (Delahaye et al., 2017). Galaxy mergers can alter the gas content of the interacting galaxies, with some gas potentially being removed from one galaxy and taken by another, or lost to the intergalactic medium. Such a removal of gas would quench star formation within clusters, leading to older populations and a subsequent decrease in the rate.

Further investigation is needed into the effect of the IMF on WD production efficiency, and on galaxy mergers causing a differing age in similar mass galaxies in different environments. This would allow further constraints on the cluster and field DTD in order to see what effects this would have on SN production over Hubble Time. A precise DTD in galaxy clusters and massive field galaxies is deferred to a future work.

4.1.2.2 The SN Ia rate in passive galaxies

We are able to estimate the effects of an age difference between the cluster and the field environments by isolating field galaxies that are passive, and thus should have older stellar populations. To calculate the SNuM in massive, passive field galaxies requires a passive field galaxy stellar mass function, which is provided by ZFOURGE. The ZFOURGE passive galaxies were identified using the rest-frame U, V, and J bands.

To estimate the total number of massive field galaxies that are passive, we compute the fraction of those with NIR coverage that pass the Tomczak et al. (2014) UVJ cut and multiply it by the total number of galaxies. We then calculate the total passive formed mass using the passive SMF in Tomczak et al. (2014) and assuming a similar SFH to clusters, as above. We can then calculate the rate per century per $10^{10}~M_{\odot}$ formed, which we find to be 0.0625 with the minimum error being $\pm 0.0069~(\text{stat.}) \pm 0.0062~(\text{syst.})$. As we have made some oversimplifications we do not know the exact error on this rate. However, assuming similar or slightly enhanced errors to our other field SNuMs, this passive rate is comparable (different at a maximum of 1.7σ) to the passive cluster rate of $0.0386~\pm 0.0040~(\text{stat.}) ^{+0.0082}_{-0.0044}~(\text{syst.})$ (again the minimum error). Additionally, fitting a straight line to the literature values in Fig. 4.4 allows us to probe the evolution of the SNuM as a function of redshift. We find that such a rate evolution has a gradient of $\sim 0.11 \pm 0.02$. Thus the average redshift difference of 0.1 between our cluster and field samples would have a related rate difference of ~ 0.011 . Shifting the cluster rate to the field redshift using this evolution brings the maximum difference to $< 1\sigma$.

Therefore it appears that while the stellar population in cluster host galaxies may be much older than those within overall field hosts, they are comparable in age or slightly older to stellar populations in passive field hosts. Another cause may be that the IMF in cluster hosts produces additional white dwarfs compared to the lower mass field hosts, but production of these white dwarfs is similar in clusters and passive field hosts.

We however note that this passive rate contains many simplifications, and more wide-reaching NIR data would be needed to allow these comparisons to be performed in a more precise manner.

4.2 Summary

From our previously identified sample of 66 cluster based and 1024 field based SNe within the DES-SN5YR sample we have calculated the mass-normalised rates of SNe Ia within these two environments. Our main findings are as follows:

- We measure a preliminary rate of the full DES-SN5YR sample normalised by the volume encompassed by the DES-SN survey, and find the overall rate to be consistent with previously measured rates from the Supernova Legacy Survey (Neill et al., 2006; Perrett et al., 2012). We also measure the evolution of this volumetric rate as a function of redshift, and find it in good agreement with both the evolution measured in Perrett et al. (2012) and the power-law fit to the redshift evolution calculated in Frohmaier et al. (2019).
- We calculate the rates of SNe Ia in cluster and field environments, and find them to be broadly consistent to within 1σ . However, at higher masses this appears to change, with the rate of cluster SNe between $(11 \le \log(M_*/M_\odot) \le 11.25)$ being lower than the field by 3.6σ . Taking into account all mass bins with a detected cluster SN, the weighted average ratio of cluster to field SNe rates is 0.594 ± 0.068 , however this average ratio is heavily driven by the final cluster mass bin.
- Integrating the overall rates of field and clusters within galaxies with $\log(M_*/M_\odot) \geq 10.0$, we find the rate of SNe Ia within clusters as a fraction of formed mass to be 0.0332 ± 0.0040 (stat.) $^{+0.0082}_{-0.0044}$ (syst.) SNe 100 yr^{-1} $10^{10} \text{ M}_\odot^{-1}$, and the corresponding field rate to be 0.086 ± 0.0069 (stat.) ± 0.0062 (syst.) SNe 100 yr^{-1} $10^{10} \text{ M}_\odot^{-1}$. However, these measurements are at slightly differing redshifts, which will account for some of this difference and both are broadly consistent with other literature cluster rates. The measured decrease could be due to cluster galaxies being older, or more quenched than their field counterparts. Thus this declining rate within clusters compared to the field indicates that galaxies at a fixed mass are older in clusters than the field. We calculate that the rate in passive field galaxies is more comparable to the cluster rate, however a more complete dataset would be valuable in verifying this result.

Interestingly, where previous studies have found an increased rate of SNe per formed stellar mass within clusters compared to the field, we find that they are, within similar galaxy types, statistically the same. This, along with the previous chapters results of similar light curve properties in samples of similar galaxy make-ups, implies that the global environment is sub-dominant in its effects on SNe properties when compared to the correlation between host galaxy properties and SNe properties. Even recent studies such as Larison et al. (2023), which find SNe closer to the centre of their cluster to be faster evolving than those further out, suggest this may be caused by a gradient in stellar population, with older galaxies closer to the cluster centre.

4.2. *Summary* 69

Despite this, clusters remain an interesting point of study. Recently, Ruppin et al. (2024) reconfirmed the dependence of x_1 on distance from cluster centre. They calculate that if this is a solely age driven effect (i.e older populations host faster declining SNe), the fraction of quenched galaxies in the centres of galaxies could reach ~ 90 per cent. Such a homogeneous environment, with very little ongoing star formation, could be an interesting target for future cosmological surveys to test the robustness of their host-property corrections.

Motivated by the seeming sub-dominance of large scale environment on type Ia supernovae, with many differences lowered when comparing SNe in similar hosts, along with the curious effect of faster declining SNe within the centres of hosts, we will investigate the properties of SNe as a function of their projected separation from their host galaxy, and any dependence on their standardisation in the next chapter.

Chapter 5

A cosmological conundrum - Galactic location and its impact on the properties and standardisation of supernova

How about we explore the area ahead of us later?

Paimon - Genshin Impact

5.1 The importance of galactocentric separation for supernova properties

In the previous chapters, we broadly investigated the trends of SN light curves and rates with their host environment, splitting them into binary categories of within a cluster or not. Such a split allowed us to probe the effects of large scale structure, different progenitor formation periods, and differences in stellar populations.

We made the assumption through most of that work that galaxies within clusters and the field contained no large population differences at fixed stellar mass. We also assumed that the galaxies themselves contained no gradients such as dust or star formation. This assumption is a great simplification.

Rather than homogeneity, galaxies often instead have gradients based on the distance from the galaxy core. Within both spiral (Simpson et al., 1995) and elliptical galaxies (Kormendy & Djorgovski, 1989), observations show gradients in their metal abundances, with inner regions

being more metal rich than the outer regions. Gradients for spiral galaxies change on the order of kpcs, with stellar metallicity (the fraction of elements within stars heavier than He) gradients of -0.05 dex/kpc often observed (Pilkington et al., 2012).

Additionally, galaxies often exhibit gradients in the age of their stellar populations. Stellar populations within spiral galaxies are typically younger in the outer regions, attributed to inside-out star formation (where the centre bulges of galaxies form first, followed by 'rings' of stellar formation) (Parikh et al., 2021). Stellar populations in elliptical galaxies on the other hand may be older in the outer regions (Baes et al., 2007), or exhibit little overall gradient. This may be due to the star formation within the nucleus of elliptical galaxies being less affected by the galactic wind, while star formation in the outer regions is quenched due to feedback from active galactic nuclei and SNe (Baes et al., 2007).

Such gradients pose an interesting conundrum for SN cosmology. These gradients inevitably lead to varying environments in which the SN progenitor will evolve from within the same host, as well as from galaxy to galaxy. Such different environments may change the astrophysics which involve the SN Ia progenitor, with different white dwarf ages, masses and compositions depending on the stellar age of the surrounding environments. Different compositions or masses may lead to the production of different amounts of Ni⁵⁶, the decay of which governs the observed light curve (Arnett, 1982). Additionally, the inter-stellar medium (ISM) may be composed of different gasses and molecules, varying the underlying reddening and extinction we observe due to line of sight effects. These environmental properties governing and altering the SN Ia explosion may affect the light curve properties we measure, such as dust reddening the emitted light, leading to different supernova colours being measured. While these differences in light curve properties such as x_1 and c_{SN} may not affect the standardised brightness, instead leading to different nuisance parameters (α/β) being calculated, dimming from dust or brightness fluctuations based on fluctuations in Ni⁵⁶ masses may lead to variations in standardised brightnesses and ultimately on cosmological measurements.

One property often not included in the standardisation of SNe is the projected separation of a SN as a function of its host galaxy radius in the direction of the SN ($d_{\rm DLR}$, see Sullivan et al., 2006, and §2.2.1). When adjusting SN brightnesses based on correlations between brightnesses and host properties, $d_{\rm DLR}$ is not considered and is for the most part, ignored in cosmological analyses. Previous work showed no clear trends between SN light curve width and $d_{\rm DLR}$ (e.g. Ivanov et al., 2000; Jha et al., 2007; Hicken et al., 2009). However, as seen in Chapter 3.1.2.5, the stretch of light curves for cluster and field-based SNe decreases at low values of $d_{\rm DLR}$, hosting faint, fast evolving SNe Ia. This is unlikely to originate from an observational bias; in these regions close to the host galaxy centres, any surface brightness effects (similar to the Shaw effect on photometric plates (Shaw, 1979; Howell et al., 2000)) or dust extinction effects would bias against the fast, faint SNe that this region seems to prefer.

Previous studies have found relations between the post-standardisation brightness of a given SN and measurements of the local specific star formation (Rigault et al., 2013, 2020). Similarly,

under luminous SN are predominately found in older galaxies (Howell, 2001). However, these studies showed no clear trends between the age of the stellar population and the supernova colour, and other studies have found trends between post-standardisation brightness and the colour of the supernova (Brout & Scolnic, 2021). Additionally, Jha et al. (2007) and Hicken et al. (2009) found a deficit of red supernova at large galactocentric separations.

Finally we reach our conundrum - no single parameter seems to completely align the standardised brightnesses of supernovae, with debate ongoing as to the effects of age or dust on these brightnesses. Motivated by the knowledge of galaxies exhibiting gradients of their properties, and that these properties seem to affect supernova brightnesses, we perform an in-depth analysis as the the effects of galactocentric separation on both the light curve properties and post-standardisation brightnesses of type Ia supernovae.

5.2 Light Curve Properties as a function of Host Galaxy Radius

We use the DES 5 year photometric sample described in Chapter 2. We apply light curve selections as described in 2.1.6. We apply a selection on SN light-curve width (SALT3 x_1) and SN rest-frame colour (SALT3 c_{SN}): $-3 \le x_1 \le 3$ and $-0.3 \le c_{SN} \le 0.3$.

5.2.1 Light Curve Properties

The SALT3 x_1 distribution as a function of d_{DLR} is shown in Figure 5.1. SNe located within the inner-most regions ($d_{DLR} \le 0.5$) of the host galaxy have a more negative x_1 on average than those located outside this region. This means that, on average, SNe within the centres of galaxies are fainter and faster evolving than SNe at higher galactic radii. Additionally, the furthest bin also exhibits a slightly decreased average x_1 . Within these regions we reach the haloes of galaxies, which are inhabited by typically older stars, likely driving the fainter and faster SNe we see in these regions.

We found a similar trend in Chapter 3. In that Chapter, we used a redshift selection of $z \le 0.7$, whereas here no such selection has been made. This may contribute to the slightly less negative mean x_1 in the inner-most bins found in this Chapter.

We also present the SALT3 $c_{\rm SN}$ distributions as a function of $d_{\rm DLR}$ in Figure 5.2. SNe within the inner-most regions and extending out to a $d_{\rm DLR}$ of ~ 1.5 appear to be slightly redder than those in the outer regions, with those below $d_{\rm DLR}$ of 1.5 having a mean colour of 0.010 ± 0.003 and those above this $d_{\rm DLR}$ having a mean colour of -0.023 ± 0.006 . This difference is significant to $\sim 5\sigma$

We show the mean values of the SALT3 x_1 and colour parameters for both inner ($d_{DLR} \le 1$) and outer ($d_{DLR} > 1$) regions in Table 5.1. We additionally present other split locations, to

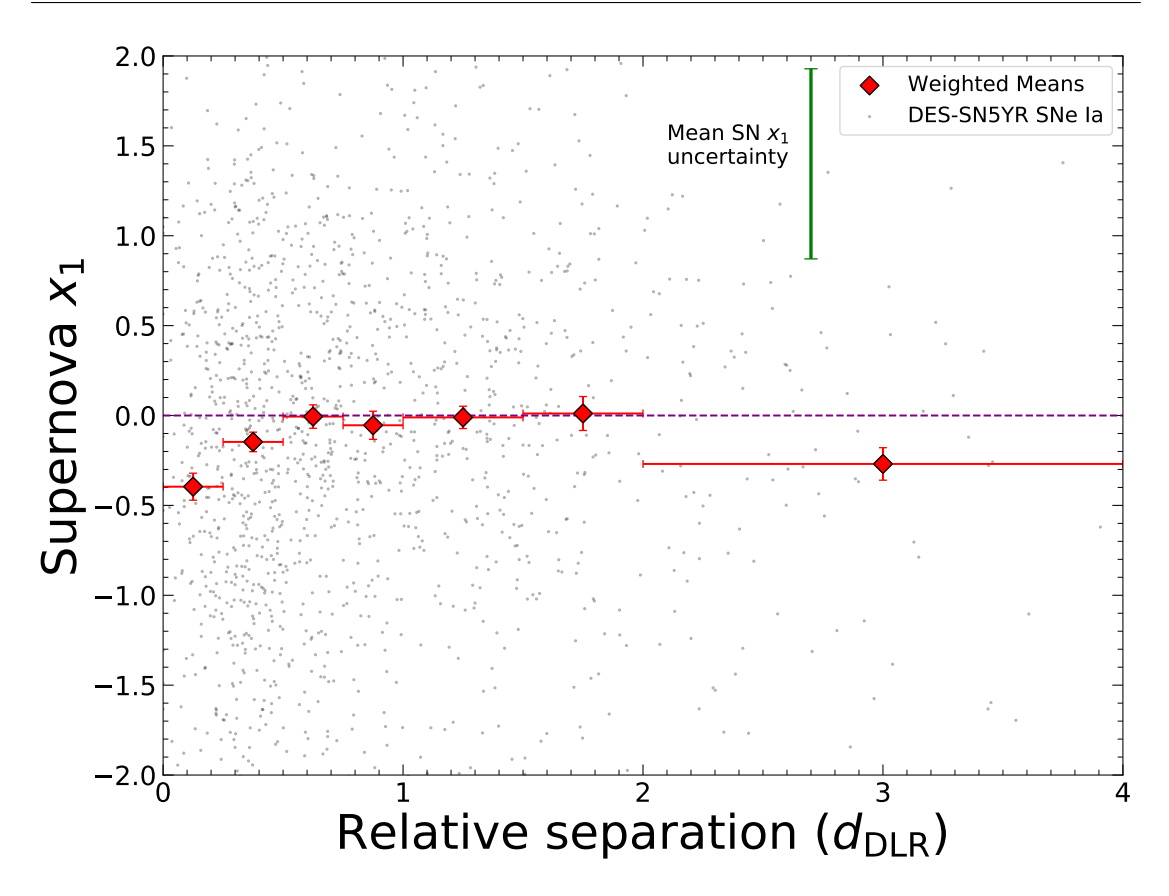


FIGURE 5.1: SALT3 x_1 for our sample as a function of d_{DLR} along with the weighted averages. We see that, on average, the light curve width is centred on 0. However, in the centre-most bins the average x_1 is more negative.

Table 5.1: Weighted mean values of SN Ia light curve properties x_1 and c_{SN} and Hubble residuals in different d_{DLR} ranges.

$d_{\rm DLR}$ range	Number	$\bar{x_1}$	$ar{c}$	Mean $\Delta\mu$
	of SNe Ia			
$d_{\rm DLR} \le 0.5$	607	-0.24 ± 0.04	0.009 ± 0.004	-0.012 ± 0.010
$d_{\rm DLR} > 0.5$	926	-0.05 ± 0.03	0.001 ± 0.003	0.008 ± 0.007
$d_{\rm DLR} \le 1.0$	1028	-0.16 ± 0.03	0.008 ± 0.003	0.001 ± 0.007
$d_{\rm DLR} > 1.0$	505	-0.07 ± 0.05	0.002 ± 0.005	-0.002 ± 0.009
$d_{\rm DLR} \le 1.5$	1294	-0.12 ± 0.03	0.010 ± 0.003	0.002 ± 0.006
$d_{\rm DLR} > 1.5$	239	-0.14 ± 0.07	-0.023 ± 0.006	-0.009 ± 0.014

investigate if there exists a more significant split location. As expected from Figures 5.1 and 5.2, the most significant x_1 difference presents at a d_{DLR} split location of 0.5, while the most significant c_{SN} difference appears at a split location of 1.5.

5.2.2 What could drive these light curve differences?

As previously discussed in Section 3.1.2.5, the increased number of fainter and faster SNe detected in the inner-most regions of their host galaxies are unlikely to originate from a

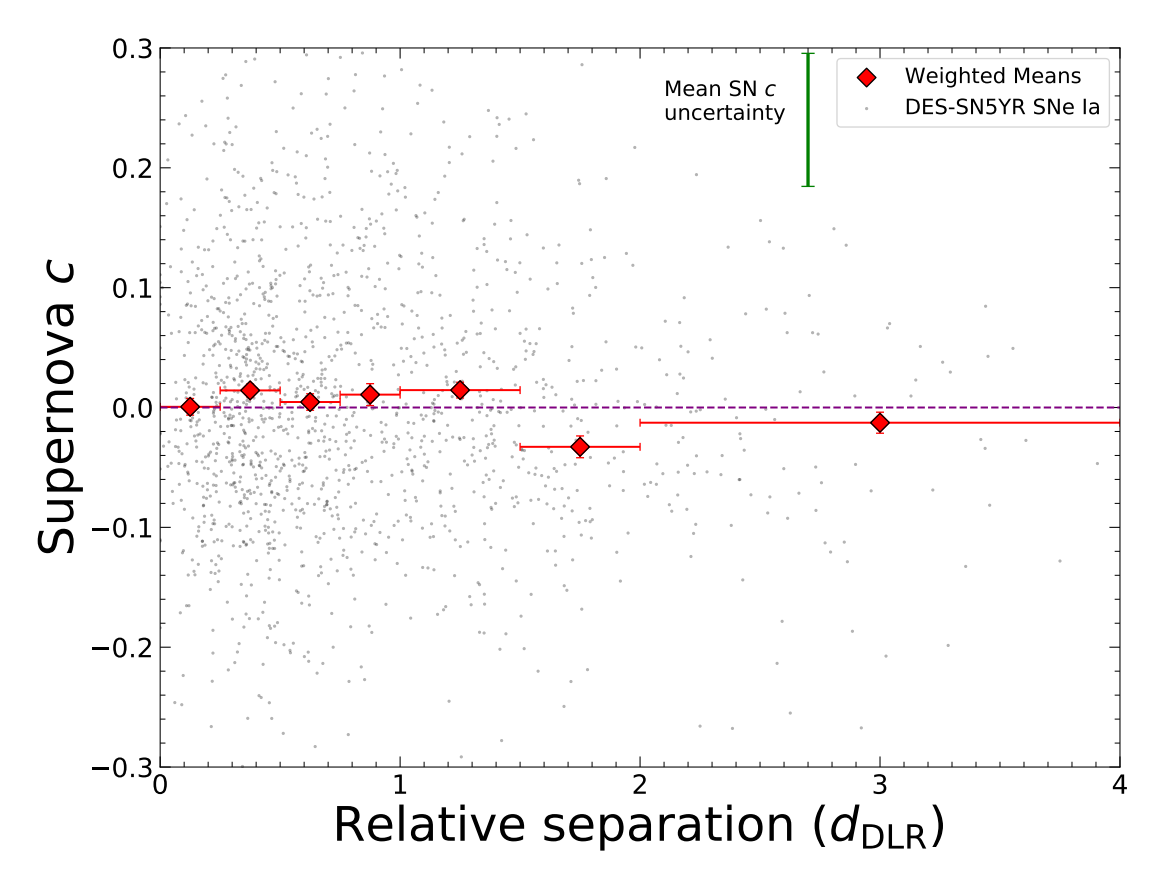


FIGURE 5.2: SALT3 $c_{\rm SN}$ for our sample as a function of $d_{\rm DLR}$ along with the weighted averages. The average colour in the inner-most regions of galaxies are redder, while outer regions become slightly more blue.

increased surface brightness bias. Such an increased brightness would instead bias us to miss these SNe, and if this was the case we would expect to preferentially find brighter, long lasting SNe within these regions. This decrease in x_1 could be due to older stellar populations within the centres of galaxies.

We additionally discussed that an increased amount of dust (and thus extinction) is unlikely to bias our results to favour fainter, faster events. However, Jha et al. (2007) and Hicken et al. (2009) show a lack of reddened SN at higher values of $d_{\rm DLR}$ and SN colour does not seem to be affected by the age of the stellar population (Rigault et al., 2020). The cause of this decrease in the fraction of red SNe may then be due to an decrease in the fraction of dust in the outer regions of galaxies.

With these changes in light curve properties, and their uncertain causes, we next investigate the post-standardised brightnesses of SN and their correlation with $d_{\rm DLR}$.

5.3 Supernova Standardisation

As a reminder, distances to the i'th supernova are calculated using the modified Tripp (Tripp, 1998b) equation:

$$\mu_{\text{obs},i} = m_{x,i} + \alpha x_{1,i} - \beta c_{i,\text{SN}} + \gamma G_{\text{host},i} - M - \Delta \mu_{\text{bias},i}. \tag{5.1}$$

 x_1 and c_{SN} are the SALT3 light curve parameters, m_x is the magnitude of the SN flux in a given band 'x', and M is the absolute magnitude. α , β and γ are global parameters determined from a minimisation over the sample to a given cosmology. $G_{host,i}$ is the relation between SN Ia luminosity and their host properties, and has historically been referred to as a "mass step" (Sullivan et al., 2010). $\Delta\mu_{bias,i}$ corrects the sample for inherent biases, determined following the method in Section 2.2.3. For the purposes of this work we make use of a '1D' bias correction, which accounts for the so called 'Malmsquist bias' (Malmquist, 1922, 1925), in which dimmer objects are missed in a magnitude limited survey such as DES-SN, and other various selection effects. This applies a shift to the brightness of a given SN as a function of its redshift, with an average correction of $|\mu_{bias}| \sim 0.016$ over our redshift range. Other bias corrections, such as the '4D' bias correction (see Popovic et al., 2021b; Vincenzi et al., 2024) model biases as a function of z, x_1 , c, and $\log(M_*)$. This framework includes an underlying model that makes assumptions about how SNe Ia and dust vary by host properties, which is part of the motivation for this chapter, and thus we elect to use only the '1D' bias corrections. However, we do compare our results to '4D' bias corrected brightnesses where relevant.

As the purpose of this work is to investigate the effects of the position in the host on SN properties and standardisation, we do not apply the $G_{host,i}$ term. This allows our sample and standardisation to remain affected by differences in host properties, and thus we may probe effects on standardisation that host properties may have.

We present the difference between our assumed cosmology of a flat Λ CDM universe with $\Omega_{\text{matter}} = 0.3$, and with a Hubble constant of $H_0 = 70 \, \text{km s}^{-1} \, \text{Mpc}^{-1}$ and the standardised brightness for each SN calculated above (the 'Hubble residual' of each given SN) in Figure 5.3. Of note is that there is no significant evolution of average Hubble residual as a function of d_{DLR} .

5.3.1 The Host Mass Step

There exists a so far unexplained problem in supernova standardisation. The apparent excess brightness of supernovae in high mass hosts by around 0.05-0.1 magnitudes (Sullivan et al., 2010; Kelly et al., 2010; Lampeitl et al., 2010; Betoule et al., 2014; Scolnic et al., 2018; Brout et al., 2022; DES Collaboration et al., 2024b) has no overall consensus to its astrophysical cause. This mass step still exists in the DES-SN 5 year sample, as can be seen in Figure 5.4. This step is highly significant at $\sim 7~\sigma$ (0.078 ± 0.011 mag), and around 4 times the size of the

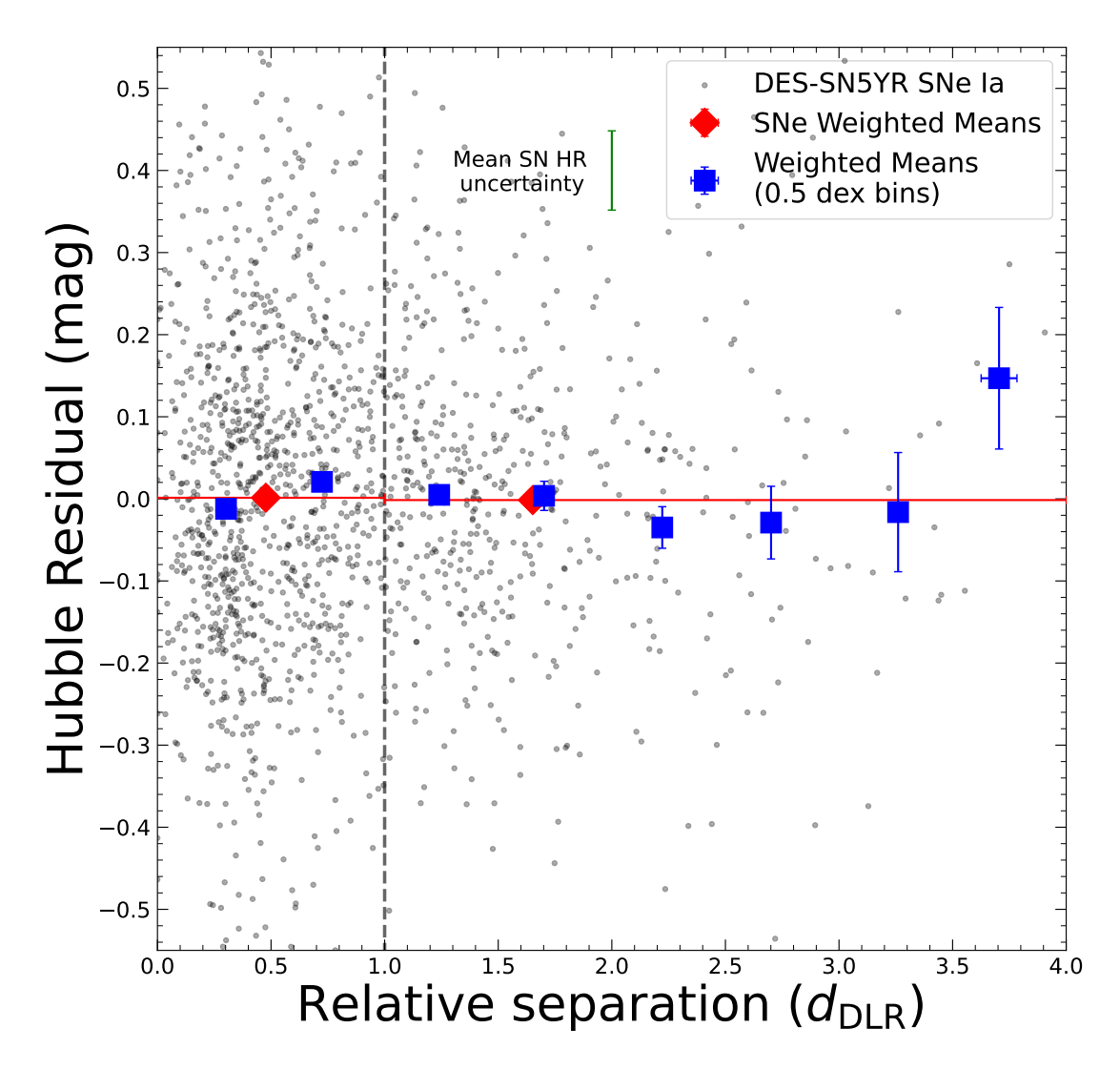


Figure 5.3: Hubble residuals for our sample as a function of $d_{\rm DLR}$. There is no significant evolution of average Hubble residual as a function of $d_{\rm DLR}$.

average bias correction we have performed. The size of the step is consistent with that found in Sullivan et al. (2010), which found a systematic increase in brightness of SNe in massive hosts of 0.06 - 0.09 mag, using SNe from the Supernova Legacy Survey (SNLS) (Guy, J and Sullivan, M et al., 2010).

Many attempts have been made to understand the astrophysical phenomena behind the mass step without simply correcting for it via γG_{host} in the Tripp equation (Eq. 5.1). Measuring and accounting for local specific star formation (hereafter LsSFR) can reduce the size of the host mass step (Rigault et al., 2020). However, such a correction introduces a LsSFR step larger than the mass step, an indication that LsSFR may be probing one of the underlying causes of the mass step (Briday et al., 2022). Re-fitting samples based on differing SN colour (and possibly dust) laws also can reduce or remove this step (Brout & Scolnic, 2021). Brout & Scolnic (2021) uses 1450 spectroscopically confirmed SNe, and finds that the difference in brightness post-standardisation seen in low and high mass galaxies depends on the SN colour, with redder SNe having a larger mass step size than bluer SNe. They refit this trend of SN Hubble residual

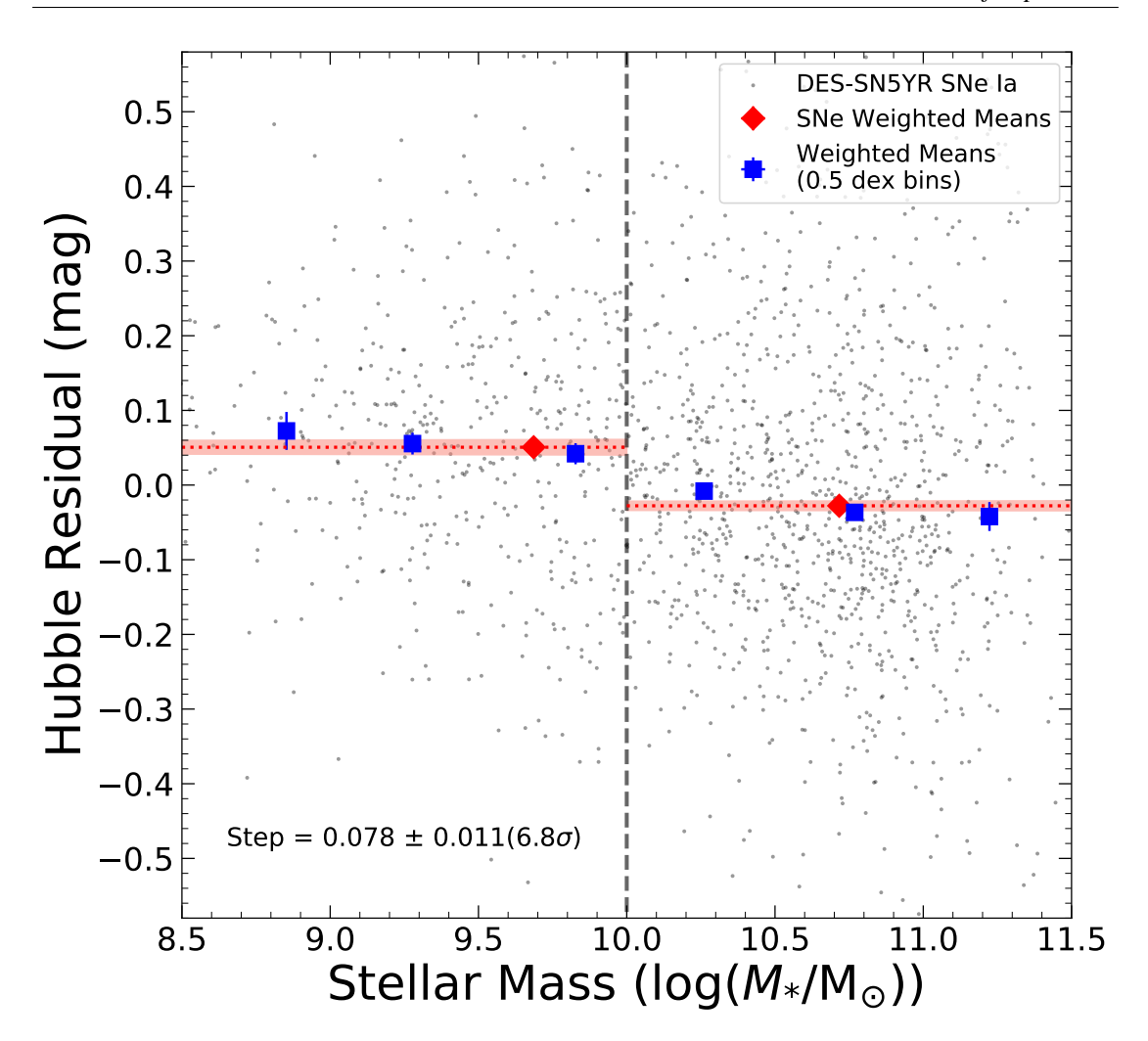


Figure 5.4: The Hubble Residuals for the DES 5 year photometric sample, fit with 1 dimensional bias corrections only as a function of their host galaxy stellar mass. When split into bins above and below a stellar mass of $10^{10} M_{\odot}$, there is a difference of 0.078 ± 0.011 magnitudes between the low and high mass weighted averages.

with the SN colour with two different dust laws, with those in low mass hosts having a mean $R_V = 2.75 \pm 0.35$ and high mass hosts having a mean $R_V = 1.50 \pm 0.25$, further developed with supporting results of an evolving R_V dependent on host galaxy properties in Wiseman et al. (2022b).

While these above attempts to explain the mass step rely on spectroscopic classification of their SNe, recent studies have shown similar trends with photometricically classified samples, such as the Amalgame sample (Popovic et al., 2024). As such while analysing any host mass step we cannot ignore the effects of star formation rate and dust driving any steps we see.

5.3.2 Host Mass Step as a function of d_{DLR}

We previously identified that SN light curve properties depend on their radial distance from their host centre. The standardisation of SNe, and therefore best fit to a cosmology, depends on

TABLE 5.2: Statistics related to the steps in SN Ia luminosity as a function of stellar mass (the mass step) in our samples.

Campla	Number	Mean $\Delta \mu$ in	Mean $\Delta \mu$ in	Size of the	Significance	r.m.s in	r.m.s in
Sample	(LM hosts, HM hosts)	low-mass hosts	high-mass hosts	mass step	of step	low-mass hosts	high-mass hosts
Full Sample	1533 (472, 1061)	0.051 ± 0.009	-0.028 ± 0.007	0.078 ± 0.011	6.8σ	0.199	0.226
$d_{DLR} \leq 1$	1028 (310, 718)	0.065 ± 0.012	-0.035 ± 0.009	0.100 ± 0.014	6.9σ	0.205	0.232
$d_{DLR} > 1$	505 (162, 343)	0.023 ± 0.014	-0.014 ± 0.011	0.036 ± 0.018	2.0σ	0.180	0.212

these properties and how they relate to the standardised brightness of the SNe. As such, we split our sample into inner $(d_{DLR} \le 1)$ and outer $(d_{DLR} > 1)$ regions and re-calculate the size of the host mass step, split at a stellar mass of $\log(M_*/M_{\odot}) = 10$. The results are shown in Figure 5.5.

SNe within the inner regions of their host galaxy have a larger mass step than in the 'whole' sample, with a step size of 0.100 ± 0.014 mag, significant at 6.9σ . We additionally calculate the root-mean-square deviation (r.m.s) for hosts on either side of the mass step as

$$\sigma_{\text{RMS}} = \sqrt{\frac{1}{N} \times \sum_{i=1}^{n} (x_i - x_0)^2}$$
 (5.2)

where N is the size of the sample, x_i is the given Hubble residual for any single SN and x_0 is the weighted mean Hubble residual for the sample.

The r.m.s on these inner region SNe is larger in both lower and higher mass hosts than in the full sample.

SNe within the outer regions however exhibit a significantly suppressed mass step, with a step size of 0.036 ± 0.018 , a significance of 2σ . The r.m.s on these SNe are also lower by ~ 0.015 mag in both high and low mass hosts than the whole sample. Due to the reduction of scatter in the Hubble residuals for this sample, it indicates a more robust standardisation for SNe in the outer regions compared to the inner regions. Values for the low/high mass hosts weighted Hubble Residuals, size of mass step, r.m.s and significance for all 3 of our samples can be found in Table 5.2

We verify the robustness of the detected decrease of the host mass step at higher $d_{\rm DLR}$'s via boot-strap resampling of the whole sample and selecting the same number of SNe as in the outer regions. As previous studies have determined a dependence on Hubble residual with colour, we weight the selection so that the resampled SNe have a similar colour distribution to those in the outer regions. We then re-calculate the size and significance of the host mass step. The results of this verification are shown in Figure 5.6. We see that on average, the step size of the resampled SNe is consistent with the whole sample, and while significant to a lesser degree due to a decreased sample size, ($\bar{\sigma} = 4.7 \pm 0.75$ for the resampled SNe vs $\sigma = 7$ for the whole sample) still above the 'typical' significance of $\sigma = 3$ for a significant result. We therefore conclude that our lack of step, and the selection required to identify it is not due to random chance.

Table 5.3: The best fit parameters and reduced χ^2 for a linear trend and a step function to Figure 5.7.

	Linear Fit	
Reduced χ^2	Gradient	Intercept
0.92	-0.041 ± 0.08	0.11 ± 0.010

Step Function					
Reduced χ^2	Step Location	A	В		
0.82	1.0	0.099 ± 0.316	0.020 ± 0.01		

To determine if the observed difference in mass step size between inner and outer regions is best fit by a single split at $d_{\rm DLR}$ = 1, we split our sample into more than two $d_{\rm DLR}$ bins. As the number of SNe often trace the profile of galaxy light (Anderson et al., 2015), we use bins that increase in size from a $d_{\rm DLR}$ of 1 so we have similar numbers of SNe in each bin. We then fit both a step function and a linear trend to the data, via χ^2 minimisation. The results of this finer binning and fitting are shown in the upper panel of Figure 5.7, and the best fit parameters and corresponding reduced χ^2 values are shown in Table 5.3. In the lower panel we show the best fit reduced χ^2 as a function of $d_{\rm DLR}$ split location. We see that a split at $d_{\rm DLR} \sim 1$ provides the best fit to the data, further reinforcing our choice of split location.

5.3.3 Line of sight effects

Some galaxies within our sample may be side on, which means that our inner region sample could be more contaminated with SNe within the outer regions, attributed to inner regions due to line of sight effects. The outer regions however should be less affected by line of sight effects, as any SNe in these regions would remain within the outer regions regardless of depth.

To investigate the effect on the host mass step within our inner region SNe, we calculate the eccentricity, $e_{\rm gal}$, of each host galaxy,

$$e_{\rm gal} = \sqrt{1 - \frac{b^2}{a^2}} \tag{5.3}$$

where *b* and *a* are the semi-minor and semi-major axis of the host galaxy. We show the distribution of host eccentricities for our inner region sample in Figure 5.8. Around 400 SNe have an eccentricity higher than 0.5, over half the sample.

We then limit our inner region sample to only those hosts we are confident are face on, i.e. those with an eccentricity below 0.5, and recalculate the host mass step. This is shown in Figure 5.9. While the significance of the host mass step decreases from $\sim 7\sigma$ to 4.0σ , its magnitude remains consistent with the inner region sample with edge-on ($e_{\rm gal} > 0.5$) galaxies included. We attribute the decrease in significance to the limiting of the sample in size, and the subsequent increase in error on the weighted means. Performing this eccentricity selection may erroneously remove face-on elliptical that are disturbed. As this is likely to affect mainly higher mass galaxies, and we see little change in the mean Hubble Residual in these galaxies we determine that this potential exclusion is not a dominant effect.

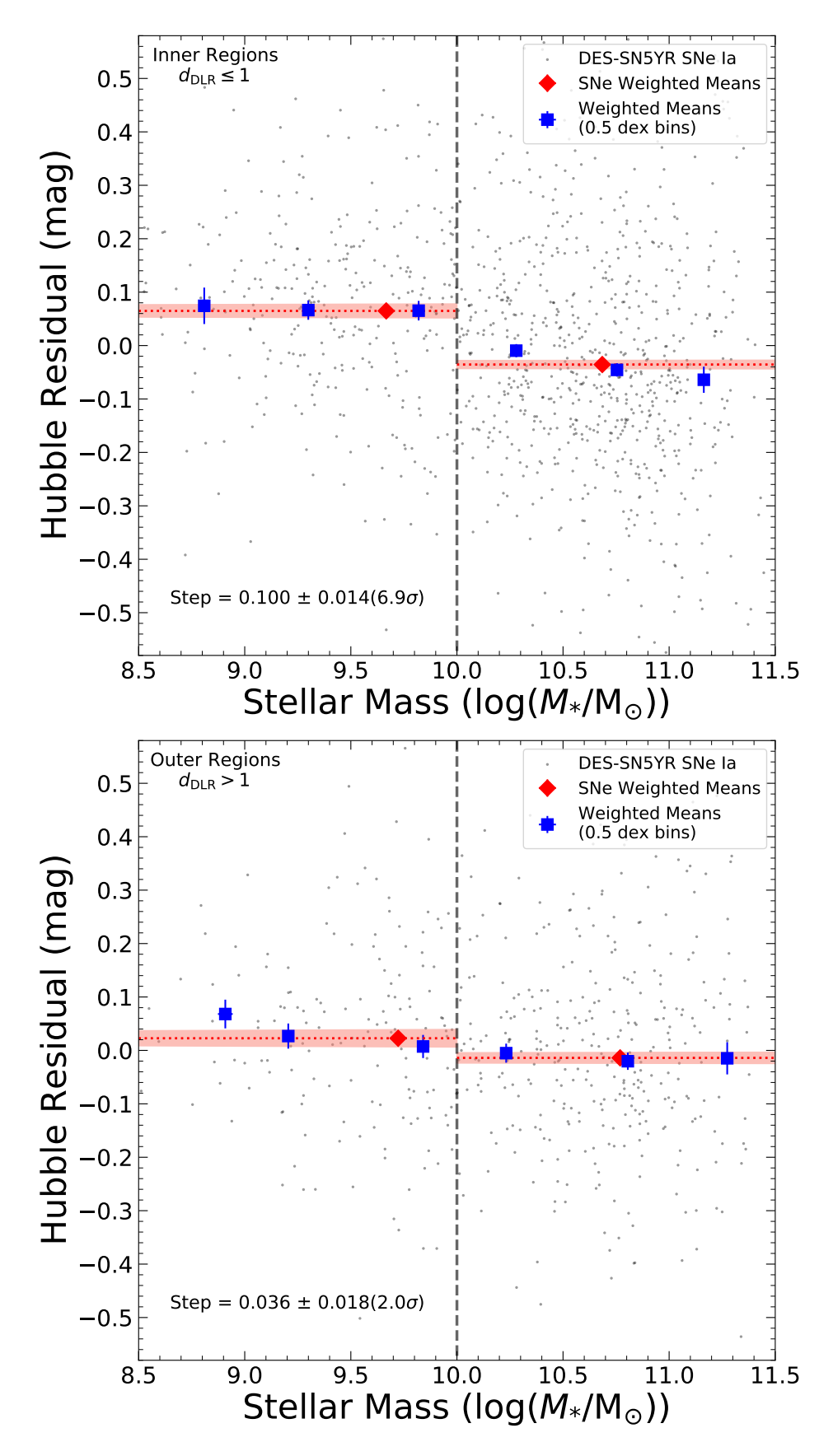


Figure 5.5: Top - As Fig. 5.4, but limited to SNe with $d_{\rm DLR} \leq 1$. The observed step between the SNe in low and high mass hosts increases to 0.100 ± 0.014 mag. Bottom - As Fig. 5.4, but limited to SNe with $d_{\rm DLR} > 1$. The observed step between the SNe in low and high mass hosts decreases to 0.036 ± 0.018 mag.

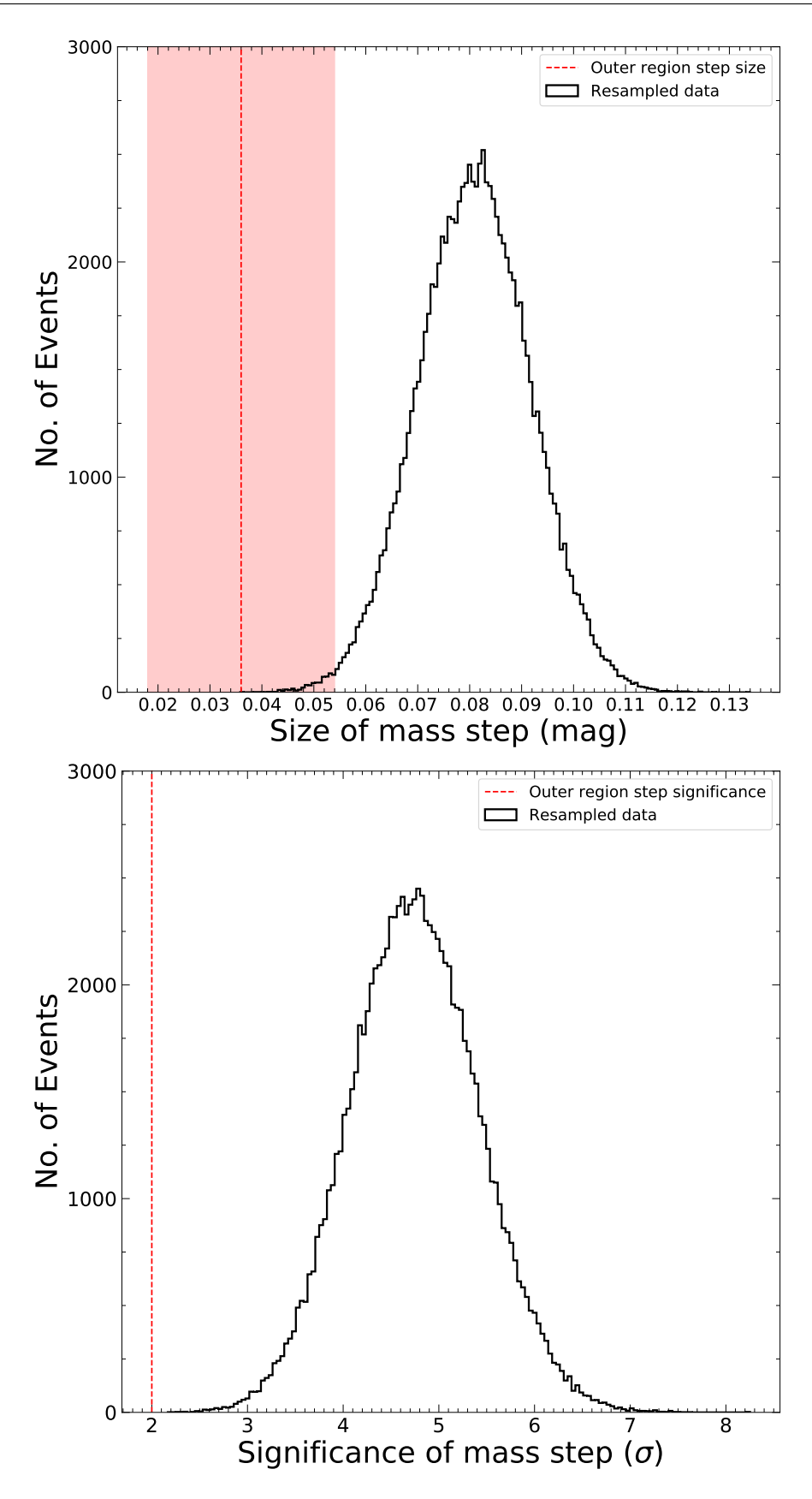


FIGURE 5.6: Upper panel: The size of the host mass step, calculated for each realisation of our resampling, outlined in Section 5.3.2. The distribution appears broadly Gaussian, centred on a step size of 0.08 mag. Such a step size is consistent with the host mass step observed in our full sample. Lower panel: As the upper panel but instead the significance of the host mass step. It is centred between $3\sigma - 4\sigma$, showing that on average, a statistically significant step is found in our resampled SNe. Shown by the dashed red line in both are size and significance of the host mass step measured in the outer regions.

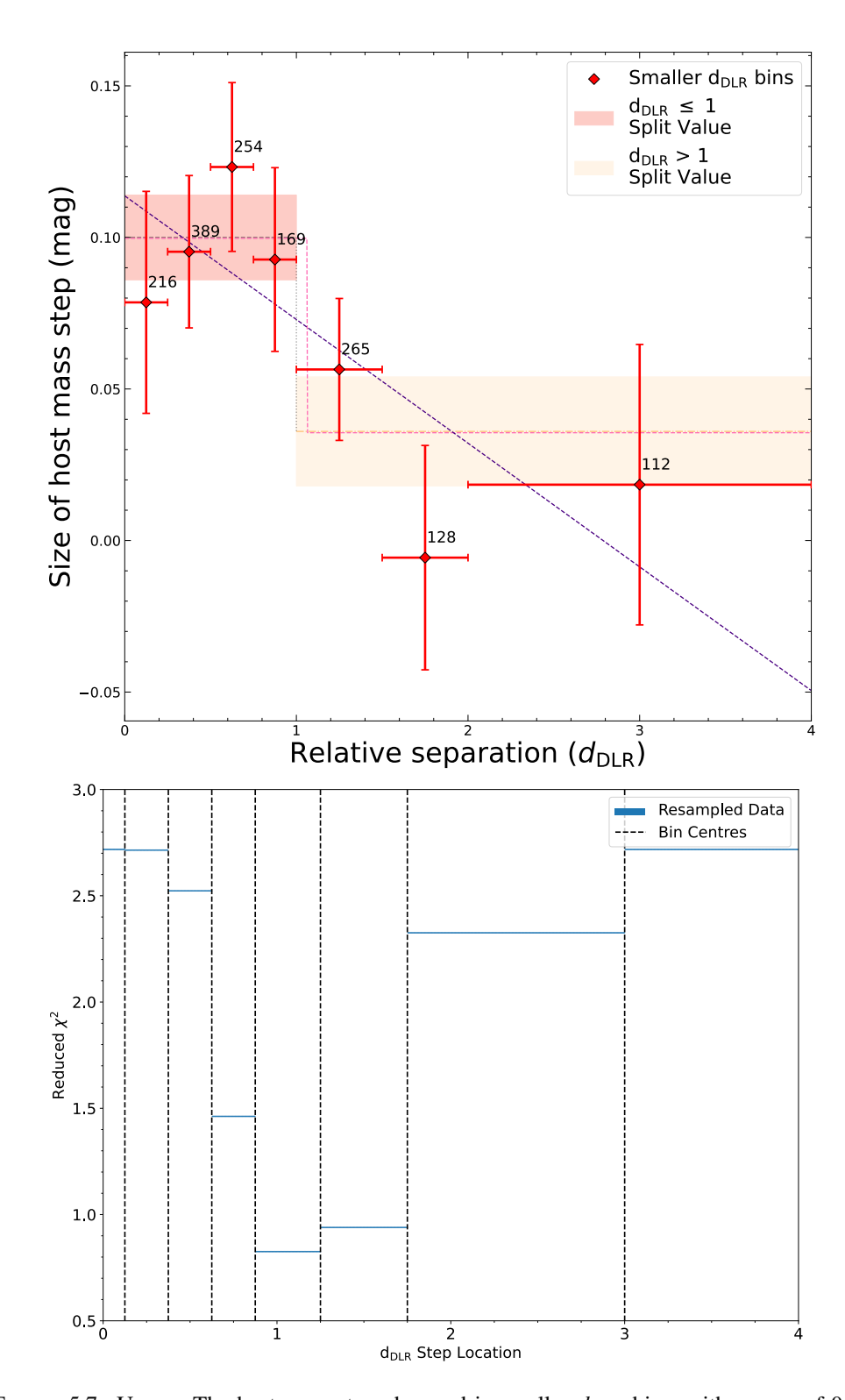


FIGURE 5.7: Upper: The host mass step observed in smaller $d_{\rm DLR}$ bins, with a span of 0.25 dex between $0 \le d_{\rm DLR} \le 1$, increasing to 0.5 dex up to a $d_{\rm DLR} \le 2$ and finally 1 dex at $d_{\rm DLR} > 2$. We fit both a step function and a linear function to our data, and find both have similar goodness-of-fit values, outlined in 5.3. Numbers show the amount of SNe within each $d_{\rm DLR}$ bin. Lower: The reduced χ^2 for differing step positions. Due to binning this only changes once the bin centres (shown in the dotted black lines) have been passed. We see that the best fit step function is located around 1.0, verifying the choice of location for our previous $d_{\rm DLR}$ split.

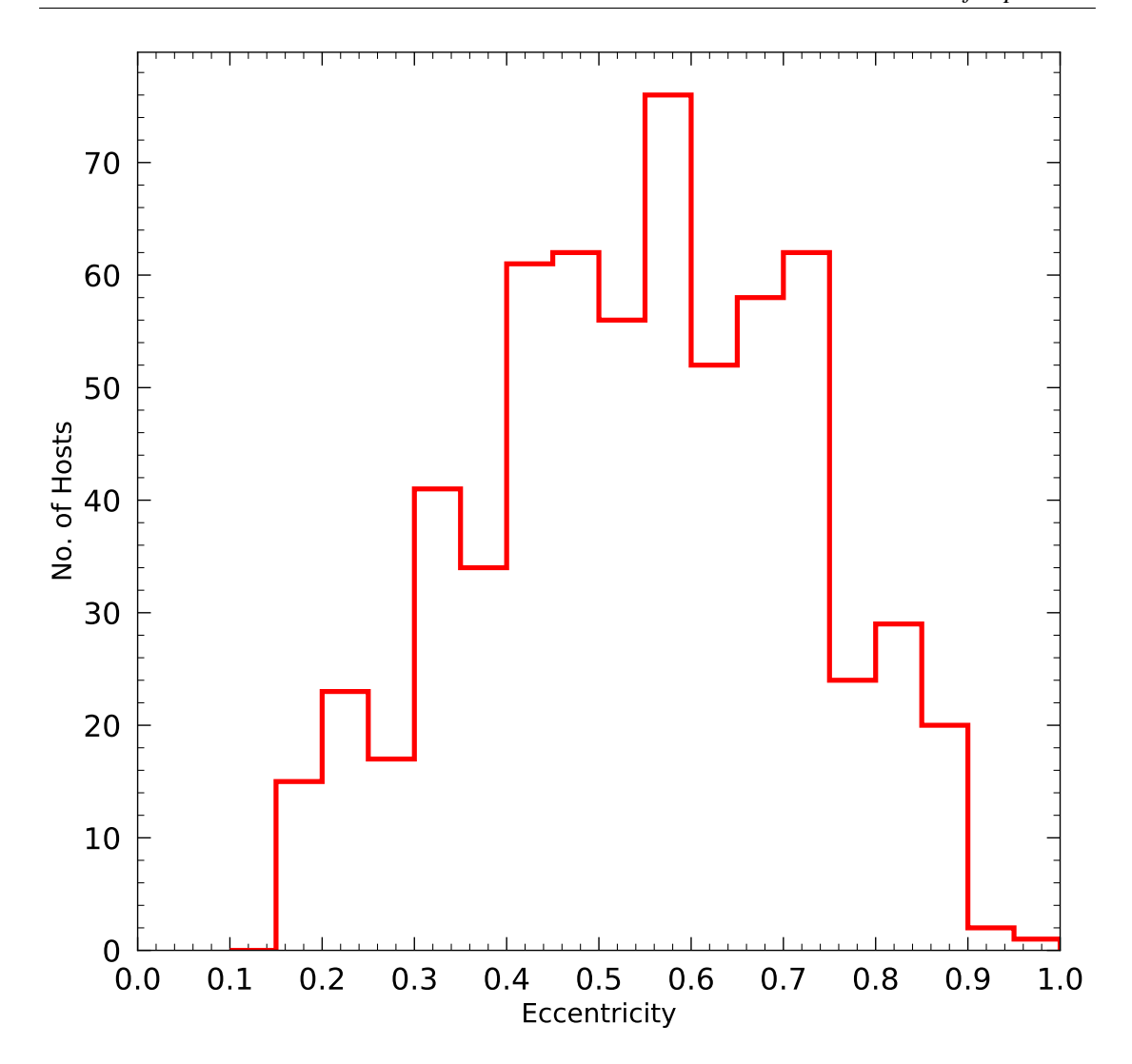


FIGURE 5.8: Eccentricities of host galaxies within our inner region sample.

This similar mass step size after limiting the potential line of sight effects from our sample implies that these effects have little to no influence on our results.

5.3.4 Other steps

Stellar mass is not the only host property that has previously had a measured 'step' in their Hubble residuals. For example, the colour of the host galaxy (e.g. Roman et al., 2018; Kelsey et al., 2021) has previously been measured to have a similar size step when compared to galaxy mass, but to a higher significance.

We find a similar result in our sample, where within the inner region there exists a 7.6σ 'colour step' (a difference in the weighted mean values of Hubble residual as a function of host colour) when splitting between red and blue hosts (defined by a split at U - R = 1 following (Kelsey et al., 2022)). Within the outer regions however, this step is still negligible. We show these steps in Fig. 5.10.

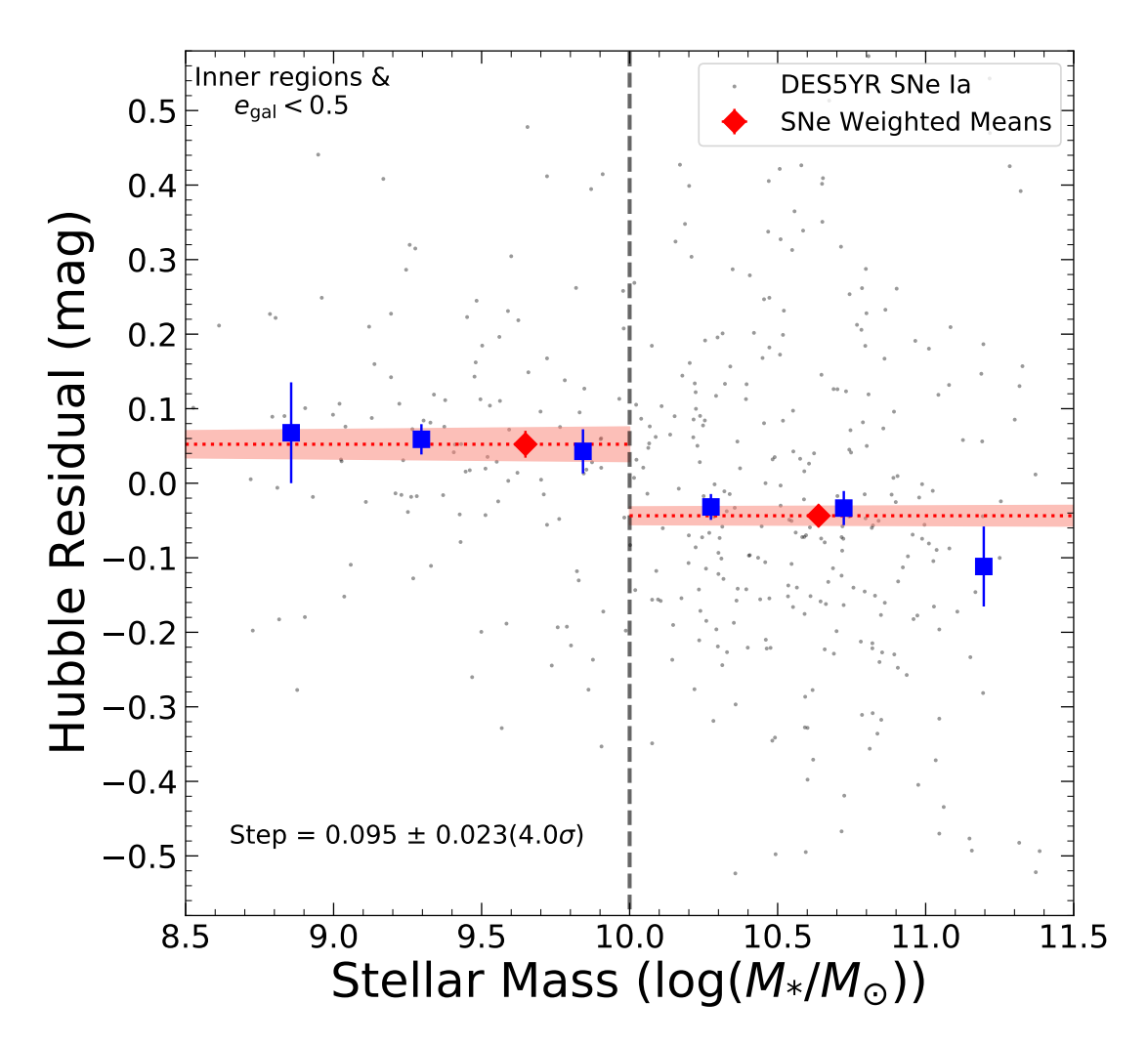


FIGURE 5.9: As the upper panel of Figure 5.5 but limited to host galaxies with an eccentricity below 0.5, calculated with Equation 5.3.

To further investigate this effect within our sample, we calculate the average Hubble residual for those in blue hosts and red hosts in $d_{\rm DLR}$ bins. We also perform a similar calculation, but instead calculate the host colour for inner and outer regions separately, with host colour measured in an aperture defined at $d_{\rm DLR}$ = 1 and an annulus defined by 1 < $d_{\rm DLR}$ < 4. We present this calculation, and compare it to the average Hubble residual in high and low mass hosts, in Fig. 5.11.

It is clear to see that any difference in the weighted mean values of Hubble residual as a function of host colour, be it local or global colour additionally is drastically reduced above a $d_{\rm DLR}$ of 1. This gives further credence that the post-standardisation brightnesses of SNe Ia within the outer regions of galaxies are less affected by the properties of their host than those in the inner regions.

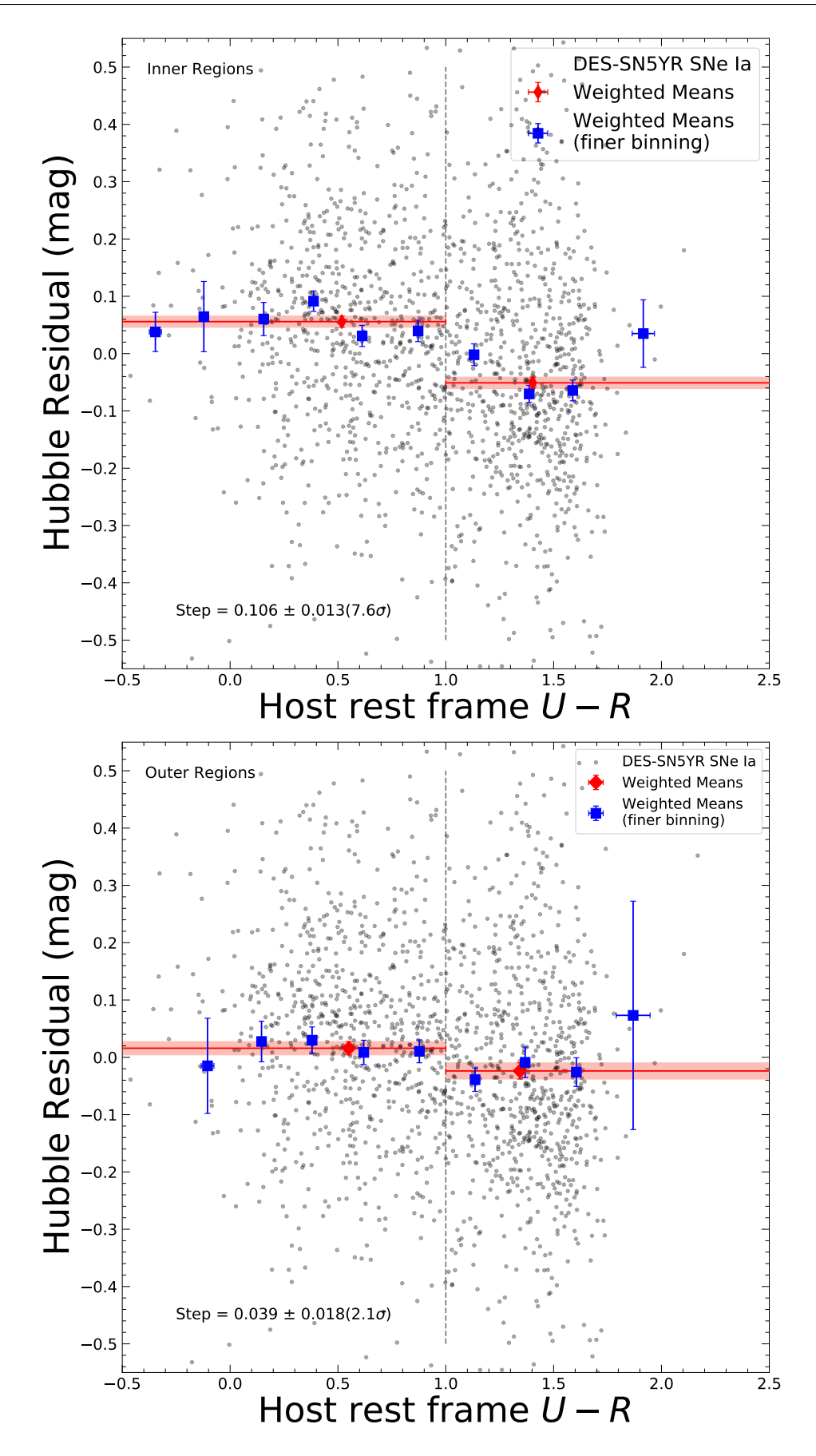


Figure 5.10: As Fig. 5.5 but for host galaxy rest-frame U-R colour. The step sizes are 0.106 ± 0.013 mag (left) and 0.039 ± 0.018 mag (right).

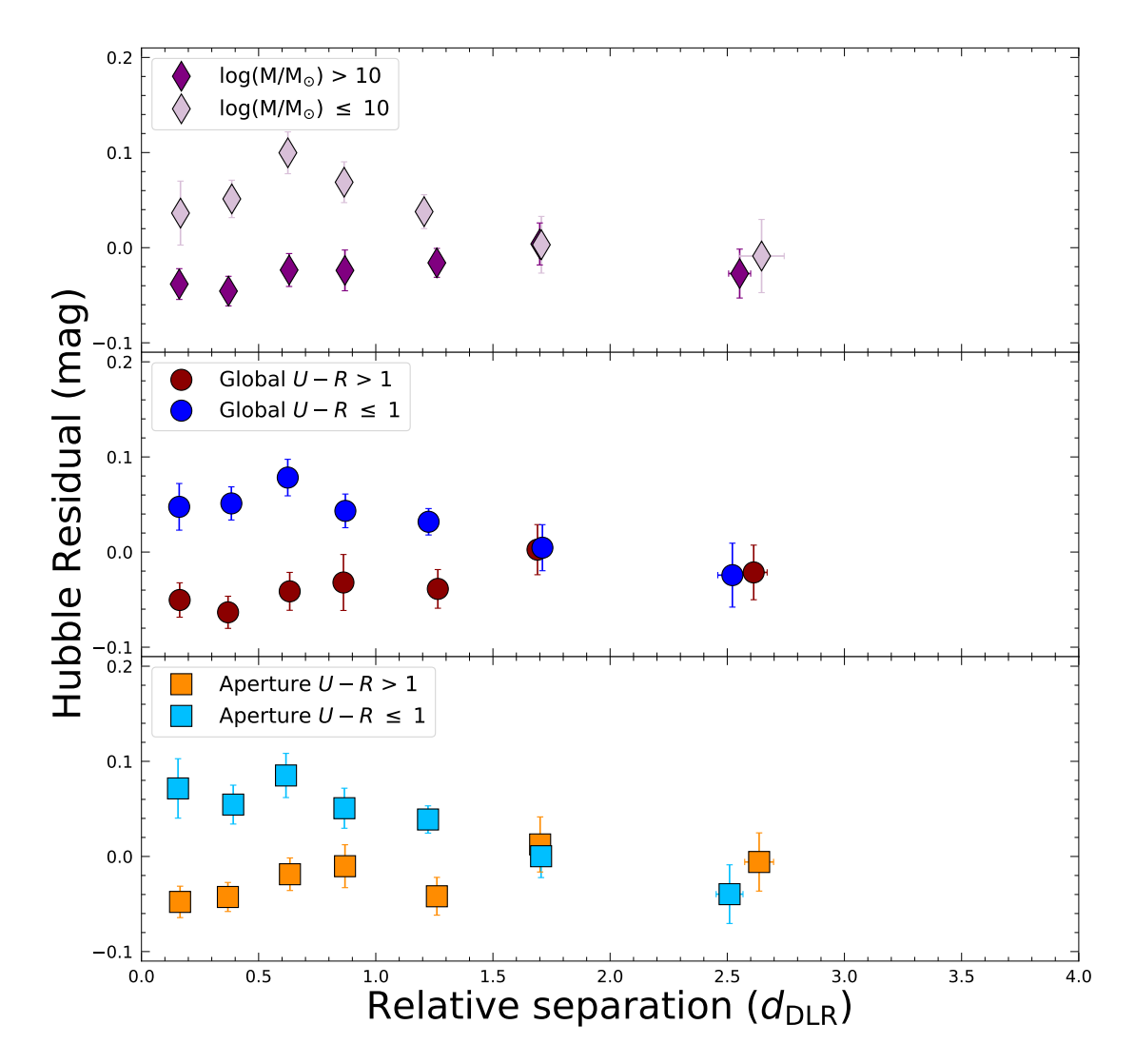


FIGURE 5.11: The host mass step observed in smaller $d_{\rm DLR}$ bins of 0.25 dex over $0 \le d_{\rm DLR} \le 1$, 0.5 dex over $1 < d_{\rm DLR} \le 2$, and 2 dex at $d_{\rm DLR} > 2$. The Hubble residuals split into low and high stellar mass samples (top panel), split by the global host galaxy rest-frame U-R colour (middle panel), and split by an aperture U-R colour (lower panel).

5.3.5 Could it be dust?

Previous studies have proposed a differing dust law in low and high mass hosts to explain the host mass step (Brout & Scolnic, 2021; Popovic et al., 2024) etc. Here we investigate if a similar effect is occurring within our samples in outer and inner regions.

We show our colour distributions in Figure 5.12, split by hosts on either side of the mass step. We assume a similar colour distribution as Brout & Scolnic (2021); Popovic et al. (2021a), where the intrinsic colour distribution for a given sample of SNe is fit by a Gaussian, and reddening by dust introduces an exponential tail.

As such, we fit both normal Gaussian (Equation 5.4) and Gaussian with an exponential tail (Equation 5.5) probability functions to each sample.

$$f(x) = \frac{\text{Amplitude}}{\sigma \sqrt{2\pi}} \times e^{\frac{1}{2} \left(\frac{x-\mu}{\sigma}\right)^2}$$
 (5.4)

$$f(x; \mu, \sigma, \tau) = \frac{\text{Amplitude} \times \tau}{2} \times e^{\frac{\tau}{2}(2\mu + \tau\sigma^2 - 2x)} \times \text{erfc}\left(\frac{\mu + \tau\sigma^2 - x}{\sqrt{2}\sigma}\right)$$
(5.5)

In both equations, μ , σ are the mean and the standard deviation of the distribution respectively. 'Amplitude' allows the peak of the distribution to shift up or down from the peak of the distribution and τ is the rate of the exponential component. 'erfc' is the complementary error function, defined as

$$\operatorname{erfc}(x) = \frac{2}{\sqrt{\pi}} \int_{x}^{\infty} e^{-t^{2}} dt.$$
 (5.6)

We calculate the least squares of both a Gaussian fit and an Gaussian plus exponential tail fit, and, after dividing the least squares by the number of free parameters, define the best fit as the model with the lowest reduced χ^2 .

We find both samples are best fit by a Gaussian with an exponential tail, with similar parameters (all parameters are within 1σ except the standard deviations, which are higher for the low mass hosts, likely due to the lower sample size) for their best fit. This, while a basic test, is an indication that dust is reddening SNe in both high and low mass hosts to a similar degree.

We additionally perform this calculation on both the SNe in the inner and the outer regions of their host galaxy. This is presented in Fig 5.13. SNe in the inner region appear similar to the full sample in Fig 5.12. However, SNe in the outer regions in low mass hosts are not best fit with an exponential tail. This may indicate that we have a lack of reddened SNe within these regions, perhaps not entirely unexpected result given the amount of dust within a galaxies increases with stellar mass (Santini et al., 2014). It is also possible that red SNe in outer regions are not reddened due to dust, and instead this shows the intrinsic colour distribution of type Ia SNe. We show the reduced χ^2 for each fit to each sample, along with the best fitting parameters in Table 5.4.

This apparent lack of reddened SNe in the outer regions of low mass hosts would be initially attributed as the cause of a lack of step we observe, as this would indicate two distinct populations in the outer regions: Low mass, dust free regions and high mass regions obscured by some dust.

We analyse this as a cause for the lack of step in Figure 5.14. The upper panel shows the Hubble residuals for our full SN sample limited to the outer regions of their host, split between low and high mass, as a function of their SALT3 colour. Critically, across all SNe colours we observe no significant difference between SNe in low or high mass hosts. While a reconfirmation of the

	High mass	High mass	Low mass	Low mass	Best fit	Best fit parameters
Sample	$\left egin{array}{c} \chi^{\mathcal{L}}_{ m red} \ & & & & & & & & & & \end{array} ight { m Eaussian only} \ \left { m E} ight $	$\chi^{z}_{ m red}$ Exponential Gaussian	$\chi^z_{ m red}$ Gaussian only	$\chi^{arsigma}_{ ext{red}}$ Exponential Gaussian	parameters high mass	low mass
					$\bar{c} = -0.071 \pm 0.009$	$\bar{c} = -0.074 \pm 0.005$
En II Comple	03.0	1 00	2 10	1 27	$\sigma = 0.009 \pm 0.006$	$\sigma = 0.060 \pm 0.004$
run sampie	6.7	1.99	5.10	17:1	$\tau = 0.080 \pm 0.012$	$\tau = 0.083 \pm 0.007$
					scale = 1.006 ± 0.029	scale = 0.99 ± 0.032
					$\bar{c} = -0.073 \pm 0.008$	$\bar{c} = -0.073 \pm 0.007$
\ \ \	1 33	0.01	2 13	1.46	$\sigma = 0.095 \pm 0.005$	$\sigma = 0.0533 \pm 0.005$
uDLR ≥ 1	1.32	0.01	3.12	1.40	$\tau = 0.084 \pm 0.010$	$\tau = 0.092 \pm 0.011$
					scale = 1.015 ± 0.025	scale = 0.983 ± 0.043
					$\bar{c} = -0.069 \pm 0.013$	2 0017 - 0004
7	100	2 11	77.0	13.8	$\sigma = 0.082 \pm 0.011$	$c = -0.017 \pm 0.004$
uDLR / 1	7.7.7	7.11	0.77	15.0	$\tau = 0.078 \pm 0.018$	0.030 ± 0.004
					scale = 0.965 ± 0.050	scale = 0.900 ± 0.047

Table 5.4: A table showing the reduced χ^2 values for both an exponential and regular Gaussian for both high and low mass hosts for each of our samples. Additionally, the best fit parameters are shown. They may also be found in the legends of Figures 5.12 and 5.13.

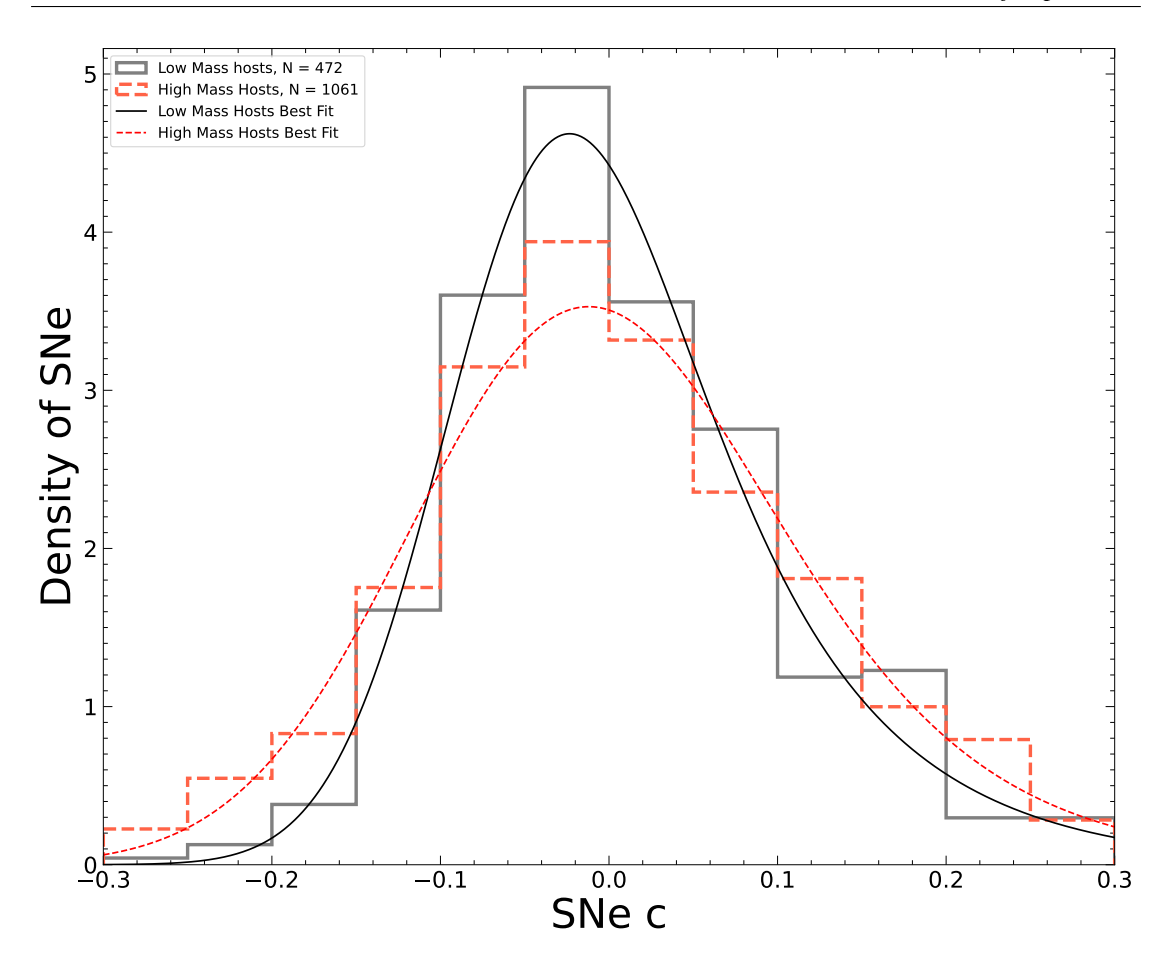


Figure 5.12: Colour distributions for our sample, split by low (black) and high (red) mass hosts. Over-plotted are the best fit to the data. In this case both high and low mass hosts are best fit by a Gaussian with an exponential tail.

lack of step previously measured in these outer regions, it does show this lack of step is not due to averaging, where blue SNe could have the opposite step size to red SNe.

Comparing this to the inner regions, we see an increasing difference between low and high mass hosts as SN colour increases. This lack of step in reddened SNe in the outer regions would point to a similar dust law (R_v) in high and low mass hosts, if methods from previous studies such as Brout & Scolnic (2021) were used, where they alter the colour component of the Tripp equation shown in Eq. 5.1 as such,

$$\beta c_{\text{SN}} \longrightarrow \beta_{\text{SN}} c_{\text{SN,int}} + (R_{\nu} + 1) E_{\text{dust}}.$$
 (5.7)

Where $R_v + 1$ is the dust law governing the B band reddening (The band SNe are typically standardised in) and E_{dust} is the colour excess due to the dust. As such populations with dust are modelled not by only an intrinsic colour with an exponential tail but include the reddening on an intrinsic colour distribution due to the effects of dust.

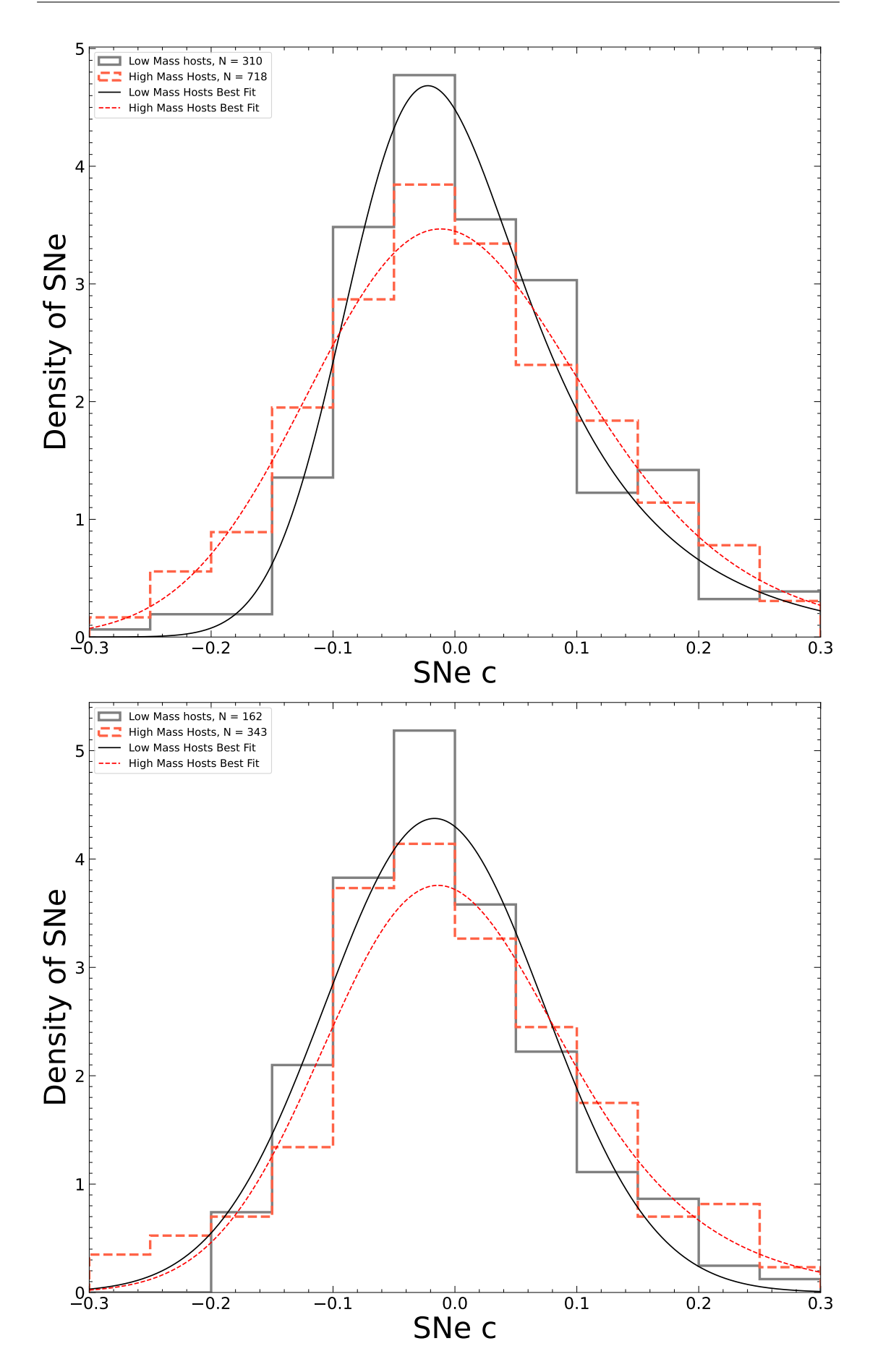


FIGURE 5.13: Same as Fig 5.12, but split by Inner (upper) and outer (lower) regions. Notably, the low mass SNe hosts in outer regions are the only distribution **not** best fit by a Gaussian with an exponential tail.

However, within the outer regions there appears to be little dust present in the lower mass hosts, as indicated by the lack of exponential tail in their SALT3 colour distributions. To reconcile this, the dust content in the outer regions may have little evolution as a galaxy grows, while the inner regions dust evolves more drastically. This would allow the outer region SNe to behave similarly while the inner region SNe would diverge.

Applying a '4D' bias correction (described in Chapter 5.3), which should correct for diverging dust parameters, we see that a step exists even in the slightly blue ($c \sim -0.05$) SNe in the inner regions, between low and high mass hosts, however we observe no such step between these two samples in the outer regions. This means the host mass step we measure in the inner regions is seemingly intrinsic, and not solely due to dust, as effects from dust on the Hubble residual would be reduced in bluer SNe. We show this effect in Fig. 5.15.

Combining all the evidence here, we see that adjusting for differing dust laws can reduce, but crucially not remove the observed step in the inner regions. However, in the outer regions there is no evolution of the dust law governing SNe $c_{\rm SN}$. As such we disfavour dust as the sole cause of this lack of host-mass step we observe in the outer regions (as such a correction still does not remove the step in the inner regions!). Instead, we observe a systematic increase in the average Hubble residual for SNe in high mass hosts, and corresponding decrease in low mass hosts in these outer regions compared to the inner regions. Consequently, the average of both high and low mass SNe's Hubble residuals is roughly 0, i.e little-to-no offset from the cosmological model. However, we cannot say that dust is not contributing to the observed step in the inner regions, only that it is not the sole cause of the step, as after dust corrections the step is reduced but not removed in these regions.

5.3.5.1 Other influences on the mass step

While we disfavour dust as the sole cause of the lack of observed step between high and low mass hosts and determine little to no influence on the step due to line of sight effects, there are other properties of SN hosts that could be driving this trend. We briefly discussed that fitting for LsSFR, a good tracer for the age of the stellar population around a given SNe, when calculating SNe distances reduces the size of the observed mass step. This method instead translates the mass step into an 'age step', with older stellar populations hosting brighter SNe after corrections, and vice versa.

We perform a similar test in Figure 5.16, where we calculate the step between globally star forming and passive galaxies, split at $\log_{10}(\text{sSFR}) = -10 \text{ yr}^{-1}$. We find that there remains a significant step in brightness between star forming and passive galaxies in the inner regions, shown in the upper panel. Again, any step present in the outer regions remains insignificant, and consistent with 0.

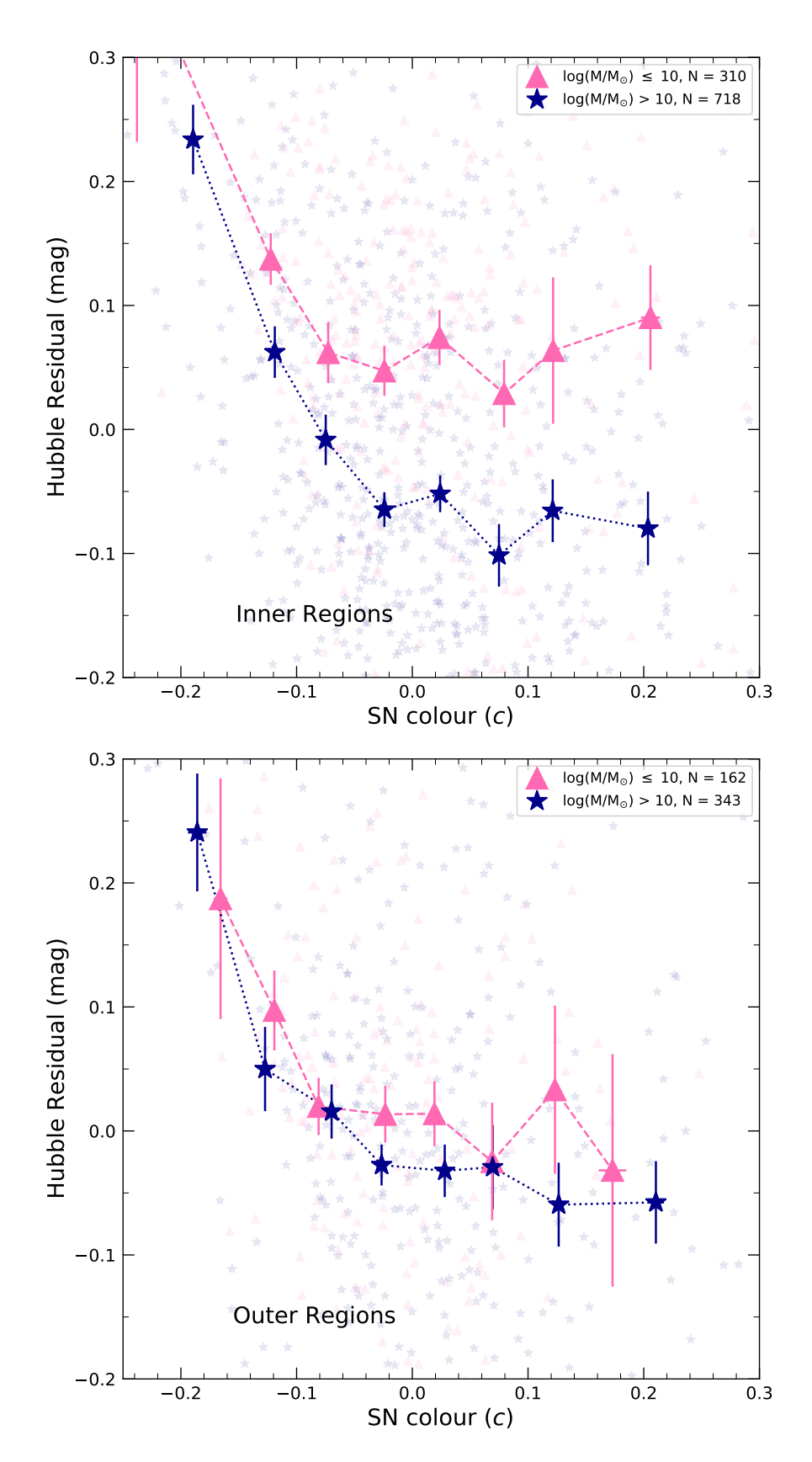


Figure 5.14: Hubble residuals for our inner (upper panel) and outer (lower panel) regions as a function of SALT3 colour. We observe no significant difference in mean Hubble residual between low and high mass hosts at any SNe colour in the outer regions.

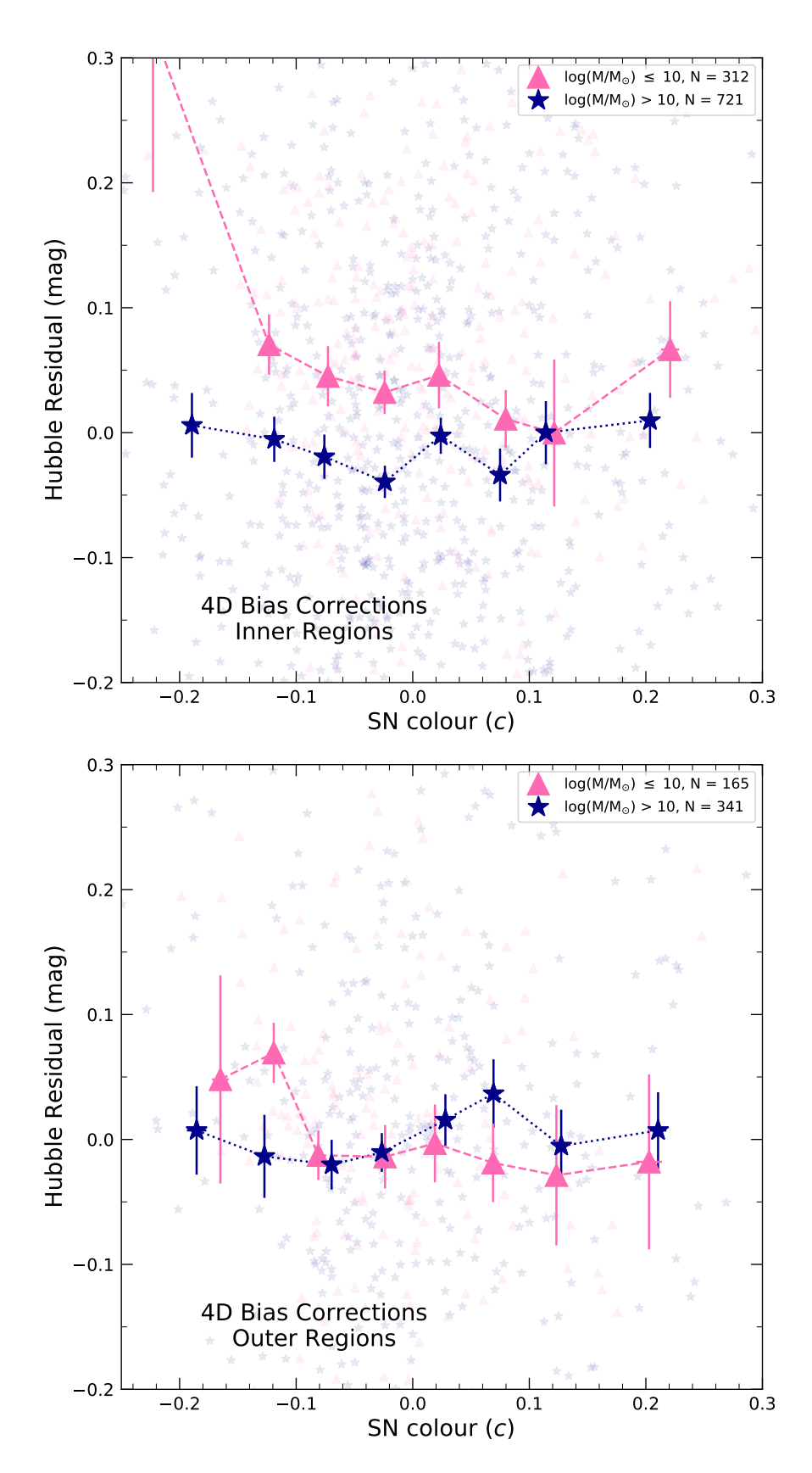


Figure 5.15: Hubble residuals for our inner (upper) and outer (lower) regions as a function of SALT3 colour $c_{\rm SN}$, plotted separately for events in low and high-mass host galaxies, after having made a BBC 4D correction for the colour-dependent selection and dust bias.

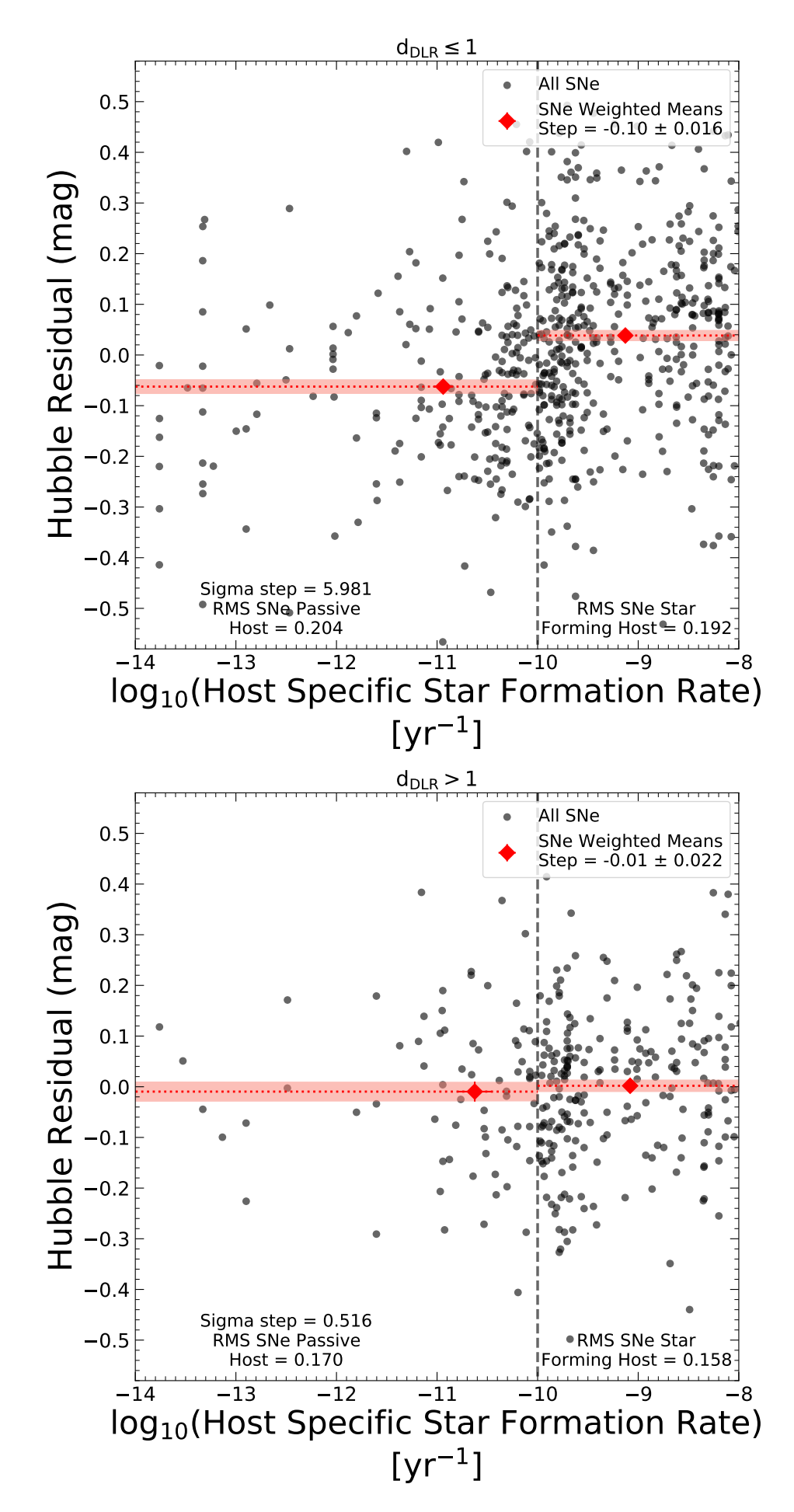


FIGURE 5.16: Hubble residuals for our inner (upper panel) and outer (lower panel) regions as a function of their host specific star formation rate, split at $log_{ssfr} = -10$.

Such a dichotomy between inner and outer regions, after disfavouring both line of sight effects and dust effects as sole contributors, remains curious. There are several possible ways to reconcile these observations.

The first is that the inner regions are more diverse in the stellar ages around a SN and dust content, while the outer regions are more homogeneous in their stellar ages and dust content, even from galaxy to galaxy. This would remove any observed age step or dust step in these outer regions, and imply that the cause of the host mass step is due to a difference in age of stellar populations and a difference in dust content in high/low mass hosts.

Secondly, we are only considering the global sSFR. In Rigault et al. (2013), it was found that $\sim 50\%$ of SNe found in locally passive environments were hosted in globally star forming galaxies. As such using the global specific star formation above may not correctly identify the stellar population about the SNe.

5.4 Summary

Using the 5 year photometrically confirmed sample for DES, we have analysed the effects on host galaxy projection on the light curve properties. We also provide a way to homogenise the brightnesses between SNe in high and low mass hosts, without the need for complex dust simulations, and only accounting for the Malmsquist bias found at higher redshifts. Our main findings are:

- We confirm previous findings that the inner most regions of galaxies ($d_{DLR} \le 1$) host faster, fainter and slightly redder SNe than in the outer regions.
- We find that the difference in SNe brightness between high and low mass hosts is consistent with 0 in the outer regions, while present at $\sim 7\sigma$ in the inner regions and full sample.
- We find that the reduction of this step is well fit by both a step function, split at $d_{\rm DLR}$ of 1, or a decreasing linear function with $d_{\rm DLR}$.
- We show that using different R_V values for dust along the line of sight to SNe that varies between low and high-mass host galaxies, can reduce but not remove the step for SNe Ia in the inner regions.
- There is no evidence that the outer regions of galaxies have dust laws that change as a function of stellar mass.
- We attempt to probe the effect of age, and find no step between SNe in star forming and passive galaxies in the outer regions. However, previous studies have found that the global star formation rate is not the most accurate probe of a SN's local environment.

5.4. *Summary* 97

Calculating $d_{\rm DLR}$ is not a computationally expensive process, and selecting SNe Ia based on $d_{\rm DLR}$ reduces the need to account for host galaxy properties to standardise SN Ia brightnesses across different galaxies. While the underlying astrophysics that $d_{\rm DLR}$'s are tracing in the DES five-year SN Ia sample remains uncertain, we have shown that the standardised distance measurements from SNe Ia in the outer regions of galaxies have little dependence on their global host galaxy properties.

Restricting a cosmological analysis to SNe Ia in the outer regions of their host galaxies reduces the sample size to around a third. This increases the statistical uncertainties on such a sample. However, the reduction in the astrophysical systematic uncertainties (and complications) gained from using such a sample, coupled with the very large sample sizes expected in future experiments such as the Rubin Observatory's Legacy Survey of Space and Time (LSST, Ivezić et al., 2019), means that such a selection is likely to be beneficial.

Chapter 6

Conclusions

You see, at this point... I'm pretty much the Queen Bitch of the Universe

Sarah Kerrigan, Omega, StarCraft: Brood

War

6.1 Conclusions

Within the contents of this Thesis we have used photometrically classified type Ia supernovae from the Dark Energy survey, primarily to determine how the effects of both large and small scale environment affect type Ia supernovae.

To do this, we have used two different samples: One with a redshift cut of $z \le 0.7$, to offset the observed differences between cluster and field hosts, and one with no redshift cut. Both samples were restricted to 'cosmologically useful' type Ia supernovae, via selections on their light curve properties (Betoule et al., 2014; Vincenzi et al., 2021). The work on large scale structure focuses on investigating the difference in light curve properties and the respective rates. The smaller scale structure work focuses mainly on the observed difference in post-standardisation brightness between high and low mass hosts, and how this varies based on projected galactocetric distance.

Our main findings are, for ease, split between the work investigating the effects of the large scale environments within cluster of galaxies and those investigating smaller, galactic scale environments.

6.1.1 Differences in light curve properties and rates between cluster and field based type Ia supernovae

For the cluster based work our main findings are as follows:

- We find a tentative indication that the light curve widths, x_1 , of cluster SNe Ia are, on average, more negative (i.e., fainter and faster evolving) than their field counterparts. Although this is an expected result, as x_1 has a known dependence on galaxy stellar mass and age, the evidence is not strong in this sample. When just comparing galaxies with similar host masses and colours, the significance drops further, perhaps implying that any differences we see are due to the lack of low-mass, young cluster hosts. We find that the colours of cluster SNe Ia statistically match those of the field, with very similar distributions.
- There is no clear relationship between a SN's x_1 and its location in its host. The exception is for the innermost SNe Ia, which have smaller values of x_1 for both cluster and field hosts.
- We calculate the rates of SNe Ia in cluster and field environments, and find them to be broadly consistent to within 1σ . However, at higher masses this appears to change, with the rate of cluster SNe between $(11 \le \log(M_*/M_\odot) \le 11.25)$ being lower than the field by 3.6σ . Taking into account all mass bins with a detected cluster SN, the weighted average ratio of cluster to field SN rates is 0.594 ± 0.068 , however this average ratio is heavily driven by the final cluster mass bin.
- Integrating the overall rates of field and clusters within galaxies with $\log(M_*/M_\odot) \geq 10.0$, we find the rate of SNe Ia within clusters as a fraction of formed mass to be $0.0332 \pm 0.0040 \; (\mathrm{stat.})^{+0.0082}_{-0.0044} \; (\mathrm{syst.}) \; \mathrm{SNe} \; 100 \; \mathrm{yr}^{-1} \; 10^{10} \; \mathrm{M}_\odot^{-1}$, and the corresponding field rate to be $0.086 \pm 0.0069 \; (\mathrm{stat.}) \pm 0.0062 \; (\mathrm{syst.}) \; \mathrm{SNe} \; 100 \; \mathrm{yr}^{-1} \; 10^{10} \; \mathrm{M}_\odot^{-1}$. However, these measurements are at slightly differing redshifts, which will account for some of this difference and both are broadly consistent with other literature cluster rates. The measured decrease could be due to cluster galaxies being older, or more quenched than their field counterparts. Thus this declining rate within clusters compared to the field indicates that galaxies at a fixed mass are older in clusters than the field. We calculate that the rate in passive field galaxies is more comparable to the cluster rate, however a more complete dataset would be valuable in verifying this result.

6.1.2 Differences in light curve properties and post-standardisation brightness of type Ia supernovae between inner and outer regions of their host galaxies

We have separated type Ia supernovae based on their projected galactocentric distance into inner ($d_{DLR} \le 1$) and outer ($d_{DLR} > 1$) regions. We have then investigated the light curve

properties and post-standardisation brightness of type Ia supernovae within these two samples. Additionally, we investigate the post-standardisation brightness as a function of various properties of the supernova's host galaxy, such as its stellar mass and specific star formation rate. Our main findings are as follows:

- We confirm previous findings of Ivanov et al. (2000); Galbany et al. (2012) and Chapter 3
 that the innermost regions of galaxies (d_{DLR}≤ 1) host faster-declining SNe than the outer
 regions.
- We show, for the first time, that the difference in SN Ia post-standardization brightnesses between high and low-mass hosts reduces from 0.078 ± 0.011 mag in the full sample to 0.036 ± 0.018 mag for SNe Ia located in the outer regions of their host galaxies (d_{DLR} > 1), while increasing to 0.100 ± 0.014 mag for SNe in the inner regions (d_{DLR} ≤ 1). The effect remains when splitting SNe Ia by their global galaxy U − R colour, or by the U − R colour in the inner aperture/outer annulus in which the SN occurred.
- We find that the decrease in magnitude of this mass step as a function of $d_{\rm DLR}$ is well fit by either a step function, split at $d_{\rm DLR}$ of 1, or a linear function declining with $d_{\rm DLR}$.
- There is no evidence that the outer regions of galaxies have dust laws that change as a function of stellar mass. Similarly, there is no evidence for an intrinsic luminosity difference between SNe Ia in the outer regions of low and high-mass galaxies.
- We attempt to probe the effect of age, and find that no step between SNe in star forming and passive galaxies in the outer regions. However, previous studies have found that the global star formation rate is not the most accurate probe of a SNe's local environment.

6.2 Looking to the future

We have shown in this Thesis that statistically significant results, based on environmental factors, can be obtained with a sample of less than 2000 type Ia supernovae. However, uncovering the underlying astrophysical phenomena driving these trends often requires further sub-samples to be selected, either based on the properties of the supernovae themselves or the host they are within. Doing such a selection invariably reduces the confidence to which you can confirm a result, due to the reduction in sample size. With our sample of 2000 photometrically confirmed type Ia supernovae, these sub-samples and selections can quickly reduce the usable sample size to a few tens of supernovae.

However, in the upcoming era of the Rubin Observatories Legacy Survey of Space and Time (LSST) sample sizes will continue to increase. LSST expects to photometrically classify hundreds of thousands of type Ia supernovae, increasing the existing sample sizes by around

two orders of magnitude. Such a wealth of data would allow for many selection cuts without significant reduction of confidence nor sample size. Selecting only outer region SNe would allow for a cosmologically useful sample without the correction of a $\gamma G_{host,i}$, possibly opening up further insights into the relationships stretch and colour have on the brightness of a given SN. Additionally, while a selection would reduce the statistical uncertainties on the cosmological parameters measured, the systematic uncertainties would be reduced. With the expected large sample sizes of LSST, using this selection may lead to an overall reduction in uncertainty compared to previous surveys. Furthermore this selection is on a simple to calculate variable (which, if LSST matches their SN to host in the same way as DES, would be computed in the host identification stage), allowing such a selection to be investigated with little additional compute time required.

Additionally, such a sample size will allow for uncertainties in cosmological parameters, such as those on the equation of state of dark energy, and the density of matter in the universe to be further reduced.

In terms of cosmological analyses, the measurement of distances are crucial, and much work has been undertaken to limit and account for variations of brightness. In (DES Collaboration et al., 2024b), much of the systematic uncertainty comes from the colour-and-host dependent scatter model. The results of this Thesis may indicate that the associated bias corrects may be overestimated in the outer regions and underestimated in the inner regions. However, the results of this potential over/underestimation would not propagate through as a bias on w, as this would require the distribution of $d_{\rm DLR}$ to evolve as a function of redshift, which it does not.

LSST's $d_{\rm DLR}$ distribution is unknown, and should it evolve with redshift (due to selection affects or a yet unknown astrophysical cause), care must be taken to account for this potential bias on w. The simplest way to investigate and account for this would be to add an additional terms to the bias corrections, correcting for a mass step in the inner region, with lower successive corrections as the SN become more removed from their host..

Appendix A

Appendix A

A.1 Investigating the effects of Cluster Richness on SNe within clusters

When selecting our cluster sample we chose to use the larger $\lambda/S \ge 5$ catalogue, potentially opening our analysis to contamination from over densities of galaxies that would not be classified as true clusters. To investigate what affect this cut has, we restrict our sample to $\lambda/S \ge 15$ and re-analyse the results presented in this paper. This re-analysis is summarised in Table A.1.

Limiting the sample with a more stringent richness cut does change the significance of our results. The colour distribution changes by a large amount, but there is still no significant difference between the two samples, with both samples having less than 1σ difference between them. For the field vs cluster x_1 distribution, it does not alter the result much, with the 'less significant' sample still having a tentative difference between the cluster and field samples, with a confidence level of around 95 per cent. Additionally the restriction shifts the result into being less significant. If the cut removed non-cluster SNe this should increase the significance

Table A.1: Significance's of our cluster vs field analysis for a richness cut of $\lambda/S \ge 5$ and for $\lambda/S \ge 15$

Comparison	K-S Test result	K-S Test result	
	$\lambda/S \geq 5$	$\lambda/S \ge 15$	
x_1	0.023	0.0507	
c	0.8005	0.4441	
Host Stellar Mass	0.0006	0.1102	
Overall Cluster Rate $(SNe \ 100yr^{-1}10^{10}M_{\odot}^{-1})^a$	0.0332 ^{+0.0091} _{-0.0060} (syst)	0.0325 ± 0.0098	

 $[^]a$ Calculated rate is for galaxies with $log(M_*/M_\odot) > 10$ as done in Section 4.1

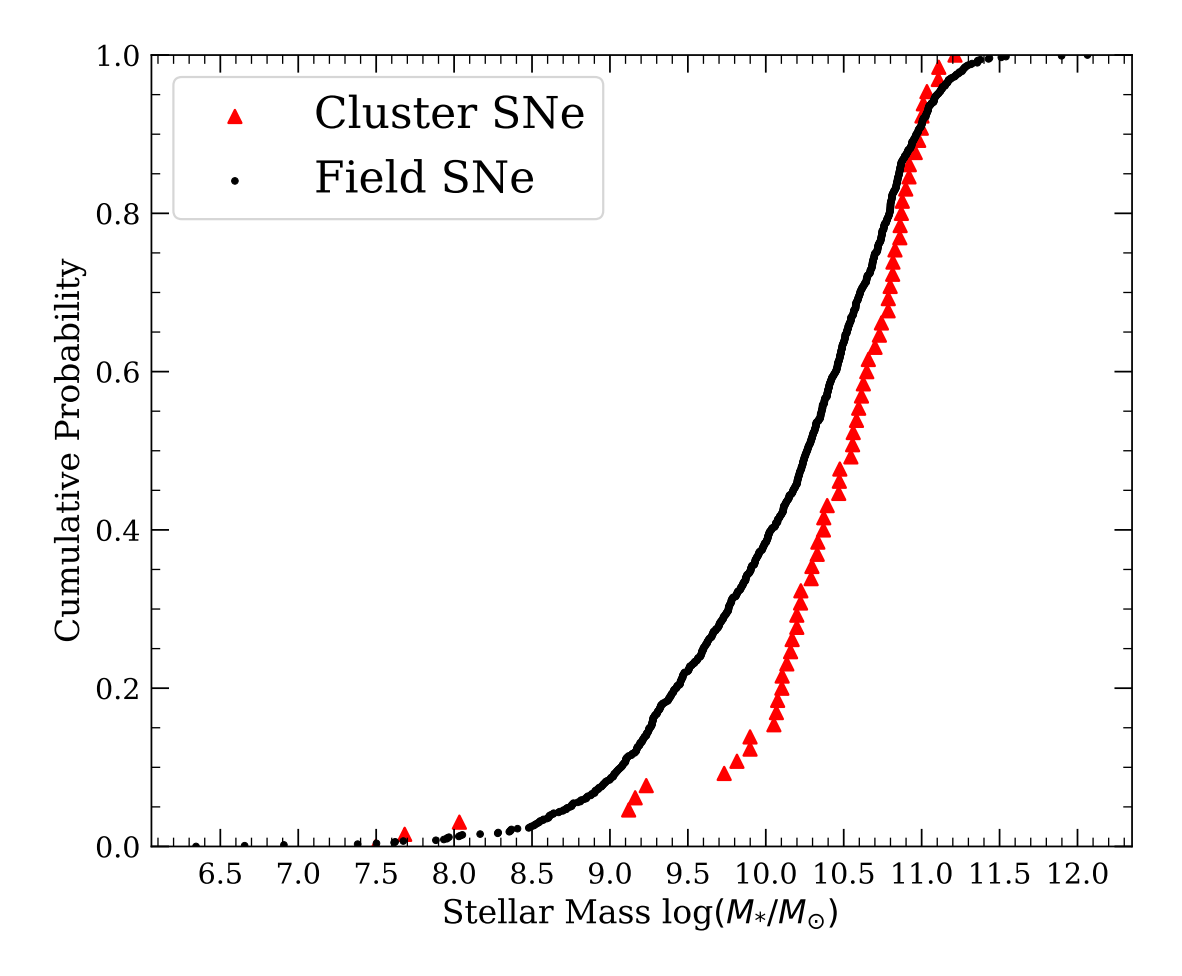


FIGURE A.1: Host galaxy stellar mass distributions for SNe Ia occurring within clusters and in the field. Shown is the CDF of our uncut sample, with clusters of richness ≥ 5 .

between our two samples, as SN x_1 values within rich galaxy clusters were previously found to be significantly different from field galaxy x_1 values, as found in Xavier et al. (2013).

The largest shift is in the host stellar masses, where restricting our sample to only higher richness clusters again decreases the significance of the difference between them. The actual distribution shapes however, do not significantly change. This is shown in Figures A.1 and A.2. We therefore attribute the drop in significance to lower statistics.

There is no significant change in the overall rate, with the two being consistent when accounting for their errors. As our investigated properties do not significantly change under a richness cut, we conclude that making such a richness cut is unnecessary, and would be unnecessarily removing cluster SNe from our sample.

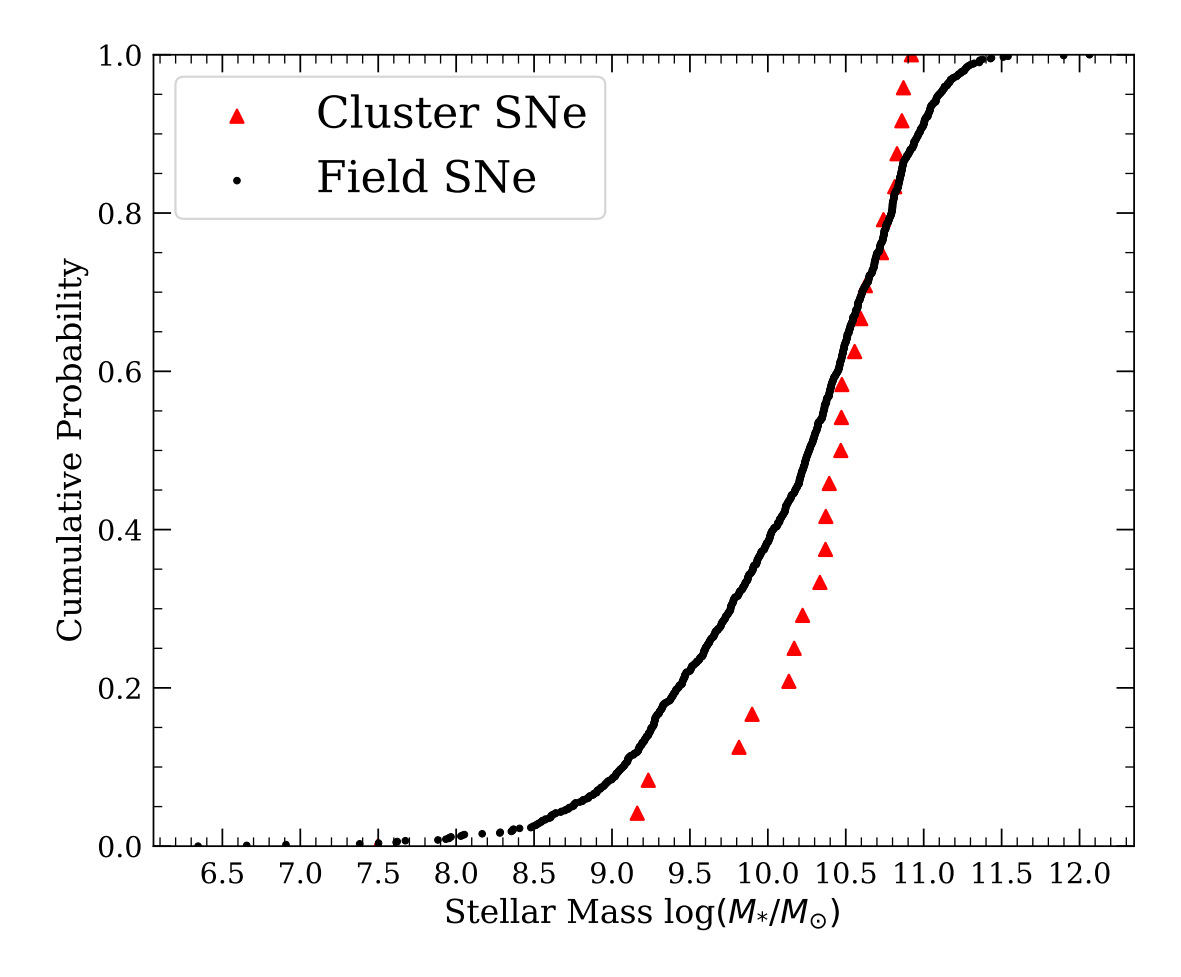


Figure A.2: Host galaxy stellar mass distributions for SNe Ia occurring within clusters and in the field. Show is the CDF of our restricted sample, with clusters of richness ≥ 15 Visually, there is little difference between this sample and A.1, with the exception of far fewer SNe within the higher richness sample.

References

Adelman-McCarthy, J. K., Agüeros, M. A., Allam, S. S., Anderson, K. S. J., et al. 2007, ApJS, 172, 634

Ahn, C. P., Alexandroff, R., Allende Prieto, C., Anderson, S. F., et al. 2012, ApJS, 203, 21

Anderson, J. P., James, P. A., Förster, F., González-Gaitán, S., et al. 2015, MNRAS, 448, 732

Arnett, W. D. 1982, ApJ, 253, 785

Astier, P., Guy, J., Regnault, N., Pain, R., et al. 2006, A&A, 447, 31

Baade, W., et al. 1934, Contributions from the Mount Wilson Observatory, 3, 73

Baes, M., et al. 2007, A&A, 467, 991

Balogh, M. L., et al. 1997, ApJ, 488, L75

Barbary, K., Aldering, G., Amanullah, R., Brodwin, M., et al. 2012, ApJ, 745, 32

Benz, W., et al. 1989, ApJ, 342, 986

Bernstein, J. P., Kessler, R., Kuhlmann, S., Biswas, R., et al. 2012, ApJ, 753, 152

Bertin, E. 2011, in Astronomical Society of the Pacific Conference Series, Vol. 442, Astronomical Data Analysis Software and Systems XX, ed. I. N. Evans, A. Accomazzi, D. J. Mink, & A. H. Rots, 435

Bertin, E., et al. 1996, A&AS, 117, 393

Bertin, E., Mellier, Y., Radovich, M., Missonnier, G., et al. 2002, ASP Conf. Ser. Vol. 281, Astronomical Data Analysis Software and Systems XI, Astron. Soc. Pac, San Francisco

Betoule, M., Kessler, R., Guy, J., Mosher, J., et al. 2014, A&A, 568, A22

Bonnett, C., Troxel, M. A., Hartley, W., Amara, A., et al. 2016, Phys. Rev. D, 94, 042005

Bower, R. G., et al. 1990, AJ, 99, 530

Brahe, T. 1969, Tychonis Brahe De nova et nullius aevi memoria prius visa stella: iam pridem anno a nato Christo 1572, mense Novembri primum conspecta, contemplatio mathematica (Culture et Civilisation)

Briday, M., Rigault, M., Graziani, R., Copin, Y., et al. 2022, A&A, 657, A22

Brout, D., et al. 2021, ApJ, 909, 26

Brout, D., Scolnic, D., Popovic, B., Riess, A. G., et al. 2022, ApJ, 938, 110

Castrillo, A., Ascasibar, Y., Galbany, L., Sánchez, S. F., et al. 2021, MNRAS, 501, 3122

Chandrasekhar, S. 1931, ApJ, 74, 81

Childress, M. J., et al. 2014, MNRAS, 445, 1898

Childress, M. J., Lidman, C., Davis, T. M., Tucker, B. E., et al. 2017, MNRAS, 472, 273

Clark, D. H., et al. 1982, in NATO Advanced Study Institute (ASI) Series C, Vol. 90, Supernovae: A Survey of Current Research, ed. M. J. Rees & R. J. Stoneham, 355–370

Colgate, S. A., et al. 1969, ApJ, 157, 623

Collins, George W., I., et al. 1999, PASP, 111, 871

Davé, R. 2008, MNRAS, 385, 147

Deibel, A., et al. 2022, Phys. Rev. C, 106, 045803

Delahaye, A. G., Webb, T. M. A., Nantais, J., DeGroot, A., et al. 2017, ApJ, 843, 126

DES Collaboration, Abbott, T. M. C., Adamow, M., Aguena, M., et al. 2024a, arXiv e-prints, arXiv:2402.10696

DES Collaboration, Abbott, T. M. C., Acevedo, M., Aguena, M., et al. 2024b, arXiv e-prints, arXiv:2401.02929

Desai, S., Armstrong, R., Mohr, J. J., Semler, D. R., et al. 2012, ApJ, 757, 83

Dilday, B., Bassett, B., Becker, A., Bender, R., et al. 2010, ApJ, 715, 1021-1035

Einstein, A. 1917, Sitzungsberichte der Königlich Preussischen Akademie der Wissenschaften, 142

Ferré-Mateu, A., et al. 2013, MNRAS, 431, 440

Ferreras, I., La Barbera, F., de La Rosa, I. G., Vazdekis, A., et al. 2013, MNRAS, 429, L15

Fioc, M., et al. 1997, A&A, 500, 507

—. 2019, arXiv e-prints, arXiv:1902.02198

Flaugher, B., Diehl, H. T., Honscheid, K., Abbott, T. M. C., et al. 2015, AJ, 150, 150

Freedman, W. L., Madore, B. F., Gibson, B. K., Ferrarese, L., et al. 2001, ApJ, 553, 47

Freedman, W. L., Madore, B. F., Hatt, D., Hoyt, T. J., et al. 2019, ApJ, 882, 34

Freundlich, J., et al. 2021, MNRAS, 502, 5882

Friedmann, M., et al. 2018, MNRAS, 479, 3563-3581

Frohmaier, C., Sullivan, M., Nugent, P. E., Smith, M., et al. 2019, MNRAS, 486, 2308

Gal-Yam, A., et al. 2003, AJ, 125, 1087

Gal-Yam, A., et al. 2002, Monthly Notices of the Royal Astronomical Society, 332, 37

Galbany, L., Miquel, R., Östman, L., Brown, P. J., et al. 2012, ApJ, 755, 125

Gardner, F. F., et al. 1965, AJ, 70, 754

Gatti, M., Sheldon, E., Amon, A., Becker, M., et al. 2021, MNRAS, 504, 4312

Gehrels, N. 1986, ApJ, 303, 336

Giacconi, R., Rosati, P., Tozzi, P., Nonino, M., et al. 2001, ApJ, 551, 624

Goldstein, D. A., D'Andrea, C. B., Fischer, J. A., Foley, R. J., et al. 2015, AJ, 150, 82

González Delgado, R. M., García-Benito, R., Pérez, E., Cid Fernandes, R., et al. 2015, A&A, 581, A103

Graham, M. J., Kulkarni, S. R., Bellm, E. C., Adams, S. M., et al. 2019, PASP, 131, 078001

Graham, M. L., Pritchet, C. J., Sullivan, M., Gwyn, S. D. J., et al. 2008, AJ, 135, 1343

Graur, O., et al. 2013, MNRAS, 430, 1746

Guglielmo, V., Poggianti, B. M., Moretti, A., Fritz, J., et al. 2015, MNRAS, 450, 2749–2763

Gunn, J. E., et al. 1972, ApJ, 176, 1

Gupta, R. R., Kuhlmann, S., Kovacs, E., Spinka, H., et al. 2016, AJ, 152, 154

Guy, J., Astier, P., Baumont, S., Hardin, D., et al. 2007, Astronomy & Astrophysics, 466, 11–21

Guy, J and Sullivan, M, Conley, A., Regnault, N., Astier, P., et al. 2010, A&A, 523, A7

Haines, C. P., Pereira, M. J., Smith, G. P., Egami, E., et al. 2015, ApJ, 806, 101

Hamuy, M., Phillips, M. M., Maza, J., Suntzeff, N. B., et al. 1995, AJ, 109, 1

Hamuy, M., Trager, S. C., Pinto, P. A., Phillips, M. M., et al. 2000, AJ, 120, 1479

Hansen, S. M., McKay, T. A., Wechsler, R. H., Annis, J., et al. 2005, ApJ, 633, 122–137

Hao, J., McKay, T. A., Koester, B. P., Rykoff, E. S., et al. 2010, ApJS, 191, 254

Hartley, W. G., Choi, A., Amon, A., Gruendl, R. A., et al. 2022, MNRAS, 509, 3547

Hayden, B. T., Gupta, R. R., Garnavich, P. M., Mannucci, F., et al. 2013, ApJ, 764, 191

Hicken, M., Wood-Vasey, W. M., Blondin, S., Challis, P., et al. 2009, ApJ, 700, 1097

Hillebrandt, W., et al. 2000, ARA&A, 38, 191

Hinton, S. R., et al. 2016, Astronomy and Computing, 15, 61

Howell, D. A. 2001, ApJ, 554, L193

Howell, D. A., et al. 2000, ApJ, 530, 166

Hoyle, F., et al. 1960, ApJ, 132, 565

Hubble, E. 1929, Proceedings of the National Academy of Science, 15, 168

Ibarra-Medel, H. J., Sánchez, S. F., Avila-Reese, V., Hernández-Toledo, H. M., et al. 2016, MNRAS, 463, 2799

Ivanov, V. D., et al. 2000, ApJ, 542, 588

Ivezić, Ž., Kahn, S. M., Tyson, J. A., Abel, B., et al. 2019, ApJ, 873, 111

Jarvis, M., Sheldon, E., Zuntz, J., Kacprzak, T., et al. 2016, MNRAS, 460, 2245

Jeffrey, N., Abdalla, F. B., Lahav, O., Lanusse, F., et al. 2018, MNRAS, 479, 2871

Jha, S., et al. 2007, ApJ, 659, 122

Jones, D. O., Scolnic, D. M., Riess, A. G., Kessler, R., et al. 2017, ApJ, 843, 6

Jones, D. O., Scolnic, D. M., Foley, R. J., Rest, A., et al. 2019, ApJ, 881, 19

Kelly, P. L., et al. 2010, ApJ, 715, 743

Kelsey, L., Sullivan, M., Smith, M., Wiseman, P., et al. 2021, MNRAS, 501, 4861

Kelsey, L., Sullivan, M., Wiseman, P., Armstrong, P., et al. 2022, MNRAS, arXiv:2208.01357

Kennicutt, Robert C., J. 1998, ARA&A, 36, 189

Kenworthy, W. D., Jones, D. O., Dai, M., Kessler, R., et al. 2021, ApJ, 923, 265

Kessler, R., et al. 2017, ApJ, 836, 56

Kessler, R., Bernstein, J. P., Cinabro, D., Dilday, B., et al. 2009, PASP, 121, 1028

Kessler, R., Marriner, J., Childress, M., Covarrubias, R., et al. 2015, AJ, 150, 172

Kim, J., Jee, M. J., Hughes, J. P., Yoon, M., et al. 2021, ApJ, 923, 101

Kormendy, J., et al. 1989, ARA&A, 27, 235

Kowal, C. T. 1968, AJ, 73, 1021

Lampeitl, H., Smith, M., Nichol, R. C., Bassett, B., et al. 2010, ApJ, 722, 566

Lampland, C. O. 1921, PASP, 33, 79

Larison, C., et al. 2023, arXiv e-prints, arXiv:2306.01088

Le Borgne, D., et al. 2002, A&A, 386, 446

Leavitt, H. S., et al. 1912, Harvard College Observatory Circular, 173, 1

Lemos, P., et al. 2023, arXiv e-prints, arXiv:2307.13083

Lianou, S., et al. 2019, A&A, 631, A38

Lidman, C., Tucker, B. E., Davis, T. M., Uddin, S. A., et al. 2020, MNRAS, 496, 19

Lintott, C. J., Schawinski, K., Slosar, A., Land, K., et al. 2008, MNRAS, 389, 1179

Lueker, M., Reichardt, C. L., Schaffer, K. K., Zahn, O., et al. 2010, ApJ, 719, 1045

Malmquist, K. G. 1922, Meddelanden fran Lunds Astronomiska Observatorium Serie I, 100, 1

—. 1925, Meddelanden fran Lunds Astronomiska Observatorium Serie I, 106, 1

Mandel, K. S., et al. 2011, ApJ, 731, 120

Mannucci, F., Della Valle, M., Panagia, N., Cappellaro, E., et al. 2005, A&A, 433, 807

Mannucci, F., Maoz, D., Sharon, K., Botticella, M. T., et al. 2008, MNRAS, 383, 1121

Maoz, D., et al. 2017, ApJ, 848, 25

—. 2014, ARA&A, 52, 107

McClintock, T., Varga, T. N., Gruen, D., Rozo, E., et al. 2019, MNRAS, 482, 1352

Minkowski, R. 1941, PASP, 53, 224

Mohr, J. J., Armstrong, R., Bertin, E., Daues, G., et al. 2012, in Society of Photo-Optical Instrumentation Engineers (SPIE) Conference Series, Vol. 8451, Software and Cyberinfrastructure for Astronomy II, ed. N. M. Radziwill & G. Chiozzi, 84510D

Möller, A., Smith, M., Sako, M., Sullivan, M., et al. 2022, MNRAS, 514, 5159

Möller, A., Wiseman, P., Smith, M., Lidman, C., et al. 2024, arXiv e-prints, arXiv:2402.18690

Moore, B., et al. 1996, Nature, 379, 613

Morganson, E., Gruendl, R. A., Menanteau, F., Kind, M. C., et al. 2018, PASP, 130, 074501

Murdin, P., et al. 2011, Supernovae (Cambridge University Press)

Möller, A., et al. 2019, MNRAS, 491, 4277-4293

Neill, J. D., Sullivan, M., Balam, D., Pritchet, C. J., et al. 2006, AJ, 132, 1126

Nersesian, A., Dobbels, W., Xilouris, E. M., Baes, M., et al. 2021, MNRAS, 506, 3986

Oppenheimer, B. D., Davé, R., Kereš, D., Fardal, M., et al. 2010, MNRAS, 406, 2325

Orellana, G., Nagar, N. M., Elbaz, D., Calderón-Castillo, P., et al. 2017, A&A, 602, A68

Palmese, A., Annis, J., Burgad, J., Farahi, A., et al. 2020, MNRAS, 493, 4591

Parikh, T., Thomas, D., Maraston, C., Westfall, K. B., et al. 2021, MNRAS, 502, 5508

Perlmutter, S., Aldering, G., Goldhaber, G., Knop, R. A., et al. 1999, ApJ, 517, 565

Perrett, K., Sullivan, M., Conley, A., González-Gaitán, S., et al. 2012, AJ, 144, 59

Phillips, M. M. 1993, ApJ, 413, L105

Pierre, M., Valtchanov, I., Altieri, B., Andreon, S., et al. 2004, J. Cosmology Astropart. Phys., 2004, 011

Pigott, E. 1785, Philosophical Transactions of the Royal Society of London Series I, 75, 127

Pilkington, K., Few, C. G., Gibson, B. K., Calura, F., et al. 2012, A&A, 540, A56

Planck Collaboration, Aghanim, N., Akrami, Y., Ashdown, M., et al. 2020, A&A, 641, A6

Popovic, B., et al. 2021a, arXiv e-prints, arXiv:2112.04456

—. 2021b, ApJ, 913, 49

Popovic, B., Scolnic, D., Vincenzi, M., Sullivan, M., et al. 2024, MNRAS, 529, 2100

Porredon, A., Crocce, M., Elvin-Poole, J., Cawthon, R., et al. 2022, Phys. Rev. D, 106, 103530

Pskovskii, I. P. 1977, Soviet Ast., 21, 675

Qu, H., et al. 2021, AJ, 162, 67

Qu, H., Sako, M., Vincenzi, M., Sánchez, C., et al. 2024, ApJ, 964, 134

Riess, A. G., et al. 1996, ApJ, 473, 88

Riess, A. G., Filippenko, A. V., Challis, P., Clocchiatti, A., et al. 1998, AJ, 116, 1009

Riess, A. G., Macri, L., Casertano, S., Sosey, M., et al. 2009, ApJ, 699, 539

Riess, A. G., Yuan, W., Macri, L. M., Scolnic, D., et al. 2022, ApJ, 934, L7

Rigault, M., Copin, Y., Aldering, G., Antilogus, P., et al. 2013, A&A, 560, A66

Rigault, M., Brinnel, V., Aldering, G., Antilogus, P., et al. 2020, A&A, 644, A176

Roman, M., Hardin, D., Betoule, M., Astier, P., et al. 2018, A&A, 615, A68

Rose, B. M., et al. 2019, ApJ, 874, 32

Rowan-Robinson, M., Lari, C., Perez-Fournon, I., Gonzalez-Solares, E. A., et al. 2004, MNRAS, 351, 1290

Rozo, E., Rykoff, E. S., Koester, B. P., McKay, T., et al. 2009, ApJ, 703, 601

Ruiter, A. J., et al. 2009, ApJ, 699, 2026

Ruppin, F., Rigault, M., Ginolin, M., Dimitriadis, G., et al. 2024, arXiv e-prints, arXiv:2406.01108

Rust, B. W. 1974, PhD thesis, Oak Ridge National Laboratory, Tennessee

Rykoff, E. S., Koester, B. P., Rozo, E., Annis, J., et al. 2012, ApJ, 746, 178

Rykoff, E. S., Rozo, E., Busha, M. T., Cunha, C. E., et al. 2014, ApJ, 785, 104

Rykoff, E. S., Rozo, E., Hollowood, D., Bermeo-Hernandez, A., et al. 2016, ApJS, 224, 1

Sako, M., Bassett, B., Connolly, B., Dilday, B., et al. 2011, ApJ, 738, 162

Santini, P., Maiolino, R., Magnelli, B., Lutz, D., et al. 2014, A&A, 562, A30

Saracco, P., et al. 2017, A&A, 597, A122

Scannapieco, E., et al. 2005, ApJ, 629, L85

Schechter, P. 1976, ApJ, 203, 297

Scolnic, D. M., Jones, D. O., Rest, A., Pan, Y. C., et al. 2018, ApJ, 859, 101

Sevilla, I., Armstrong, R., Bertin, E., Carlson, A., et al. 2011, arXiv e-prints, arXiv:1109.6741

Shappee, B. J., Prieto, J. L., Grupe, D., Kochanek, C. S., et al. 2014, ApJ, 788, 48

Sharon, K., et al. 2007, ApJ, 660, 1165

Sharon, K., Gal-Yam, A., Maoz, D., Filippenko, A. V., et al. 2010, ApJ, 718, 876

Shaw, R. L. 1979, A&A, 76, 188

Shchekinov, Y. A., et al. 2022, Universe, 8, 212

Shen, K. J., et al. 2017, ApJ, 851, L50

Sicoli, P., et al. 2024, Icarus, 420, 116165

Simpson, J. P., et al. 1995, ApJ, 444, 721

Smith, M., Nichol, R. C., Dilday, B., Marriner, J., et al. 2012, ApJ, 755, 61

Smith, M., D'Andrea, C. B., Sullivan, M., Möller, A., et al. 2020a, AJ, 160, 267

Smith, M., Sullivan, M., Wiseman, P., Kessler, R., et al. 2020b, MNRAS, 494, 4426

Speagle, J. S., et al. 2014, The Astrophysical Journal Supplement Series, 214, 15

Sullivan, M., Le Borgne, D., Pritchet, C. J., Hodsman, A., et al. 2006, ApJ, 648, 868

Sullivan, M., Conley, A., Howell, D. A., Neill, J. D., et al. 2010, MNRAS, 406, 782

Taam, R. E. 1980, ApJ, 242, 749

The LSST Dark Energy Science Collaboration, Mandelbaum, R., Eifler, T., Hložek, R., et al. 2018, arXiv e-prints, arXiv:1809.01669

Tomczak, A. R., Quadri, R. F., Tran, K.-V. H., Labbé, I., et al. 2014, ApJ, 783, 85

Toy, M., Grayling, M., Frohmaier, C., Wiseman, P., et al. 2022, Transient Name Server Classification Report, 2022-2756, 1

Toy, M., Wiseman, P., Sullivan, M., Frohmaier, C., et al. 2023, MNRAS, 526, 5292

Toy, M., Wiseman, P., Sullivan, M., Scolnic, D., et al. 2024, arXiv e-prints, arXiv:2408.03749

Tripp, R. 1998a, A&A, 331, 815

—. 1998b, A&A, 331, 815

Truran, J. W., et al. 1967, Canadian Journal of Physics, 45, 2315

Tutukov, A. V. 1981, in IAU Symposium, Vol. 93, Fundamental Problems in the Theory of Stellar Evolution, ed. D. Sugimoto, D. Q. Lamb, & D. N. Schramm, 137–153

van der Burg, R. F. J., McGee, S., Aussel, H., Dahle, H., et al. 2018, A&A, 618, A140

van der Burg, R. F. J., Muzzin, A., Hoekstra, H., Lidman, C., et al. 2013, A&A, 557, A15

van Dokkum, P. G. 2008, ApJ, 674, 29

Vincenzi, M., Sullivan, M., Graur, O., Brout, D., et al. 2021, MNRAS, 505, 2819

Vincenzi, M., Brout, D., Armstrong, P., Popovic, B., et al. 2024, arXiv e-prints, arXiv:2401.02945

von Spaeth, O. 2000, Centaurus, 42, 159

Watson, C., Tran, K.-V., Tomczak, A., Alcorn, L., et al. 2019, ApJ, 874, 63

Weidemann, V. 1968, ARA&A, 6, 351

Whelan, J., et al. 1973, ApJ, 186, 1007

Wilman, D. J., Balogh, M. L., Bower, R. G., Mulchaey, J. S., et al. 2005, MNRAS, 358, 88

Wiseman, P., Smith, M., Childress, M., Kelsey, L., et al. 2020, MNRAS, 495, 4040

Wiseman, P., Sullivan, M., Smith, M., Frohmaier, C., et al. 2021, MNRAS, 506, 3330

Wiseman, P., Vincenzi, M., Sullivan, M., Kelsey, L., et al. 2022a, MNRAS, 515, 4587

—. 2022b, MNRAS, 515, 4587

Xavier, H. S., Gupta, R. R., Sako, M., D'Andrea, C. B., et al. 2013, MNRAS, 434, 1443

Yuan, F., Lidman, C., Davis, T. M., Childress, M., et al. 2015, MNRAS, 452, 3047

Zhao, F.-Y., et al. 2006, Chinese J. Astron. Astrophys., 6, 635

Zheng, Z., Wang, H., Ge, J., Mao, S., et al. 2017, MNRAS, 465, 4572

Zwicky, F. 1940, Reviews of Modern Physics, 12, 66